# CZECH TECHNICAL UNIVERSITY IN PRAGUE
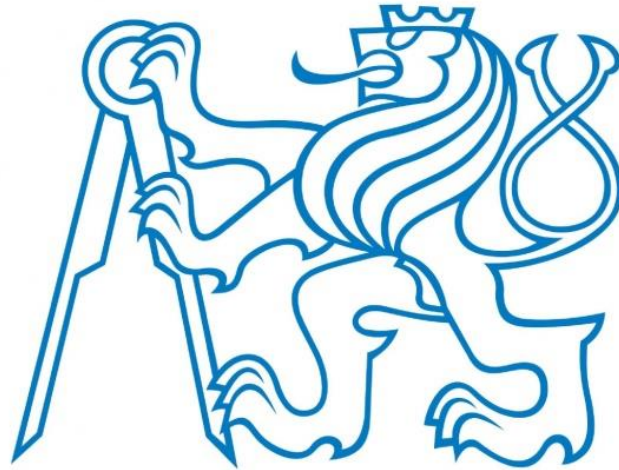
# FACULTY OF MECHANICAL ENGINEERING

## DEPARTMENT OF AUTOMOTIVE, COMBUSTION ENGINE AND RAILWAY ENGINEERING



# Design of 12V and 400V Lithium – Ion Battery Pack for an Electric Vehicle with Immerisve Cooling

**Author: Kanishka Mathur**

**Supervisor: doc. Ing. Pavel Mindl Csc.**

**Program: Master of Automotive Engineering**

**Specialization: Advanced Powertrain Design**

**August 2021**

# ABSTRACT

The following master's thesis is concerned with the development of a 12V and 400V lithium-ion immersive cooled battery. Lithium-ion batteries must be explicitly designed for a Classic Mini Cooper. The design and manufacture of the 12V battery and the modelling of the 400V battery for heat generation and SOC curve are all part of this thesis project. To obtain the heat generation data and SOC curve, a battery model was created in MATLAB Simulink. The heat exchanger was designed with 3M Novec 7200 cooling fluid based on heat generation.

**Keywords**

12V, 400V Lithium-Ion, Battery, Immersive Cooling, SOC, Heat Exchanger, Battery Modelling

# ABSTRAKT

Následující diplomová práce se zabývá vývojem 12V a 400V lithium-iontové chlazené baterie. Lithium-iontové baterie musí být výslovně navrženy pro Classic Mini Cooper. Součástí tohoto projektu je návrh a výroba 12V baterie a modelování 400V baterie pro výrobu tepla a křivka SOC. Pro získání dat o generování tepla a křivky SOC byl v MATLAB Simulink vytvořen model baterie. Výměník tepla byl navržen s chladicí kapalinou 3M Novec 7200 na základě výroby tepla.

**Klíčová slova**

Lithium-iont 12V, 400V, baterie, pohlcující chlazení, SOC, výměník tepla, modelování baterií

# Declaration

I, Kanishka Mathur, declare that this thesis and the work presented in it, titled "Design of 12V and 400V Lithium-Ion battery pack for an Electric Vehicle with immersive cooling", are my own and has been generated by me as the result of my original research. I confirm that this work was completed entirely or primarily while pursuing a master's degree in Automotive Engineering at Czech Technical University. This thesis has been clearly mentioned where any element of it has previously been submitted for a degree or other qualification at this University or another institution. When I consult other people's published work, I always make sure to credit them. I always give the source when I quote from other people's work. This thesis is totally my work, with the exception of such quotes. I've acknowledged all major sources of assistance. None of this work has been published before submission.

Date: Friday, August 13, 2021                                        Signature:

# ACKNOLEDGEMENT

# NOMENCLATURE

| | |
|---|---|
| $V_t^{dis}$ | Terminal Voltage while discharging |
| $V_t^{cha}$ | Terminal Voltage while charging |
| $E_{eq}$ | Equilibrium State Voltage |
| $\eta_{dis}$ | Discharging polarization Voltage |
| $\eta_{cha}$ | Charging Polarization Voltage |
| $A_{copper}$ | Copper plate cross-sectional area |
| $R_C$ | Copper resistance per unit cm |
| $R_{total\ copper}$ | Copper plate total resistance |
| $V_{drop,copper}$ | Voltage drop across the copper plate |
| I | Current |
| $L_{total,copper}$ | total length of copper plates |
| $R_{total,copper}$ | Total resistance of copper plate |
| $Q_{resistance}$ | Heat generated due to resistance |
| $L_{nickel}$ | Length of Nickel Plate |
| $R_{total,\ nickel}$ | Total resistance of nickel plate |
| $A_{nickel}$ | Area of Nickel Playte |
| $Q_{nickel,copper}$ | Total heat generated due resistance in nickel and copper plates |
| $R_{total}$ | Total resistance of copper and nickel plate |
| $R_{busbar}$ | Resistance of busbar |
| $Q_{busbar}$ | Heat generated in busbar due to resistance |
| $R_{internal,total}$ | Total internal resistance of the cells |
| $Q_{cells}$ | Heat generated in cells due to resistance |
| $Q_{battery}$ | Total heat generated in the battery |
| $W_{cells}$ | Weight of the cells |
| $W_{cell\ holder}$ | Weight of cell holders |
| $W_{fluid}$ | Weight of cooling fluid |
| $W_{Al}$ | Weight of the aluminium case |
| $W_{battery}$ | Weight of the battery |
| $W_{miscellaneous}$ | Miscellaneous Weight |
| $E_{gen}$ | Energy generated in the battery |
| $\Delta T_{novec}$ | Increase in Novec fluid temperature |
| $W_{cells,400}$ | Weight of the cells in 400V battery |
| $W_{cellholder,400V}$ | Weight of the cell holder in 400V battery |
| $W_{battery\ case,400V}$ | Weight of the 400V battery case |
| $W_{fluid,400V}$ | Weight of the cooling fluid in 400V battery |
| $W_{miscellaneous,400v}$ | Miscellaneous weight in 400V battery |
| $W_{batter,400V}$ | Weight of the 400V battery |
| $F_t$ | Tractive force |
| $F_{RR}$ | Rolling Resistance |
| g | acceleration due to gravity |
| f | coefficient of rolling resistance |
| Cd | Drag Coefficient |
| A | Vehicle frontal area |
| $\delta$ | Coefficient of rotational inertia |
| $F_{aero}$ | Aerodynamic resistance force |

| | |
|---|---|
| $F_{acc}$ | Acceleration resistance force |
| $P_{wheels}$ | Power required at the wheels |
| $P_{motor}$ | Power required from the motor |
| $P_{battery}$ | Power required from the battery |
| $\eta_{motor}$ | Motor efficiency |
| $\eta_t$ | Transmission Efficiency |
| $\eta_{converter}$ | Converter efficiency |
| $R_{int}$ | Internal Resistance |
| $n_{series}$ | Number of cells in series |
| $n_{parallel}$ | Number of cells in parallel |
| $R_{cell}$ | Internal resistance of a cell |
| $I_{dc}$ | Discharge current |
| $I_C$ | Charge Current |
| $V_{OCV}$ | Open circuit voltage |
| $P_{req}$ | Power required |
| $C$ | Battery Capacity |
| $I_{tot}$ | Total current |
| $Q_{gen}$ | Heat generated |
| $R_{tot}$ | Total resistance |
| $q$ | heat generated |
| $m_{air}$ | mass of air |
| $C_{P,air}$ | Heat capacity of the air |
| $T_{air,in}$ | Inlet air temperature |
| $T_{air,out}$ | Air outlet temperature |
| $m_{novec}$ | Mass of Novec fluid |
| $T_{novec,in}$ | Inlet temperature of Novec fluid |
| $T_{novec,out}$ | Outlet temperature of Novec Fluid |
| $D_{hydraulic}$ | Hydraulic Diameter |
| $A_{tube}$ | Tube cross sectional area |
| $P_{tube}$ | Perimetere of tube |
| $A_{radiator}$ | Total radiator area |
| $A_b$ | Base surface area |
| $A_f$ | Single fin surface area |
| $A_{fin,base}$ | Total fin/base surface area |
| $A_{external}$ | Total eternal surface area |
| $A_{internal}$ | Total internal surface area |
| $L_{radiator}$ | Length of radiator |
| $H_{radiator}$ | Height of radiator |
| $W_{radiator}$ | Width of radiator |
| $W_{tube}$ | Width of tube |
| $H_{tube}$ | Tube height |
| $L_{fin}$ | Length of fin |
| $H_{fin}$ | Fin thickness |
| $N_{tube}$ | Number of tubes |
| $L_C$ | Corrected length |
| $Re_{novec}$ | Reynolds number of Novec |
| $\rho_{novec}$ | Novec 7200 fluid density |

| | |
|---|---|
| $v_{novec}$ | Velocity of Novec fluid |
| $Re_{air}$ | Reynolds Number of air |
| Nu | Nusselt number |
| $h_{air}$ | heat transfer coefficient of air |
| $\eta fin$ | Fin efficiency |
| $\eta_o$ | Overall efficiency |
| UA | Overall heat transfer coefficient |
| $h_{novec}$ | heat transfer coefficient of novec |
| $C_r$ | Heat capacity ratio |
| K | Coefficient |
| $q_{predicted}$ | predicted heat transfer |
| $q_{max}$ | maximum heat transfer |
| $G_{a,w}$ | mass flux parameter |
| $f_n$ | Novec side friction factor |
| $\Delta P_{novec}$ | pressure drop of novec fluid across heat exchanger |
| fa | Air side friction factor |

# List Of Abbreviations

| | |
|---|---|
| WLTP | Worldwide harmonized light vehicles test procedure |
| SOC | State of Charge |
| ESS | Energy Storage System |
| HEV | Hybrid Electric Vehicle |
| EOL | End Of Life |
| DOD | Depth of Discharge |
| PHEV | Plugin Hybrid Electric Vehicle |
| BEV | Battery Electric vehicle |
| CE | Coloumb Efficiency |
| EE | Energy Efficiency |
| VE | Voltage Efficiency |
| TMS | Thermal Management System |
| PCM | Phase Change Material |
| SAE | Society of Autmotive Engineers |
| USABC | United States Advanced Battery Consortium |
| EDTA | Electric Drive Transportation Association |
| EVAA | Electric Vehicle Association of America |
| ISO | International Organisation for Standardization |
| SOE | State of Energy |
| SOH | State of Health |
| SOP | State of Power |
| EM | Electrochemical Model |
| ECM | Equivalent Circuit Model |

# Table of Contents

# 1  Introduction

Lithium-ion (Li-ion) batteries are now omnipresent. Our watches, cellphones, tablets, computers, portable appliances, GPS gadgets, handheld games, and just about everything else we carry with us today are all powered by them. Moreover, they are also beginning to power our neighbourhoods, residences, and vehicles, or perhaps it is more apt to say that batteries power transportation when addressing transportation applications. Lithium-ion batteries' rise to prominence and domination is due to their high power density compared to other rechargeable battery systems, which was achieved by designing and developing high-energy-density electrode materials. Moreover, batteries are unique in energy storage products as they both create energy via chemical processes and store the energy within the same device. Other energy storage devices require the power to be generated in one place & stored in another. For example, in an automobile, the energy is created through the refining the liquid crude oil, it is then transferred to service stations, where it is again stored until purchased and stored again as liquid fuel in a tank, it is finally converted into energy (& work) in the combustion process of an internal combustion engine.

## 1.1  Project Goals

This project aims to design a 12V and a 400V lithium-ion battery, which is cooled by immersive cooling for an electric vehicle. The vehicle is a Classic Mini Cooper. We are converting it into an electric vehicle. Lithium-ion cells are to be studied to understand the heat generation inside the cells and the optimum temperature for their working. The battery pack modelling in Matlab SIMULINK is to be done to get the SOC and heat generated in the battery pack during a WLTP cycle. An immersive cooling system has to be designed along with its heat exchanger to get optimum battery pack cooling.

# 2  Literature Review

## 2.1  Battery fundamentals

In this section, we shall discuss the construction and working principles of a battery. Afterwards, we will discuss the lithium-ion cells' basic terminology and characteristics and their comparison with other cell chemistry.

## 2.1.1 Battery

Most simply, a battery is an electrochemical means of storing energy that operates by converting chemical energy into electrical energy. A battery is a device that uses an electrochemical redox reaction to directly convert the chemical energy contained in its active material into electrical energy.

Batteries are basically classified into two types: either primary or secondary. The main distinction is whether or not the batteries are rechargeable. Primary batteries are not rechargeable; they are one-time-use batteries that must be thrown after usage. Simple alkaline batteries, which are used in many household gadgets, are an example of this. Secondary batteries are multi-use, rechargeable batteries that can be charged multiple times. The chemistry and operational characteristics of a rechargeable battery determine how long it can be used.

## 2.1.2 Components of a battery

There are mainly five components of a battery. The cathode is the "positive" half of the battery cell, which is made up of a substrate coated with the active material. The substrate in lithium-ion batteries is frequently an extremely thin aluminum layer. The anode, or "negative" half of the battery cell, is commonly comprised of a thin copper substrate coated with active anode material. A "separator" substance is sandwiched between these two halves, preventing the two halves from contacting and causing a short circuit. These three components are assembled to form the electrodes and are either wound or stacked to form what is referred to as a jellyroll. The enclosure, which is usually a container or pouches into which the jellyroll is inserted, is the fourth component of a lithium-ion battery. A metal can, a plastic housing, or a polymer-type "pouch" might all be used. After that, the fifth component, an electrolyte, is added to the solution. The electrolyte is the medium that allows ions to move freely throughout the cell. Many other parts may be included in a battery cell, such as a current interrupt device (CID) or a positive thermal coefficient (PTC), which is a resettable thermal fuse. However, these are not included in all cell types of chemistries.
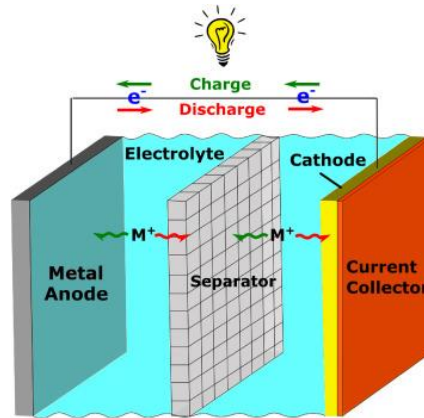
*Figure 1 Diagram showing Anode , cathode , separator and electrolyte in a Battery*

Distinct battery types have different performance characteristics, making them suitable for various applications. In Table 1 several of the most common nonlithium-based chemistry types are compared. The table is not all-inclusive but offers a good summary of some of the significant nonlithium chemistries used in ESS. For example, traditional lead-acid offers the shortest cycle life and lowest energy density and lowest cost. Secondary battery chemistries such as lead-acid, nickel-cadmium (NiCd), NiMh, sodium-sulphur, and sodium nickel chloride were used in many early automotive electrification attempts. NiMh remains the most used battery chemistry for hybrid electric vehicles today (HEVs).

| | Lead Acid | Nickel Cadmium | Nickel Metal Hydride | Sodium Sulfur | Sodium Nickel Chloride |
|---|---|---|---|---|---|
| Chemistry descriptor | PbA/LAB | NiCd | NiMh | NaS | NaNiCl |
| Specific energy (Wh/kg) | 30–40 | 40–60 | 30–80 | 90–110 | 100–120 |
| Energy density (Wh/L) | 60–70 | 50–150 | 140–300 | 345 | 160–190 |
| Specific power (W/kg) | 60–180 | 150 | 250–1000 | 150–160 | 150 |
| Power density (W/L) | 100 | 210 | 400 | – | – |
| Nominal voltage (per cell) (V) | 2.0 | 1.2 | 1.2 | 2.0 | 2.6 |
| Cycle life | 300–800 | 1000–2000 | 500–1500 | 1000–2500 | 1000 |
| Self-discharge (% per month) | 3–5% | 20% | 30% | 0% | 0% |
| Operating temperature range (°C) | −20 to +60 | −40 to +60 | −20 to +60 | 300 to 400 | 300 to 400 |
| Cost (per kWh) | $150–$200 | $400–$800 | $200–S300 | $350 | $100–$300 |
| Maintenance | 3–6 months | 30–60 days | 60–90 days | None | None |

*Table 1 Different types of batteries comparison*

In our research, we focus mainly on lithium-ion chemistry.

## 2.2 Lithium-Ion Cells

The first commercial lithium-ion chemistry was introduced to the market in 1990 based mainly on the work of Dr John Goodenough of the University of Texas. From its introduction in 1991 to the early 2000s, sales of lithium-ion grew in demand to become the highest volume cell manufactured in the world with about 660 million small cylindrical cells and another 700 million small polymer (pouch)-type cells manufactured annually in 2013. Lithium-ion quickly became the battery of choice for most small electronics because it contained much higher energy density than comparable cells on the market.

In a lithium-ion battery, energy flow is created as the lithium-ions within the cathode are transferred through an electrolyte medium into anode, this represents a charging event. A discharging event is represented by the lithium-ions being transferring through an electrolyte medium from anode into the cathode. This seems counterintuitive for most of us, but when the battery discharges, the ions pass from anode to cathode. In the diagram below, a charging event is being shown. The lithium-ions pass from the cathode material through the electrolyte to the separator and then again through the electrolyte and to the anode material. This action creates a voltage flow up the copper current collector and to the positive current collector in a closed circuit loop.
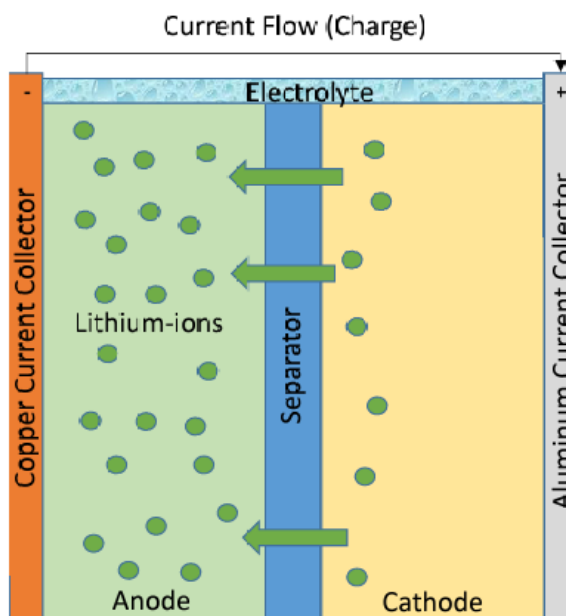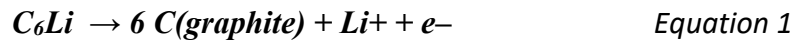


*Figure 2 Flow of Lithium Ions in cell when charging*

During discharge, lithium is then oxidized from Li to Li + (0 to +1 oxidation state) in the lithium-graphite anode through the following reaction:

$$C_6Li \rightarrow 6\ C(graphite) + Li+ + e– \qquad Equation\ 1$$

The cell can be recharged by reversing these reactions. Lithium ions leave the lithium cobalt oxide cathode and migrate back to the anode in this scenario. They are reincorporated into the graphite network after being reduced to neutral lithium. These lithium ions migrate through electrolyte medium to cathode, where they are incorporated into lithium cobalt oxide through the following reaction, which reduces cobalt from a +4 to a +3 oxidation state :

$$Li1-xCoO2\ (s) + x\ Li+ + x\ e- \rightarrow LiCoO2\ (s) \qquad Equation\ 2$$
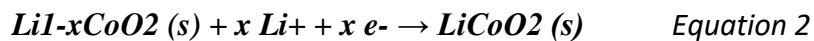
One of the other benefits of lithium-ion chemistries over nickel- and lead-based batteries is the higher voltage. Typical NiMh and NiCd rechargeable cells operate at about 1.2–1.5 V nominal, whereas lithium-ion cells typically operate between 3.2 and 3.8 V nominal. Having a higher voltage is essential in that it means that we need to connect fewer cells in series in order to achieve our desired pack voltage. For instance, a NiMh battery pack with 350 V may require 292 cells to achieve that voltage (350 V/1.2 V = 292 cells). On the other hand, a lithium-ion-based battery pack would only require 98 cells to achieve the same system voltage (350 V/3.6 V = 98 cells). Lithium-ion batteries have a lower rate of self-discharge in addition to higher voltage and energy density. This means that its natural capacity loss over time when the batteries are in storage is less than that of other chemistries, with many lithium-ion chemistries losing only 1–5% per month. Capacity loss during storage comes in two types, reversible and permanent. Reversible capacity loss is the energy lost during storage but regained once the battery is cycled again. The percentage of a loss that will never be recovered is known as permanent loss. Virtually all lithium-ion chemistries have some amount of reversible capacity loss over time, some of which are generally always permanent.

Finally, lithium-ion chemistries tend to have a much better cycle life than the other chemistries. Where PbA may only get 300–500 cycles before it reaches its end of life (EOL), lithium-ion can achieve thousands of complete discharge cycles before reaching its EOL during 100% depth of discharge (DOD) cycles. If we look at partial cycles, the lithium-ion battery will be able to achieve tens of thousands of cycles as the DOD is

reduced. For example, let's look at a typical lithiumion chemistry. It may achieve 1000 cycles using 100% DOD, but if we take that same cell and use only 80% of its total usable energy, we will find that we can now get several thousand cycles.

## 2.2.1 Electrolytes

The electrolyte is essential for transferring positive lithium ions from the cathode to the anode. Lithium salt, such as LiPF6, in an organic solution is the most often used electrolyte. There are mainly two types of electrolytes details of which are mentioned below.

## 2.2.2 Types of electrolytes

- Liquid electrolyte

Liquid electrolytes in the lithium-ion batteries consist of lithium salts, like $LiPF_6$, $LiBF_4$ or $LiClO_4$ in an organic solvent, like ethylene carbonate, dimethyl carbonate & diethyl carbonate. The liquid electrolyte acts as a conductive channel for cations flowing from negative to positive electrodes during the discharge. At room temperature (20 °C (68 °F), typical conductivities of liquid electrolyte are in the 10 mS/cm range, increasing by 30–40% at 40 °C (104 °F) and decreasing somewhat at 0 °C (32 °F).

- Solid Electrolytes

Recent advances in battery technology involve using solid as the electrolyte material. The most promising of these are ceramics.

The solid ceramic electrolytes are mostly lithium metal oxides, allowing lithium-ion transport through solid more readily due to intrinsic lithium. The main benefit of a solid electrolyte is that there is no risk of leakage, which is a serious safety issue for batteries with liquid electrolytes.

Ceramic and glassy solid ceramic electrolytes are the two primary kinds of solid ceramic electrolytes. Ceramic solid electrolytes are highly organized substances containing ion transport channels in their crystal structures. Perovskites and lithium super ion conductors (LISICON) are two common ceramic electrolytes. Glassy solid electrolytes are amorphous atomic structures having similar elements to ceramic solid electrolytes, but with greater conductivities altogether driven by strong conductivity at grain boundaries.

## 2.2.3 Cathode Materials

LiCoO2 or LiMn2O4 are commonly used as cathode materials. The pseudo tetrahedral structure of cobalt-based materials enables for two-dimensional lithium-ion diffusion.

Because of their high theoretical specific heat capacity, high volumetric capacity, low self-discharge, high discharge voltage, and outstanding cycle performance, cobalt-based cathodes are suitable. The material's high cost and low thermal stability are two drawbacks. The cubic crystal lattice system used in manganese-based materials allows for 3D lithium-ion diffusion. Manganese cathodes are appealing because manganese is inexpensive and could theoretically be utilized to create a more efficient, longer-lasting battery if its restrictions are addressed. The tendency of manganese to dissolve into electrolyte during cycling, resulting in poor cycling stability for the cathode, is one of the limits. The most typical cathodes are made of cobalt. Other materials, on the other hand, are being investigated in order to reduce prices and improve battery life.

Due to its low cost, great safety, and high cycle durability, LiFePO4 is a possibility for large-scale production of lithium-ion batteries, such as those used in electric vehicles, as of 2017.Some of the most common Cathode materials are mentioned below:-

- Lithium Nickel Manganese Cobalt oxides ("NMC" , $LiNi_xMn_yCo_zO_2$ )
- Lithium Nickel Cobalt Aluminium Oxides ( "NCA", $LiNiCoAlO_2$)
- Lithium Manganese Oxide ("LMO", $LiMn_2O_4$)
- Lithium Iron Phosphate ("LFP", $LiFePO_4$)
- Lithium Cobalt Oxide ($LiCoO_2$, "LCO")

## 2.2.4 Anode Materials

Graphite and other carbon compounds have traditionally been used to make negative electrode materials. These materials were chosen because they are plentiful, electrically conductive, and can intercalate lithium ions to retain electrical charge with minimal volume expansion.. Some of the materials that can be used as Anode are mentioned below:-

- Graphite
- Lithium Titanate
- Hard Carbon
- Tin/Cobalt Alloy
- Silicon / Carbon

## 2.2.5  Separator

The separator is the next component to consider within the lithium-ion cell. The anode and cathode are separated by a separator, which is usually made of plastic or ceramic. The

separator material must be able to tolerate the corrosive hydrocarbon (HC)-based electrolytes used in lithium-ion cells while also preserving the isolation of the two electrodes within the cell when in use. The separator's principal function is to separate the anode from the cathode. An internal short circuit occurs when the two parts of the electrode come into touch, resulting in cell failure. As a result, the separator is critical in any lithium-ion cell design.

Some cells employ polypropylene or polyethylene plastic to partition the anode and cathode. They prevent short-circuiting while still allowing lithium ions to travel from the anode to the cathode. Many cell manufacturers employ a trilayer PP/PE/PP structure to allow the middle layer to melt at greater temperatures while maintaining cathode and anode separation. PE melts at 135 degrees Fahrenheit, while PP melts at 155 degrees Fahrenheit. Because the pores of PP begin to melt at high temperatures, the flow of lithium-ion cells is impeded.

Some manufacturers are using ceramic layered separators in their cells because they can withstand higher temperatures and so boost the cell's safety.

Table 2 below summarizes performance characteristics of some of the most common lithium-ion chemistries that are in use today, including nickel manganese cobalt (NMC), nickel cobalt aluminum (NCA), lithium iron phosphate (LFP), lithium titanate (LTO), lithium manganese oxide (LMO), and lithium cobalt oxide (LCO).

| | Lithium Iron Phosphate | Lithium Manganese Oxide | Lithium Titanate | Lithium Cobalt Oxide | Lithium Nickel Cobalt Aluminum | Lithium Nickel Manganese Cobalt |
|---|---|---|---|---|---|---|
| Cathode chemistry descriptor | LFP | LMO | LTO | LCO | NCA | NMC |
| Specific energy (Wh/kg) | 80–130 | 105–120 | 70 | 120–150 | 80–220 | 140–180 |
| Energy density (Wh/L) | 220–250 | 250–265 | 130 | 250–450 | 210–600 | 325 |
| Specific power (W/kg) | 1400–2400 | 1000 | 750 | 600 | 1500–1900 | 500–3000 |
| Power density (W/L) | 4500 | 2000 | 1400 | 1200–3000 | 4000–5000 | 6500 |
| Volts (per cell) (V) | 3.2–3.3 | 3.8 | 2.2–2.3 | 3.6–3.8 | 3.6 | 3.6–3.7 |
| Cycle life | 1000–2000 | >500 | >4000 | >700 | >1000 | 1000–4000 |
| Self-discharge (% per month) | <1% | 5% | 2–10% | 1–5% | 2–10% | 1% |
| Cost (per kWh) | $400–$1200 | $400–$900 | $600–$2000 | $250–$450 | $600–$1000 | $500–$900 |
| Operating temperature range (°C) | –20 to +60 | –20 to +60 | –40 to +55 | –20 to +60 | –20 to +60 | –20 to +55 |

*Table 2 Lithium-Ion Chemistries comparison*

## 2.2.6 Types Of Lithium Ion Cell Forms

There are essentially three main types of lithium-ion cell form factors:

- Small cylindrical,
- Large prismatic,
- Pouch (or polymer) cells.

The 18650 cylindrical cell is the most common lithium-ion cell format today, with about 660 million cells made each year. The 18650 designation denotes a cell with a diameter of 18 mm and a length of 65 mm. Except for Tesla which uses high volume 18650 cells, nearly all major automakers have recognized "small" cylindrical cells as being mostly suitable for HEV-type power uses in vehicle applications. The majority of auto manufacturers, on the other hand, use huge rectangular or cylindrical prismatic cells or flat "pouch"-type cells for plug-in hybrid electric vehicle (PHEV) and battery electric vehicle (BEV) applications. The fundamental reason for this is that a high number of cells are required to achieve the requisite voltage and energy, which implies that there are much more connections with small cells than with bigger cells, and hence many more possible failure locations in small cell assemblies.
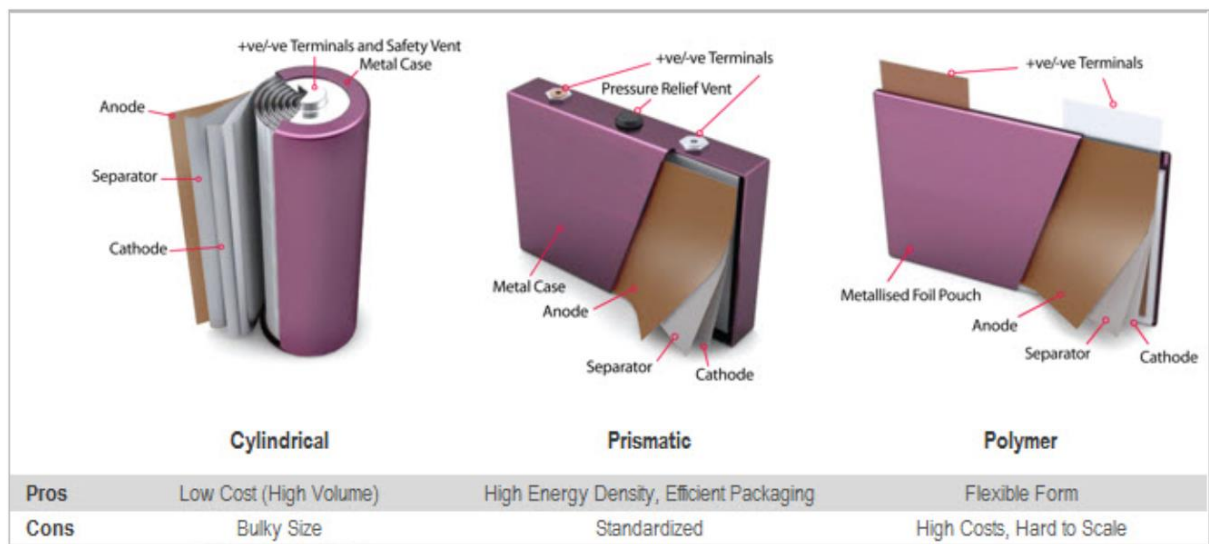


*Figure 3 Cylindrical, Prismatic and Polymer type of lithium-ion cell*

## 2.3  Battery Characteristics

### 2.3.1 OCV – Open Circuit Voltage

When no external load is attached, Battery OCV refers to the potential difference between the positive and negative electrodes. As a result, the battery receives no external current. After the open circuit is made in the discharging/charging operation, the battery OCV can go up/down quickly.

### 2.3.2 Terminal Voltage

When a load is applied, the voltage between the battery terminals is called terminal voltage.The cell terminal voltage Vt deviates from its equilibrium state voltage Veq when current runs through it; this deviation is known as polarization voltage or overvoltage. Three key components make up the polarization voltage:

• The resistances in the bulk of the electrolyte, separators, electrodes, current collectors, and other connectors generate an ohmic overvoltage drop.

• Activation overvoltage, commonly known as "electrode losses," is connected to charge transport at each electrode/ electrolyte interface.

• Overvoltage concentration linked to the depletion or accumulation of active materials near the electrode surface.

In practical batteries, cell voltage for discharging can be expressed as

$$V_t^{dis} = E_{eq} - \eta^{dis} \qquad\qquad \textit{Equation 3}$$

while cell voltage undergoing charging

$$V_t^{cha} = E_{eq} + \eta^{cha} \qquad\qquad \textit{Equation 4}$$

where $\eta^{dis}$ and $\eta^{cha}$ represent the polarization voltages for charging and discharging processes, respectively.

### 2.3.3 Cut off voltage

Many battery types, including lead-acid batteries, cannot be depleted below a certain level without causing irreparable harm to the battery. This level is known as the "cut-off voltage," and it is determined by the battery's type, temperature, and discharge rate.

### 2.3.4 Internal Resistance

The resistance within a battery, which is normally varied for charging and discharging, is also affected by the state of charge of the battery. The battery efficiency falls as the internal

resistance rises, and thermal stability suffers as more of the charging energy is transferred to heat.

### 2.3.5 Battery Capacity

The mass of active elements present in the battery determines "battery capacity," which is a measure (usually in Amp-hr) of charge held by the battery. The capacity of a battery refers to the maximum amount of energy that may be extracted from it under specific conditions. However, the battery's real energy storage capacities may differ greatly from its "nominal" quoted capacity, as battery capacity is highly dependent on the battery's age and history, charging and discharging regimens, and temperature. A battery's capacity is measured in 'Ampere Hours.' The ampere-hour of a battery is the number of hours the battery can deliver a current equal to the discharge rate at the battery's rated voltage.

## 2.3.6 Energy Capacity

The total Watt-hours available when the battery is discharged at a specific discharge current (given as a C-rate) from 100 percent state-of-charge to cut-off voltage is the "energy capacity" of the battery. Multiplying the discharge power (in Watts) by the discharge time yields energy (in hours). Energy, like capacity, diminishes when the C-rate rises.

## 2.3.7 Battery charge and discharge rate

The charge and discharge rates of the battery are defined by the battery C rates. The rate at which a battery is depleted in relation to its maximum capacity is measured by its C rating. A 1C rate, for example, signifies that the discharge current completely discharges the battery in 1 hour. As a result, a battery with a capacity of 100Ah may deliver 100 Amps for one hour.

## 2.3.8 State of Charge
## 2.3.9 Depth of Discharge

The percentage of battery capacity that is been discharged is expressed as the percentage of maximum capacity. A discharge to at least 80% DOD is referred to as a deep discharge.

## 2.3.10 Battery Efficiency

Efficiency is a key factor in secondary battery systems, since it refers to how well a battery can transfer energy from one form to another, usually including changes in electrical and chemical energy. The secondary battery is often measured using voltage efficiency (VE), Coulomb efficiency (CE), and energy efficiency (EE). The CE of a battery is the ratio of charge and

discharge capacity (Qdischarge/Qcharge) within a particular voltage window. The voltage differential between charge and discharge operations involving internal resistance and other polarizations determines VE. EE is the product of CE and VE (EE = CE VE). Inefficiencies are influenced by a variety of parameters, including current density, temperature, membrane/separator choices, and electrolyte conductivity.

## 2.4 Battery Pack Design

A lithium-ion battery pack is a collection of interconnected subsystems that work together to keep the battery healthy and well. The lithium-ion batteries are the heart of the pack, and the number of them varies depending on the application. To achieve the desired voltage and energy, the cells can be connected in a variety of ways.

## 2.5 Series Cell Connection

When we connect a group of cells in series, we must connect the cell's negative terminal to the positive terminal of the other cell until all the cells are connected. Hence, the positive terminal of the first cell and the negative terminal of the last cell is our cell pack's main positive and negative terminal. This configuration is used to increase the overall voltage of the pack. This does' t increase the capacity of the pack.
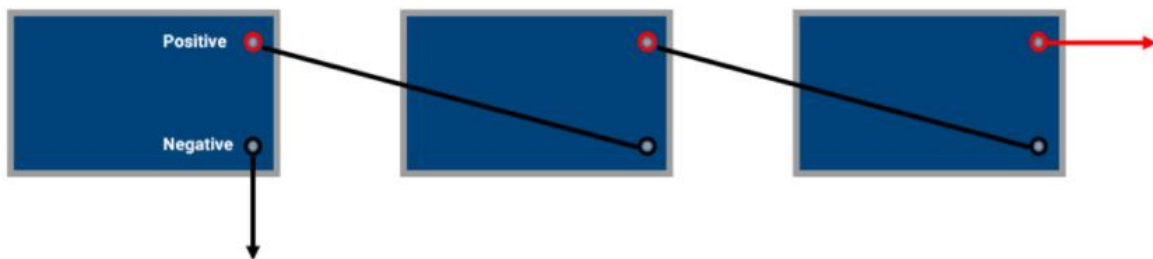
Hence a battery configuration of 4s means that 4 cells are connected in series . If one cell voltage is 3.6V , we can calculate the total voltage of the pack in the following way:-

Battery configuration = ns

Where 'n' is the number of cells in series, hence

Total voltage = n . V    ( volts)

where V is the nominal voltage of the cell. So for a 4s configuration we will get 14.4V .



*Figure 4 Cell Series connection*

## 2.5.1 Parallel Cell Connection

When we connect a group of cells in parallel , we must connect the negative terminal of the cell to the negative terminal of the other and so on through the string of batteries, and we have to do the same with the positive terminal. This configuration increases the amp-hour capacity, but the voltage remains the same.

Hence battery configuration of 4p means that 4 cells are connected in parallel . And total capacity is 4 times the cell capacity. Suppose we have a cell with capacity = 3 Ah

Battery configuration = mp

Where 'm' is number of cells connected in parallel, hence

Total capacity = m . Ah   ( Ah)

Therefore for a 4p configuration, we will have a cell pack 12 Ah capacity.



*Figure 5 Cell Parallel connection*

We can make a combination of series and parallel connections to get the desired voltage and capacity. For example we have a cell of 3.6 V and 3Ah capacity used in 4s4p configuration . Therefore we have a cell pack of -

Cell pack voltage = 4 . 3.6 = 14.4 V

Cell pack capacity = 4 . 3 = 12 Ah

## 2.5.2 Cell Holder

A cell holder is either a separate plastic holder mounted using screws, glue, eyelets, double-sided tapes, or other ways, or a plastic case with the shape of the housing moulded as a compartment or compartments that take the battery or batteries. The battery holders may have a lid to keep the batteries in place and protect them, or they may be sealed to keep the batteries from leaking and causing harm to the electronics and components. For lithium-ion applications,

the cell holder material is essential as it must hold and protect the cells simultaneously. Below are some qualities that a cell holder material must have –

- High dielectric strength
- High melting point
- Compatible with Immersive cooling fluid
- High stiffness
- High dimensional stability
- High machinability
- High availability
- Low price
- Low density

Thermoplastics are the best material for cell holders as they are dielectric and also are able to handle higher temperatures. Some of the thermoplastics that are used in the industry are mentioned below.

| Polymer type | Abbreviation | Tradenames |
|---|---|---|
| Polytetrafluoroethylene | PTFE | Teflon, Hostaflon, Fluon |
| Ethylene tetrafluoroethylene | ETFE | Tefzel |
| Polychlorotrifluororethylene | PCTFE | Kel-F, Aclon |
| Perfluoroalkoxy | PFA | Teflon |
| Polyoxymethylene acetal copolymer | POM | Kemetal, Delrin, Ultraform |
| Ultrahigh molecular weight polyethylene | UHMWPE | Hostalen |

*Table 3 List of thermoplastics*

| Polymer | Advantages | Disadvantages |
|---|---|---|
| PTFE | Outstanding chemical resistance, Low friction , High operational Tmax | Low stiffness , strength and hardness |
| ETFE | Good creep . tensile and wear properties. | Expensive , Attacked by esters , aromatics |
| PCTFE | Stiffer than PTFE | Very expensive , Attacked by – Esters , ethers and halogenated hydrocarbons. |
| PFA | Highest Tmax of fluoroplastics | Very expensive , Low stiffness, strength and hardness |

| POM | Tough and stiff . Good abrasion , creep and chemical resistance . | Attacked by acid and alkalis |
|---|---|---|
| UHMWPE | Good abrasion and chemical resistance | Low Tmax |

*Table 4 Comparison of thermoplastics*

## 2.5.3 Battery Enclosure

Enclosures for modules and packs can be made of plastics, steel, aluminum, fiberglass, or composite materials. In almost every scenario, we'll employ a combination of these materials in our battery design. Metals that can be used for enclosure:-

**Steel** – Steel has a number of advantages, including high strength and inexpensive cost. A steel enclosure, on the other hand, must typically have some weldments or other mounting attachments, as well as mounting structures and durability. This lengthens the material's processing time and raises its cost. Multiple firms are currently attempting to improve the strength of steel while also reducing its weight and mass to make it more competitive with low-weight aluminum applications.

**Aluminium** - Enclosures made from aluminum might be stamped, die-cast, or machined blocks. Aluminum is lighter than steel, but it demands more material thickness to meet strength requirements, particularly in pressed items. Die casting is another way that can be utilized to work with aluminum. This can be accomplished by either high-pressure die casting (HPDC), which provides the best strength, porosity, and surface quality but is difficult to tool. Sand casting is less expensive to tool, but the component quality is sometimes poor, necessitating additional finishing operations. Plaster casting combines the best of both worlds: it is relatively inexpensive to tool and produces finishes that are nearly as good as HPDC. The porosity of the flow, which can cause weak places in the final result, is one of the most difficult aspects of plaster casting. If our item isn't too complicated, we can machine our case from an aluminum block using CNC.

**Use of Plastic as Enclosure :-**

Plastic enclosures may be used in some smaller battery systems. If the battery does not have large structural demands, these systems are more likely to employ plastic. The enclosure merely needs to surround and protect the lithium-ion cells in some hybrid and stop-start-type automobile batteries with minimal structural demands. Plastics and polymers are used in a

variety of applications, from internal to even enormous battery packs. A composite cover may be used in conjunction with a metal foundation for some of the bigger automobile ESSs. The Chevrolet Volt, for example, is built of a sheet moulded composite made of a lightweight vinyl ester resin with haydite nanoclay filler and 40% glass fibres. In layman's terms, the Chevrolet Volt's cover is composed of fibreglass. The Volt and its sister car, the Ampera, use lithium-ion pouch-type cells, which are separated by a plastic "end" and "repeating frames" in their systems. These are injection-molded plastic components produced from BASF's nylon 6/6 grade and Ultramid 1503-2F NAT, a 33 percent glass-filled, hydrolysis-stabilized material. Another issue involving plastics and polymers is their flame retardant ratings. V stands for vertical flame rating, and the flame retarding ratings vary from V0 to V2. We must utilize non-flammable polymers in our battery cases.

## 2.6  Thermal issues in Lithium-Ion Batteries

The high power density of lithium-ion batteries can be a disadvantage because it causes the batteries to lose heat during the energy conversion process. In batteries, heat is generated from three basic sources, namely: [1]

(1) activation losses due to interfacial kinetics

(2) concentration losses due to transport of species,

(3) joule heating movement of charged particles causing ohmic losses.

To extract the best possible performance from the cells, they have to be operated within the optimum temperature range. This effect was studied by Khateed et al., who concluded from their research in [2] that "the electrochemical performance of the Li-ion battery chemistry, charge acceptance, power and energy capability, the operating temperature very much controls cycle life and cost". According to [3], the preferred temperature range providing maximum power capability and acceptable thermal aging is between 20°C and 40°C for Li-ion cells and the temperatures must be limited to a certain value between 50 °C and 60 °C to maintain the cell in a safe temperature zone and prevent accelerated ageing. Temperature non-uniformity that develops in battery packs as they age is another crucial factor that must be considered. Thermal imbalance in cells has a substantial impact on battery system performance. The Arrhenius equation states that as cell temperature rises, the battery reaction expands exponentially, leading cells at higher temperatures to degrade more quickly than those at lower temperatures. The lifespan of the entire battery pack is reduced as a result of this degradation.

In the operating temperature range of 30 - 40 °C, each degree of temperature rise reduces the Li-ion cell's lifespan by around two months. As a result, a management system must adjust for the heat imbalance in cells in order to extend the battery's life. The thermal issues affecting lithium-ion batteries discussed above bring to light the significant safety concerns that need to be accounted for while implementing lithium-ion batteries. It can thus be concluded that "effective heat dissipation and thermal runaway are the major concerns in the commercialization of lithium-ion batteries for high power applications. As a result, an efficient thermal management system is essential to maximize the battery pack's performance by:

(1) keeping the battery temperature within the operational range

(2) Improving battery pack temperature uniformity.

A thermal management system would ensure that cell temperatures remained within the operational range, allowing for appropriate power output while maintaining temperature stability.

## 2.7 Temperature effects on Battery Characteristics

- **Effects of heat**

The chemical reactions that take place inside a battery are affected by rising temperatures. The chemical reactions inside the battery speed up as the battery's temperature rises. Higher temperatures have a number of consequences for lithium-ion batteries, including improved performance and storage capacity. According to a Scientific Reports research institute study, increasing the temperature from 25 to 45 degrees Celsius increased maximum storage capacity by 20%. However, there is a drawback to this increased performance: the battery's lifecycle shortens over time. According to the same study, lifespan degradation was substantially more pronounced at higher temperatures when the battery was charged at 45 degrees versus 25 degrees. At 25 degrees, battery performance dropped by only 3.3 percent for the first 200 cycles; at 45 degrees, performance degraded by 6.7 percent. That's a more than twofold increase in deterioration. Due to greater degradation at higher temperatures, battery lifecycles can be substantially shortened when exposed to excessive heat on a regular basis. While heat exposure boosts battery capacity briefly, the damage it causes to the lifetime might cause long-term issues, so extended heat exposure should be avoided.
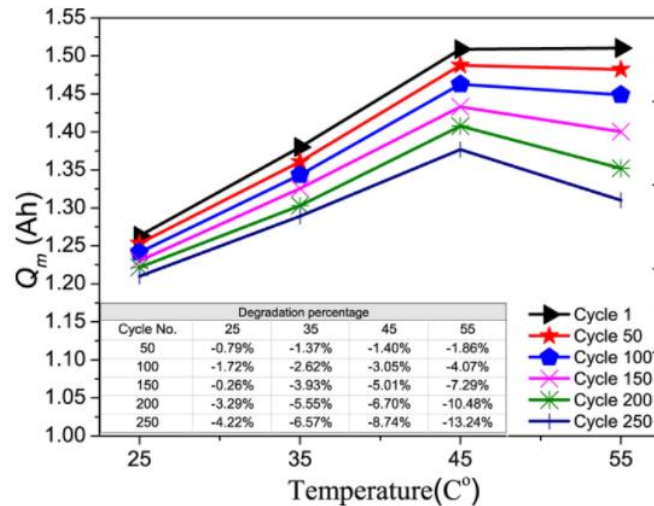
**Degradation percentage**

| Cycle No. | 25 | 35 | 45 | 55 |
|---|---|---|---|---|
| 50 | -0.79% | -1.37% | -1.40% | -1.86% |
| 100 | -1.72% | -2.62% | -3.05% | -4.07% |
| 150 | -0.26% | -3.93% | -5.01% | -7.29% |
| 200 | -3.29% | -5.55% | -6.70% | -10.48% |
| 250 | -4.22% | -6.57% | -8.74% | -13.24% |

*Figure 6 Degradation percentage at different cycles and temperatures*

- **Effects of Cold**

  Long-term exposure to cold temperatures has an adverse effect on battery performance and safety. When the temperature drops, the battery's internal resistance rises. This means that charging the battery involves more work, reducing the capacity. However, it's crucial to remember that capacity loss is influenced by charge and discharge rates, and the impact of cold weather varies depending on the chemistry of the battery. At -17° C, a lead-acid battery might only offer half of its nominal capacity.

  The operating temperatures of the batteries fluctuate depending on the sort of battery we're using. Lithium-ion batteries, for example, may be charged and discharged at temperatures ranging from 0 to 45 degrees Celsius (however, if you operate at such high-temperature levels you do run into problems mentioned earlier). Lead-acid batteries, on the other hand, may be charged and discharged at temperatures ranging from -20°C to 50°C. It's critical to understand what charging temperatures a battery can handle. Because ion combinations are slow, charge uptake reduces if batteries do not run at the acceptable temperature. Furthermore, applying a high current can cause pressure to build up inside sealed batteries, resulting in explosions. The following chapter addresses the many types of thermal management strategies, such as active cooling and passive cooling, and gives a detailed literature study on them.
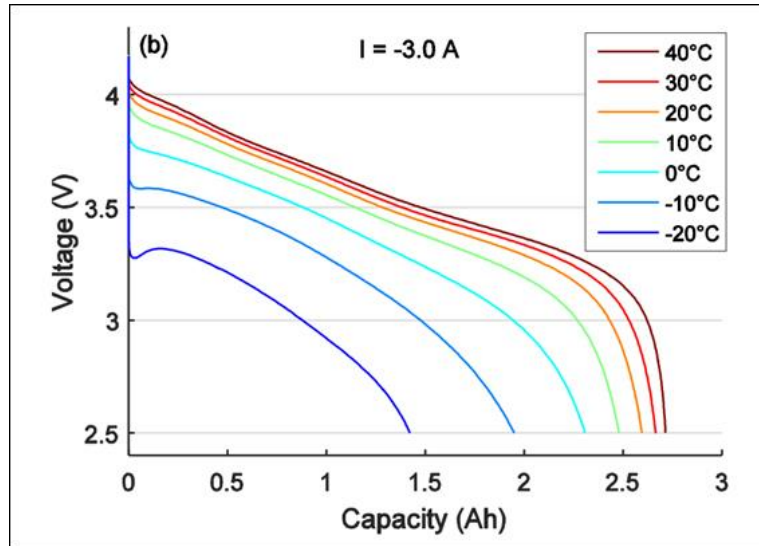
*Figure 7 Discharge curve at different temperatures*

## 2.8 Thermal Management Systems

The basic goal of a thermal management system (abbreviated as TMS in this text) is to keep temperatures within the required operating range by regulating temperatures uniformly inside a battery pack. The features of a thermal management system found in battery packs should normally include the following.

1. Favourable environment for all the cells to operate within the optimum temperature range in order to optimize the battery performance and life
2. It should work towards reducing the temperature non-uniformity amongst the different cells in order to minimize the electrical imbalance

As a result, a temperature management system within Li-ion battery packs must be efficiently designed and executed. Many aspects influence the design of an effective TMS, including the heat generation rate of the cells, energy efficiency, and temperature-dependent performance sensitivity. The choice of heat transfer medium is also influenced by the TMS design, which is intrinsically reliant on the type of management system. As a result, the various types of thermal management systems can be categorised as follows:

1. Active cooling TMS, wherein a built-in source provides the heating at cold temperatures and cooling at hot temperatures respectively

2. Passive cooling TMS, a system in which the ambient environment surrounding the batteries is used

Thermal management can be accomplished by the use of air or liquid systems, thermal storage phase change material, insulation, or a mix of the active and passive methods outlined above.
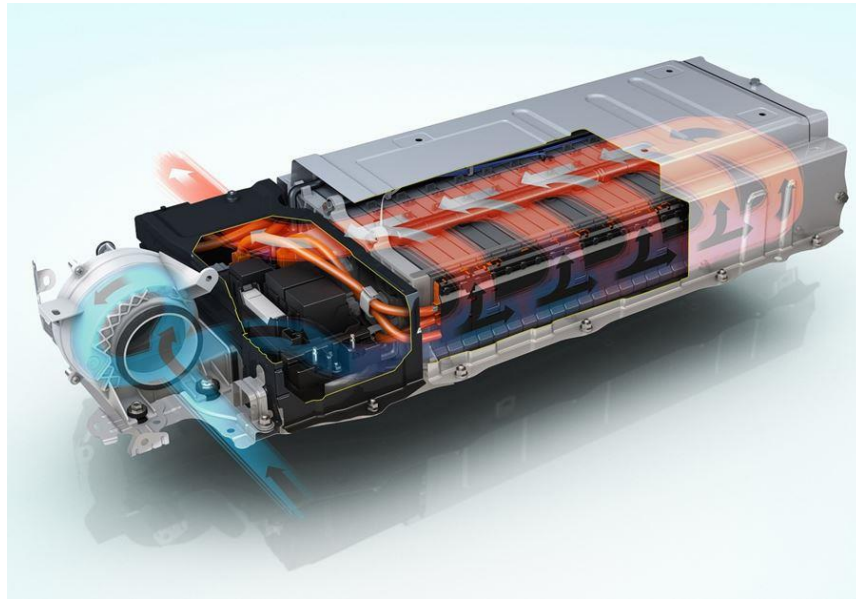
## 2.8.1 Air Cooling And heating

The heat medium in the air system is air. The intake air can come straight from the atmosphere or the cabin, or it can be conditioned after passing through the air conditioner's heater or evaporator. The first is referred to as a passive air system, while the latter is referred to as an active air system. Additional cooling or heating power can be provided through active systems. Active systems have a power limit of 1 kW, however passive systems can offer hundreds of watts of cooling or heating power. [4] Both are referred to as forced ventilation systems since air is delivered by blowers in both circumstances. The schematic diagram of the system is shown in the following figure.
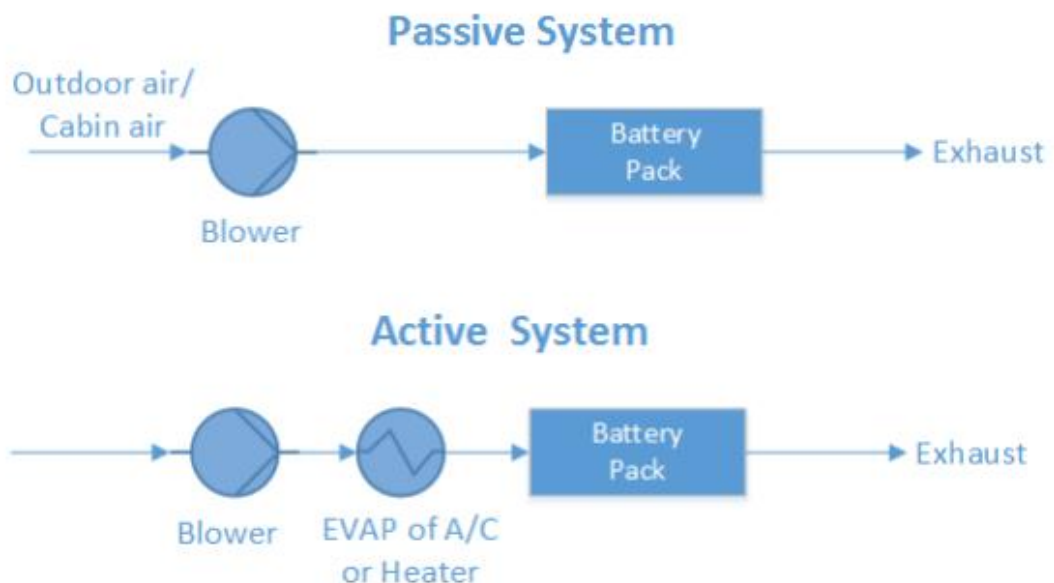


*Figure 8 Schematic of active and passive cooling system*

The battery system in cars like the Toyota Prius and Nissan Leaf is air cooled. However, even with high-powered blowers, air cannot transmit as much heat as a liquid system.

This causes issues in electric vehicles in hot areas, such as increased temperature variation in battery pack cells. Noise from the blower can also be an issue.



*Figure 9 Toyota Prius battery cooling system*

## 2.8.2 Liquid Cooling and Heating

Liquid, in addition to air, is a heat transfer fluid that is utilized for heat transfer. There are two types of liquids that are appropriate for thermal management systems in general. One is a dielectric liquid, like mineral oil, that can come into direct contact with the battery (direct contact liquid). The other is a conductive liquid, such as a combination of ethylene glycol and water, that can only make indirect contact with the cell (indirect contact with the liquid). Different designs are developed for different liquids. The common arrangement for direct contact with liquids is to submerge the module in mineral oil. A sheath around the battery modules, individual tubes around each module, mounting the battery modules on a cooling/heating plate, or integrating the battery modules with plates and cooling/heating fins are all conceivable configurations for indirect contact with liquid. In both of these groups, the indirect contact system is the preferred method of achieving better separation between the battery module and the environment, resulting in improved safety. The liquid system can be classified as either a passive or active system, depending on the radiator used for cooling. In passive liquid systems, the radiator used for cooling is the radiator. The system has no heating capacity. Figure 3.3 shows the system schematic of the passive liquid system. The heat transfer fluid circulates in the recirculating pump. The heat from the battery pack is absorbed by the circulating fluid and released through the radiator. The temperature

difference between the ambient air and the coil has a significant impact on cooling capacity. The fan behind the radiator can help with heat dissipation, but the passive liquid system will fail if the ambient air temperature is higher than the battery temperature or the gap between the two is too small.
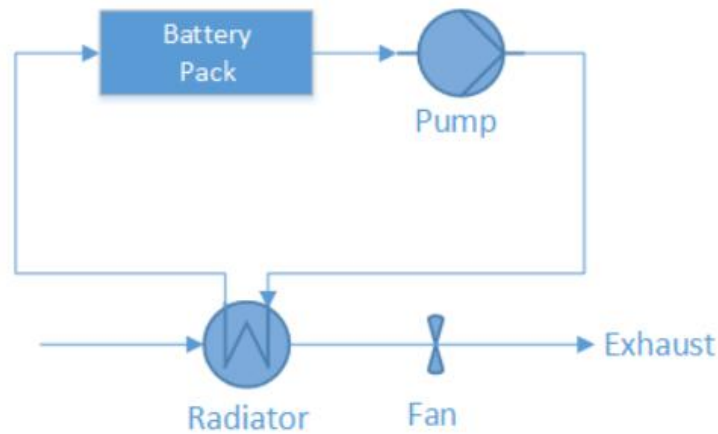


*Figure 10 Schematic of liwuid cooling system*

Figure 11 shows the systematic scheme of an active liquid system. There are two loops in total. The upper loop is referred to as the primary loop, while the lower loop is referred to as the secondary loop. The primary loop is comparable to the loop in a passive liquid system, where a pump circulates the heat transfer fluid. The air conditioning loop (A/C loop) is the secondary loop. Instead of being a radiator, the upper heat exchanger serves as an evaporator (EVAP) for cooling and connects both loops. During heating, a four-way valve is switched, and the upper heat exchanger functions as a condenser (COND) and the lower heat exchanger functions as an evaporator. The heat pump loop is another name for the heating operation loop.
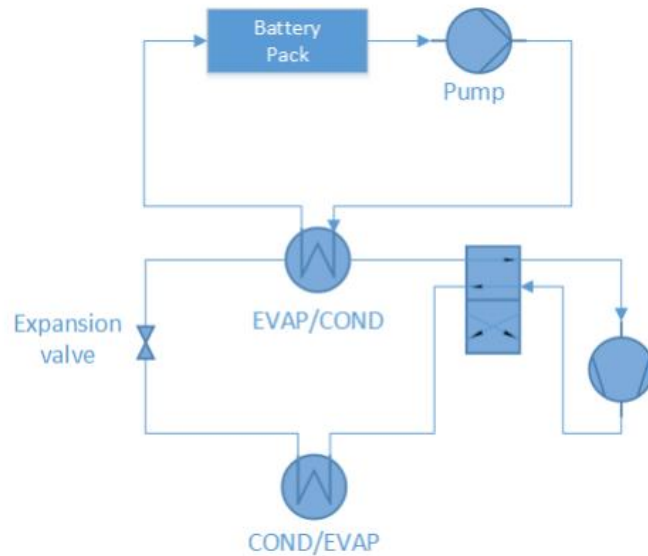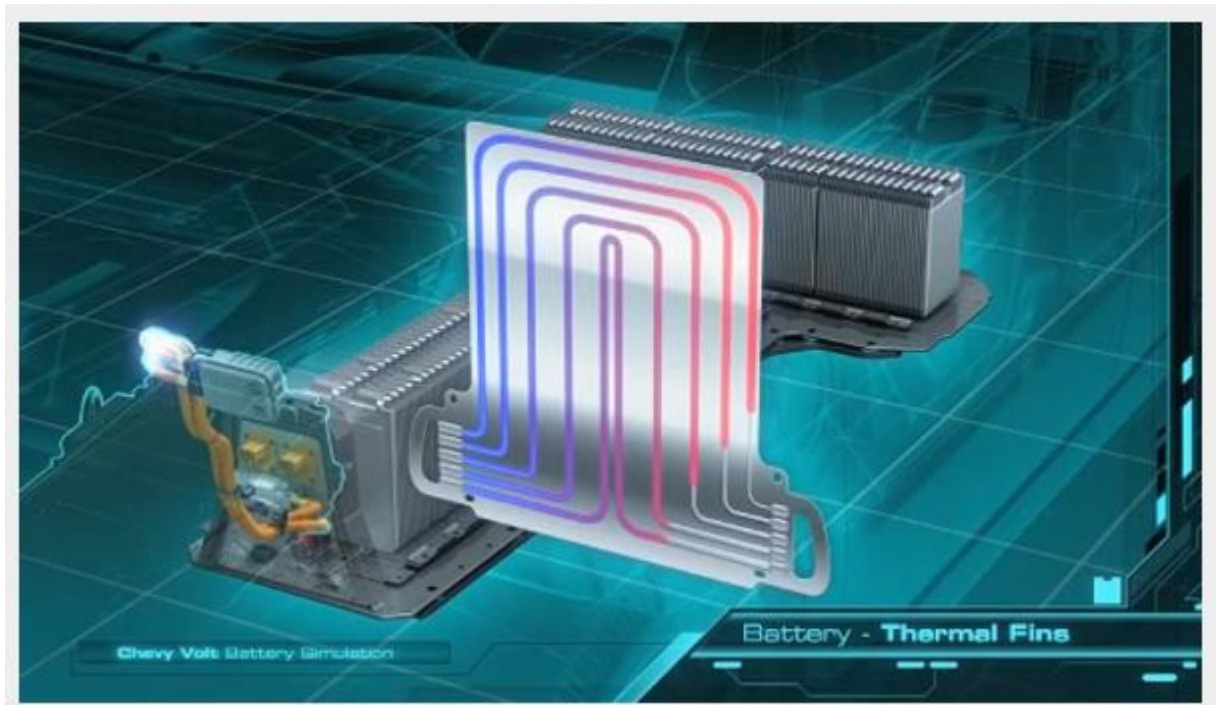
*Figure 11 Active Liquid Cooling system*

Liquid glycol is used as a coolant in Tesla's (and GM's) thermal management systems. Both the GM and Tesla systems use a refrigeration cycle to transfer heat. To keep the cells cold, a glycol coolant is circulated throughout the battery pack. This is a challenging task given Tesla's 7,000 cells to cool.
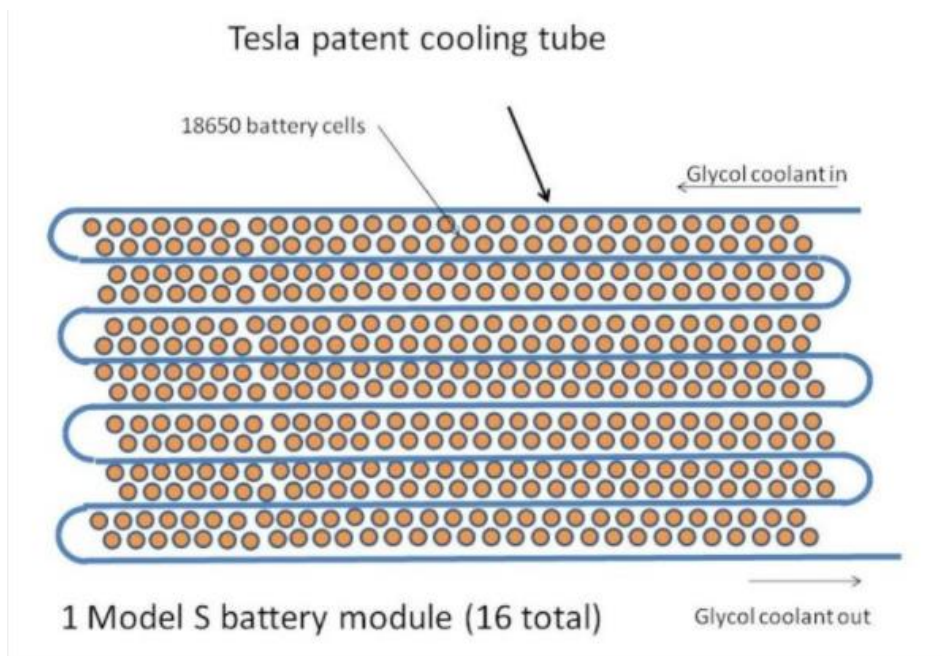


*Figure 12 Tesla cooling system of one module*

The Tesla Model S battery cooling system consists of a patented serpentine cooling pipe that winds through the battery pack and carries a flow of water-glycol coolant; thermal contact with the cells is through their sides by thermal transfer material.



*Figure 13 GM Chevrolet Volt cold plates interwoven with battery cells as liquid cooling system*

Koenisegg regera is one of the only commercial vehicle with battery cooled by immersion. Rimac developed immersion cooling technology for Koenisegg.
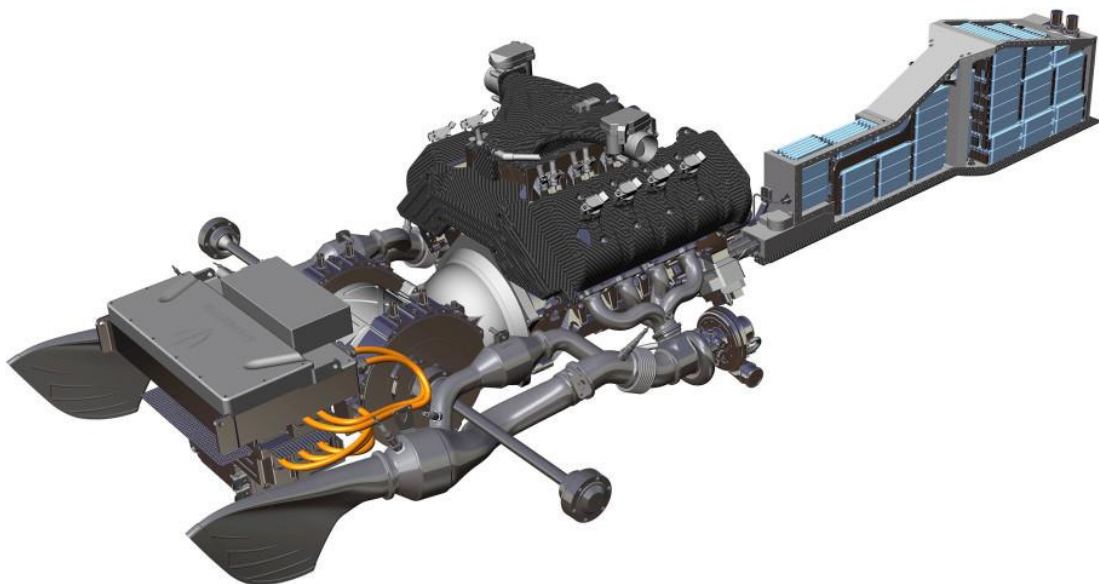


*Figure 14 Koenisegg Regera Battery pack*

## 2.8.2.1　　Types of Dielectric Fluid

There are four primary dielectric fluids - **Error! Reference source not found.**

- **Mineral Oil:** Mineral oil is the most common dielectric fluid encountered by technicians. Because of its long record of dielectric strength and thermal performance, this liquid is a top choice for outdoor transformers. Mineral oil's main problem is that it's a flammable liquid with low biodegradability, which limits its use and storage.

- **Silicone:** Silicone has typically been the insulating fluid of choice when a less flammable liquid is required. It has a relatively high ignition temperature, making it appropriate for usage indoors and in vaulted spaces. Silicone, on the other hand, has a number of drawbacks, including chemical by-products and a high cost of use. It has a similar dielectric strength to mineral oil and a higher specific gravity than mineral oil, however it is not biodegradable.

- **Hydrocarbon:** Fluids containing highly refined petroleum oils have fire-resistant qualities, making them appropriate for use in applications that require a less flammable liquid. These fluids have good insulating and cooling properties, but their ignition point is lower than silicone's, and they are also more expensive than mineral oil. Hydrocarbon fluid is completely biodegradable and has a specific gravity and power factor similar to mineral oil.

- **Natural Ester:** Natural ester fluid is a top choice when it comes to environmental impact because it is made from non-toxic natural oils (such as soy) and is completely biodegradable. They are self-extinguishing and absorb moisture better than other liquids, making them excellent for interior applications. When compared to other fluid types, natural esters have the highest dielectric strength. Natural esters have two primary drawbacks: greater costs and a larger power factor, which can result in higher operating temperatures.

## 2.8.3 Direct Refrigerant Cooling & heating

Similar to active liquid system, a direct refrigerant system (DRS) consists of an A/C loop, but DRS uses refrigerant directly as heat transfer fluid circulating through battery pack. The systematic layout is in Figure 11
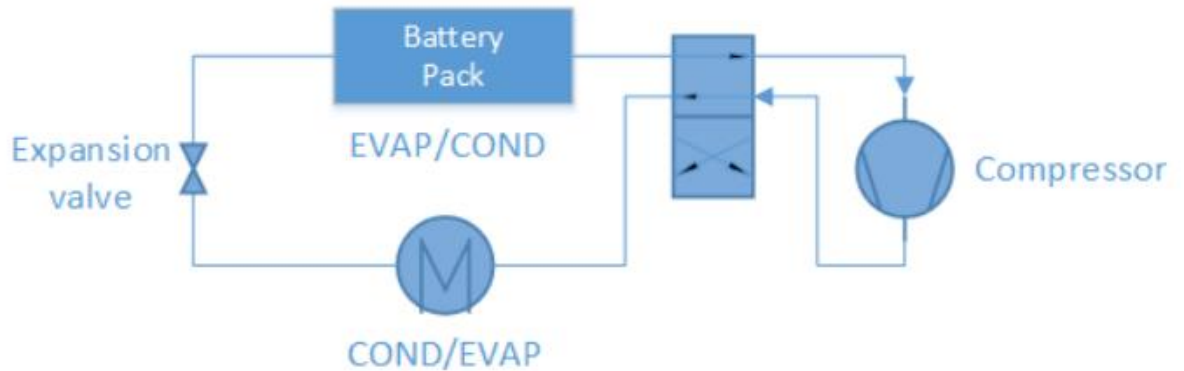


*Figure 15 Schematic of DRS System*

## 2.8.4 Phase Change Material

During melting, heat is absorbed by PCM and stored as latent heat until latent heat is up to the maximum. Temperature is kept at melting point for a period, and temperature increase is delayed. Therefore, PCM is used as a conductor & buffer in battery thermal management systems. Figure 3.6 shows the working mechanism of PCM on battery cells. Also, PCM is always combined with air cooling system or liquid cooling system to manage battery temperature.
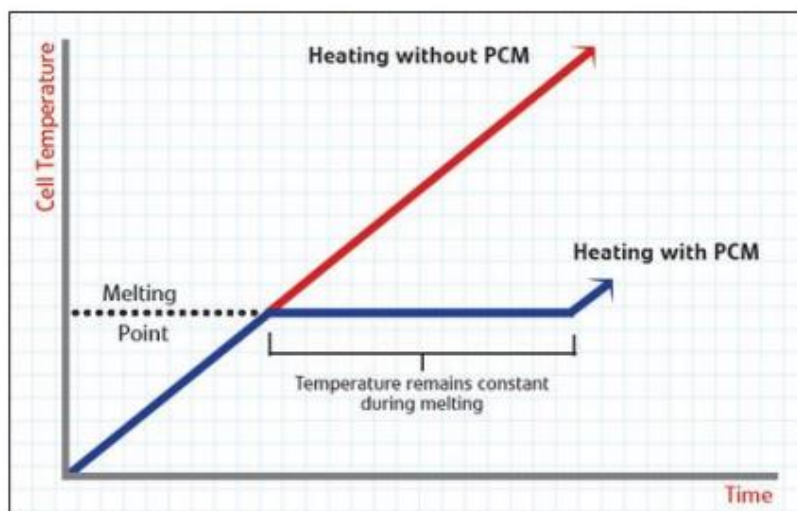


*Figure 16 Graph showing cell temperature with and without PCM material*

## 2.9 Battery Management System

The Battery Management System (BMS), while it may have many other names, is the central control unit of the battery pack. It is essentially (and quite literally) the "brains" of the operation. The BMS is a combination of several component systems, including a host or master controller (a Printed Circuit Board (PCB)), a series of "slave" control boards (depending on system typography), sensors, and software that makes everything work together.

Functions of BMS :-

- Estimating State of charge
- Estimating state of health
- Monitoring cell current, voltage and temperature
- Controlling the battery charging profile
- Isolating the battery pack from source and load
- Limiting power and thermal transient and extremes
- Controlling passive cell balancing


- **Cell Balancing**

  When designing a lithium battery pack with numerous cells in series, it's critical to include electronic components that constantly balance the cell voltages. This is important not just for the battery pack's performance but also for its long life cycles. Lithium cells are susceptible to increased cell breakdown if they are overheated or overcharged. If a lithium-ion battery voltage exceeds 4.2 V by even a few hundred millivolts, they can catch fire or explode due to a thermal runaway condition. When the cells are fully charged, cell balancing is the act of balancing the voltages and states of charge among them. There are no two cells that are alike. The condition of charge, self-discharge rate, capacity, impedance, and temperature properties are always somewhat different. Even if the cells are the exact model, manufacturer, and production lot, this is true. Although manufacturers sort cells by similar voltage to match them as closely as possible, there are still minor differences in the impedance, capacity, and self-discharge rate of individual cells that can eventually lead to a voltage divergence over time.

  For most traditional battery chargers to identify full charge, the voltage of the entire string of cells must reach the voltage regulation point. Individual cell voltages can vary as long as the overvoltage protection limitations are not exceeded. At full charge termination, however, weak cells (those with lesser capacity / higher internal

impedance) tend to show higher voltage than the remainder of the series cells. Continuous overcharge cycles then deteriorate these cells even more. The weaker cells' greater voltage upon charge completion accelerates capacity decline. If the maximum suggested charging voltage is exceeded by even ten percent, the degradation rate will rise by thirty percent.

## 2.9.1 Cell Balancing Techniques

When the cells are fully charged, the fundamental solution of cell balancing equalizes the voltage and state of charge among them. Cell balancing is usually classified into two types:

• Passive

• Active

**Passive Cell Balancing**

The approach of passive cell balancing is simple and uncomplicated. It uses a dissipative bypass route to discharge the cells. This bypass can be built into the integrated circuit or external to it (IC). In the case of a low-cost system, such an approach is advantageous. Because all of the surplus energy from a higher energy cell is wasted as heat, the passive technique is less ideal to utilize during discharge due to the apparent influence on battery run time..

**Active Cell Balancing**

Charge is transferred between battery cells using capacitive or inductive charge shuttling in active cell balancing. Because energy is supplied to where it is needed rather than being drained off, it is substantially more efficient. Of course, the requirement for additional components at a higher cost comes as a trade-off for the increased efficiency.

For low voltage battery like 12V,there are mainly two types of BMS that exist according to types of ports , common port and separate port circuit diagram of which is shown below.

BMS common / separate charge and discharge port
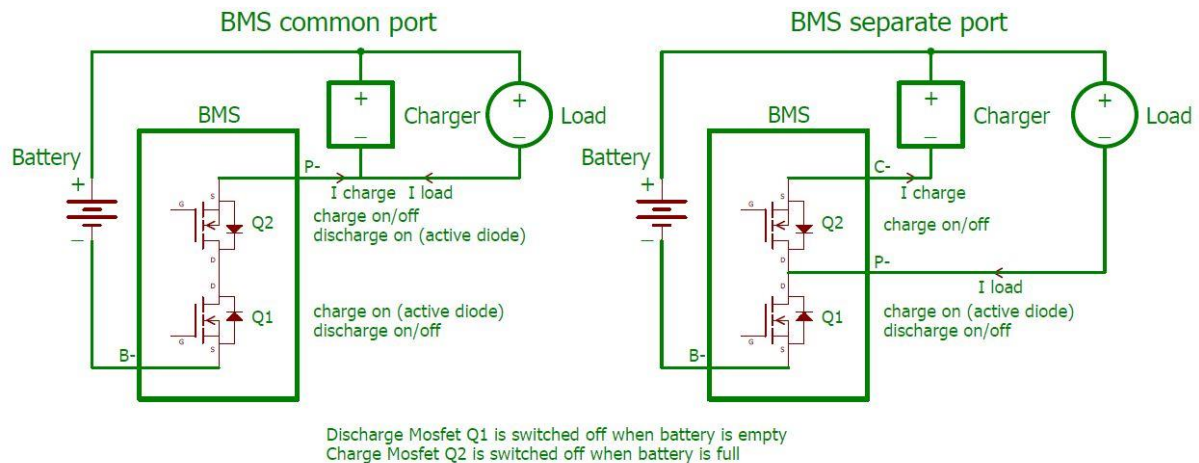


*Figure 17 Circuit diagram of common and separate port BMS*

### Separate Port

Separate ports BMS configuration has 2 advantages :

• Because the discharge current does not flow through charge Mosfet Q2, there is less loss.

• Charge Mosfet Q2 can be smaller than discharge Mosfet Q1.

Mosfets are turned on & off as follows:

Discharging

• Discharge Mosfet Q1 is on & switched off when the battery is depleted.
• Charge Mosfet Q2 is on and inactive diode mode

Charging

• Discharge Mosfet Q1 is on and inactive diode mode
• Charge Mosfet Q2 is on and switched off when the battery is full

### Common Port

Current direction detection is required by a common port BMS. Using a common port BMS to control MOSFETs is more difficult than using a separate port BMS. There are two scenarios when the battery voltage is at its lowest:

1. When charging, Q1 and Q2 must be on
2. Discharging is not allowed, Q1 must be off

As a result, Q1 is only active during charging, requiring the addition of a charge current sensing circuit. There is no need for a charge current detecting circuit in a separate port BMS. There are two scenarios when the battery voltage is at its maximum:

1. When discharging, Q1 and Q2 must be on
2. Charging is not allowed, Q2 must be off

As a result, Q2 is only active when discharging, necessitating the addition of a discharge current detecting circuit.According to its structure, the BMS for high voltage battery packs can be split into four groups.

- **Centralized**

  A centralized BMS (Figure 18) consists of a single assembly from which a bundle of wires (N + 1 wires for N cells in series) is sent to the cells.
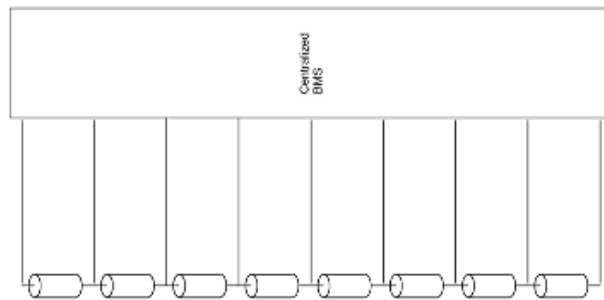


*Figure 18 Scehmatic of Centralized BMS*

- **Modular**
  A modular BMS (Figure 19) is similar to a centralized BMS, except that it is separated into many, identical modules, each with its own bundle of wires connected to one of the pack's batteries. One of the modules is usually labeled as a master because it is the one that administers the entire pack and communicates with the rest of the system, while the others serve as basic remote measuring stations. A communication link transfers the readings from the other modules to the master module.
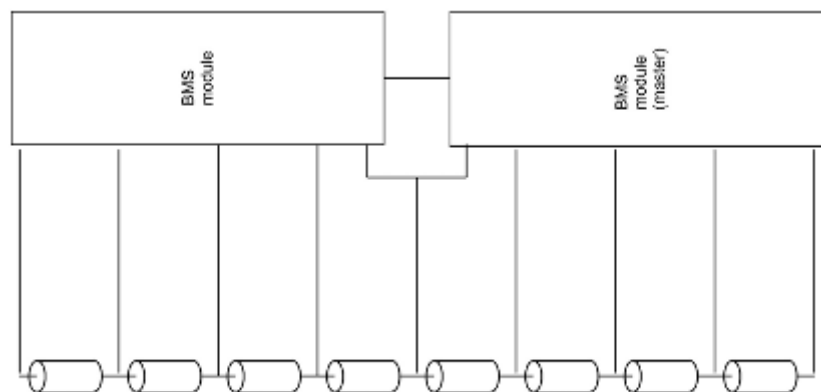


*Figure 19 Modular BMS*

- Master Slave
  In the same way as a modular system uses numerous identical modules (slaves), each sensing the voltage of a few cells, a master-slave BMS does. The master, on the other

and, is distinct from the modules since it does not measure voltages and instead focuses on computation and communication.
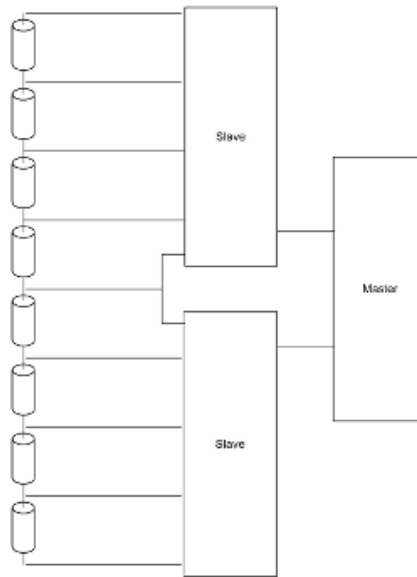


*Figure 20 Topology showing master and slave BMS*

- **Distributed**
  A distributed BMS differs from other topologies in a number of ways (in which the electronics are grouped and housed separately from the cells). The electronics of a distributed BMS are contained on cell boards that are physically attached to the cells being measured. A distributed BMS employs only a few communication lines between the cellboards and the BMS controller, rather than many tap cables between cells and electronics. The computation and communication are handled by the BMS controller (a BMS controller is not required in some simpler implementations).
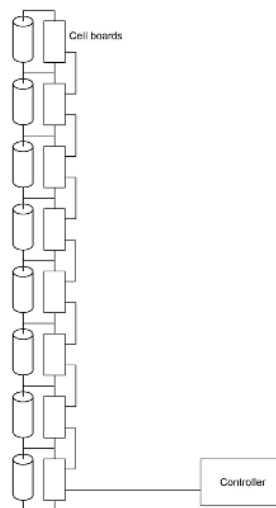


*Figure 21 Distributed BMS*

## 2.10 Battery Standards

Organisations like Society of Automotive Engineers and the International organization for standardization as well as industry groups and coalitions are helping the commercialization of the automotive and industrial lithium ion battery. Modern day organizations such as the United States Advanced Battery Consortium LLC (USABC), the Electric Drive Transportation Association (EDTA), and the National Alliance for Advanced Battery Technology (NAATBatt) are actually successors to one of the earliest electric vehicle (EV) industry trade groups called the Electric Vehicle Association of America (EVAA) which was formed in 1909 and lasted for only seven years. EVAA members included electric power generating companies, vehicle manufacturers, and energy storage battery makers.

Some of the tests and standards that are done by most of the electric vehicle manufacturesrs are mentioned below .

| Identifier | Application | Title |
|---|---|---|
| IEC 62660-2:2010 | (H)EV | Secondary lithium-ion cells for the propulsion of electrical road vehicles - Reliability and Abuse Testing. |
| IEC 62660-1:2010 | (H)EV | Secondary lithium-ion cells for the propulsion of electrical road vehicles - Performance Testing. |
| IEC 62660-2:2010 | (H)EV | Secondary lithium-ion cells for the propulsion of electrical road vehicles - Reliability and Abuse Testing. |
| IEC 62660-1:2010 | (H)EV | Secondary lithium-ion cells for the propulsion of electrical road vehicles - Performance Testing. |
| IEC 62660-3:2016 | (H)EV | Secondary lithium-ion cells for the propulsion of electrical road vehicles - Safety requirements |
| ISO 12405-1:2011 | (H)EV | Test specifications for packs and systems - High-power applications. |
| ISO 12405-2:2012 | (H)EV | Test specifications for packs and systems - High-energy applications. |
| ISO 12405-3:2014 | (H)EV | Test specification for lithium-ion traction battery packs and systems - - Part 3: Safety performance requirements. |
| ISO 6469-1:2009 | (H)EV | Electrically propelled road vehicles – Safety specifications – Part 1: On-board rechargeable energy storage system (RESS) |
| SAE J2929:2013 | (H)EV | Electric and Hybrid Vehicle Propulsion Battery System Safety Standard - Lithium-based Rechargeable Cells. |
| SAE J2464:2009 | (H)EV | Electric and Hybrid Electric Vehicle Rechargeable Energy Storage System (RESS) Safety and Abuse Testin |
| SAE J1798 WIP | (H)EV | ecommended Practice for Performance Rating of Electric Vehicle Battery Modules under development |
| UL 2580:2013 | (H)EV | Outline of investigation for batteries for use in electric vehicles. |
| QC/T 743-2006 | (H)EV | Automotive Industry Standard of the People's Republic of China - Lithium-ion Batteries for Electric Vehicles. |
| DOE-INL/EXT-15- 34184 | (H)EV | U.S. DOE Battery Test Manual for Electric Vehicles |

*Table 5 Table showing different Battery standards and their title*

All the standards mentioned above comprise a series of tests, some of which are mentioned below.

- Self-discharge tests—help the battery designer to determine how much energy is lost over time as the battery sits in storage.
- Cold-cranking tests—show how much power the battery can provide at low temperatures to "crank" the vehicle's engine and restart it
- Thermal performance testing—describes how much power and energy are available at different temperatures.
- Energy efficiency test—describes the "round trip energy efficiency" of a battery cell or system. In essence, this tells us how efficient the overall system design is and how much energy is lost during use.
- Cycle life testing—determines how many complete charge/discharge cycles at a predefined set of operating conditions a battery is achieved.
- Calendar life testing—as it is unrealistic to test a battery for its full expected life, which could be 10–15 years or more, it is important to get some idea of how long the battery lasts in calendar years. Therefore, that is precisely the purpose of this test (FreedomCAR Program Electrochemical Energy Storage Team, 2003).
- Mechanical abuse testing—which covers crush, penetration, drop, immersion, rollover, and shock testing
- Thermal abuse testing—which includes thermal stability, simulated fuel fire, high-temperature storage, rapid discharge and charge, and thermal shock cycle testing
- Electrical abuse testing—including overcharge and overvoltage, short circuit, overdischarge and voltage reversal, and partial short circuit (Sandia National Laboratories, 2006).

## 2.11 Battery Modelling

State of charge (SOC), state of energy (SOE), state of health (SOH), and state of power (SOP) are all estimated using battery modeling . These states are difficult to monitor directly, so they must be inferred using battery models. To characterize such properties, electrochemical models (EMs), black-box models, and equivalent circuit models (ECMs) have been utilized. To train black box models like neural network (NN) models, a substantial amount of experimental data is required. The resulting NN models can only be employed in similar working conditions to the experimental data because the parameters of the trained NN models have no physical relevance. This restricts the use of NN models in on-board BMSs for electric vehicles. Electrical circuits are used in ECMs to describe battery terminal behavior. They can be easily embedded into BMSs and are compatible with the circuits of BMSs for EVs.

- **Electrochemical Model**
  To describe the electrochemical reaction occurring inside batteries, EMs use partial differential equations (PDEs). These models are generally accurate, but their computational weight is too expensive to integrate into electric vehicle (EV) on-board battery management systems (BMSs). EMs use thermodynamics and electrochemical kinetics equation to describe physical and electrochemical processes in the anode, separator, and cathode regions of batteries. A pseudo-two-dimensional (P2D) model for lithium-ion batteries has been presented based on theories of porous electrodes and concentrated solutions (LiBs). The diffusion equation of lithium ions inside active

particles and electrolytes, the solid phase balance equation, and the electrolyte phase balance equation are all coupled nonlinear PDEs in three regions of LiBs.

- **Black Box Models**
  Black box models may mimic a complex interaction between external factors and battery internal electrochemical reaction processes, such as the relationship between SOC and battery terminal voltage and discharge current, without knowing the internal electrochemical reaction process. Although batteries appear to be simple, they are actually exceedingly complex electrochemical systems, as detailed in EMs. To begin with, they represent a collection of physically and chemically interconnected processes that turn chemical energy into electrical energy and vice versa. Second, there are some side reactions, such as corrosion and self-discharge, in addition to the main electrochemical reaction. Third, ambient conditions, as well as charging and discharging current profiles, have a significant impact on battery performance. Black box models, such as NN models, use automatic training to replicate the learning process of a human brain in order to obtain essential patterns within a multi-dimensional information domain.

  A NN model is made composed of an input layer, certain hidden layers, and an output layer. Adaptable weights connect each neuron in the NN to other neurons in the previous layer. Knowledge is typically kept as a series of weighted connections. Training is the process of applying a learning algorithm to modify the connection weights in an ordered manner, in which the input is supplied to the NN together with the desired output, and the weights are then adjusted so that the NN tries to create the desired output.
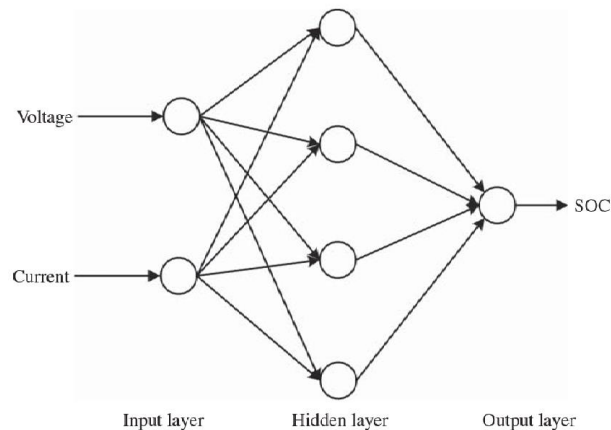


*Figure 22 NN Model for the Relationship of SOC to terminal Voltage and current for a battery*

- **Equivalent Circuit Models**
  BMS formation in EVs has been explored using ECMs. They are models with a small number of parameters that are lumped together. The ECM can show both static and dynamic properties. The equilibrium potential or open circuit voltage (OCV), which is represented by an ideal voltage source, describes the static characteristic. The OCV is commonly used to estimate SOC since it is monotonically related to SOC, aging levels, and operating temperatures. Combining polarization and hysteresis voltages with ohmic

resistance and resistance–capacitor (RC) networks describes the dynamic characteristic.

Based on the analysis of battery terminal voltage behavior, a general n- RC model is presented in Figure 23. Ri represents the internal resistance which is the sum of electrode material resistance, electrolyte resistance, diaphragm resistance, and contact resistance. RC networks denote the polarization effects with polarization resistance RD i and polarization capacitor CD i , i = 0, 1, … , n . i L is the load current (positive for discharge and negative for charge), U t is the terminal voltage, and U D i is the polarization voltage. According to Kirchhoff's current law, the relationship between output voltage and input current can be expressed by

$$U_t(s) = U_{oc}(s) - i_L(s)\left(R_i + \frac{R_{D1}}{1 + R_{D1}C_{D1}s} + \cdots + \frac{R_{Dn}}{1 + R_{Dn}C_{Dn}s}\right)$$
$$(n = 0, 1, 2, \cdots\cdots)$$

which leads to the transfer function as

$$G(s) = \frac{U_t(s) - U_{oc}(s)}{i_L(s)} = -\left(R_i + \frac{R_{D1}}{1 + R_{D1}C_{D1}s} + \cdots + \frac{R_{Dn}}{1 + R_{Dn}C_{Dn}s}\right)$$

- **Internal Resistance Model**
  When n = 0, the n-RC model is simplified to a R int model, the relationship between the output voltage and the input current under this model is expressed as

  $$G(s) = \frac{U_t(s) - U_{oc}(s)}{i_L(s)} = -R_i$$
  $$U_{t,k} = U_{oc,k} - R_i i_{L,k}$$

  where $U_{t,k}$ denotes the terminal voltage, $U_{OC,k}$ denotes the OCV, and $i_{L,k}$ stands for the load current at $k^{th}$ sampling time.
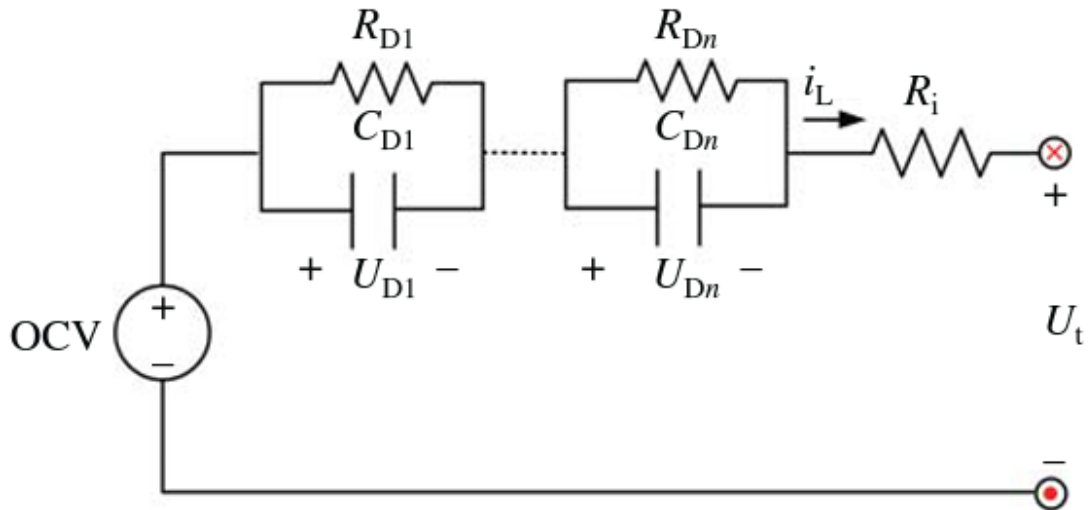


*Figure 23 n-RC Model for a lithium-ion battery*

# 3  12V Battery Design

## 3.1  Design Constraints

### 3.1.1 Battery Parameters

- Number of cells in series

  Our requirement is 12V . Hence the number of cell in series depends on the cell voltage of the cell that we choose. For example, the nominal voltage of lithium-ion cells vary from 3.3-3.V. Therefore, we must have 4 cells in the series.

- **Number of cells in Parallel**

  The number of cells in parallel depends on the capacity of the battery . Daniel Cela and Patrik Alerman published in their report that a 12V lithium ion battery must be of at least 25 Ah [5]. Therefore depending on the capacity of individual cell , the number of cells is chosen. Hence a battery with above-mentioned minimum capacity and voltage. The battery must also comply with USABC  guidelines for 12V battery minimum requirements . It should also be able to pass all the USABC tests for 12V battery . USABC stands for - United States Advanced Battery Consortium

## 3.2  Selection of cells

Currently, different automotive companies use different types of cells. But a wide variety of batteries are made from cylindrical cells. Therefore, mainly two types of cell chemistry was considered , Lithium-ion and Lithium Iron Phosphate. Both have different specifications and different applications.



*Figure 24 Usage of different kinds of cells by different companies*

For lithium-ion , SONY Morata 18650 and Samsung 21700 was considered and for lithium iron phosphate, Lithium werks was considered . Specifications of both the cells are mentioned below :-

| Parameters | Sony | Lithium Werks | Samsung |
|---|---|---|---|
| Model | US18650VTC6 | ANR26650m1B | 30T 21700 |
| Nominal voltage | 3.6 | 3.3 | 3.6 |
| Max charge voltage | 4.2 | 3.6 | 4.2 |
| Discharge end voltage | 2 | 2 | 2.5 |
| Capacity(mAh) | 3 | 2.5 | 3 |
| Max continuous discharge current(A) | 20 | 50 | 35 |
| Peak discharge Current theoretic(A) | 35 | 120 | 61.25 |
| Peak discharge cuurent time (s) | 4 | 10 | 4 |
| C-rate | 6.67 | | 11.67 |
| Diameter(mm) | 18.5 | 26.46 | 21.20 |
| Height (mm) | 65.2 | 65.65 | 70.40 |
| Weight(g) | 45.5 | 77 | 69 |

*Table 6 Different lithium ion cell comparison*

## 3.3 Cell Pack Design

Various battery-pack designs were considered , keeping weight and space efficiency in mind.

Cell to cell distance for SONY 18650 – 19.5mm

Cell to cell distance for Lithium Werks 26650- 27.5

Cell to cell distance for Samsung 21700 – 22.5

| | Cell | Cell in series | cell in parallel | Total no. Of cells | Batter capacity (Ah) | Peak discharge current(A) | Weight of batteries (g) |
|---|---|---|---|---|---|---|---|
| **Battery pack design** | Sony 18650 | 4 | 20 | 80 | 60 | 700 | 3640 |
| | Sony 18650 | 4 | 30 | 120 | 75 | 1050 | 5460 |
| | Sony 18651 | 4 | 28 | 112 | 84 | 980 | 5096 |
| | Lithium werks 26650 | 4 | 6 | 24 | 15 | 720 | 1848 |
| | Lithium werks 26650 | 4 | 8 | 32 | 20 | 960 | 2464 |
| | Lithium werks 26650 | 4 | 12 | 48 | 30 | 1440 | 3696 |
| | Lithium werks 26650 | 4 | 24 | 96 | 60 | 2880 | 7392 |
| | Samsung 21700 | 4 | 20 | 80 | 60 | 1225 | 5520 |
| | Samsung 21700 | 4 | 30 | 120 | 90 | 1837.5 | 8280 |
| | Samsung 21700 | 4 | 28 | 112 | 84 | 1715 | 69 |

*Table 7 Comparison of battery pack design with SONY, Samsung and Lithium werks cell*

According to our minimum battery required mentioned before , only three of the above battery configurations can be chosen , SONY 18650 – 4s20p , 4s30p & Lithium werks – 4s25P. According to USABC guidelines , the weight for the 12V battery should be 10Kgs. As one lithium werks cell weighs 1.6 times more than SONY 18650 and has 16% less capacity , cell configuration with SONY cells were selected . After careful considerations final configuration

of 4s28p was selected . After selecting the configuration, we have to approximate the weight of the battery .

For overall battery weight calculation , all the components of the battery were considered , which include , Cell holders , Battery case , Nickel and copper plates . Our 12V battery will be cooled by immersive cooling method hence fluid weight is also been considered.

## 3.4  Cell Holder Weight

Keeping cell to cell distance of 19.5mm drawing of the 4s28p configuration was made in Solidworks to get the dimensions of cell holders and battery case. Honeycomb pattern was selected as it is the most space-efficient pattern.
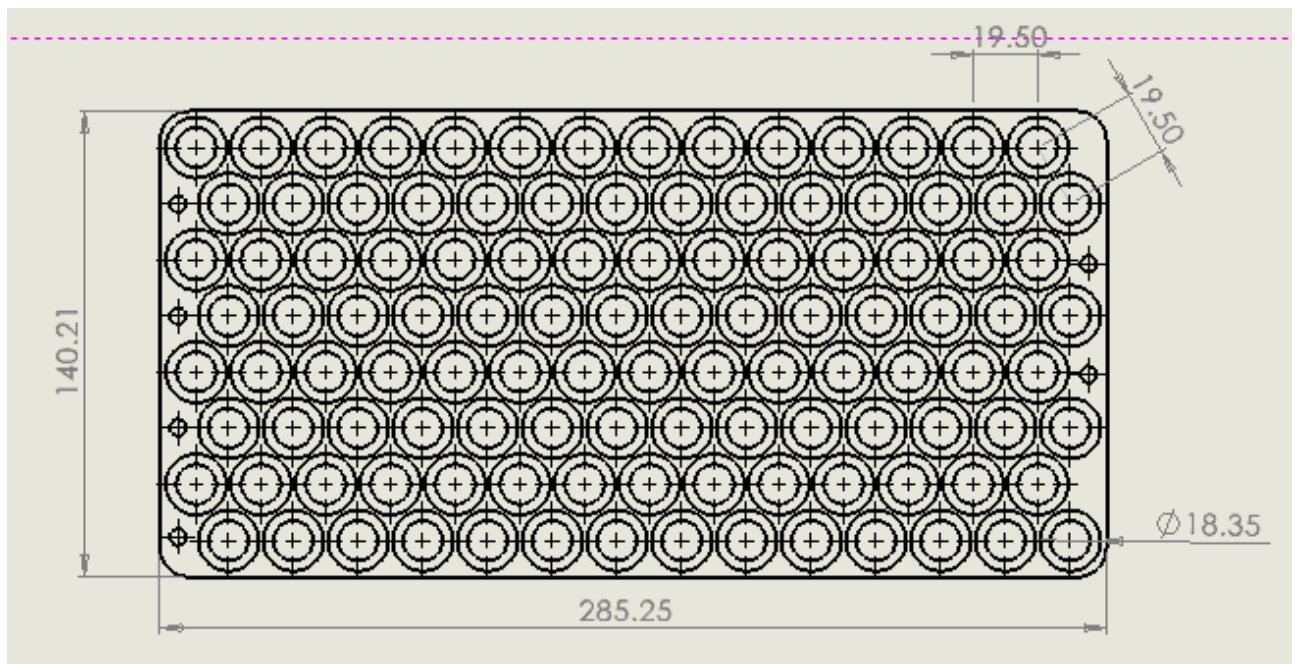


*Figure 25 Cell holder drawing with cell to cell distance of 19.5 mm*

## 3.4.1 Cell Holder Material

Among various thermoplastics stated in Table 8, Polyoxymethylene was selected , mainly because of its easy availability and cost-effectiveness and its strength . POM plastic is a semi-crystalline thermoplastic with high mechanical strength and rigidity. Acetal polymer has good sliding characteristics and with excellent wear resistance, as well as low moisture absorption.

Good dimensional stability & particularly good fatigue strength, excellent machining ability, makes POM polymer a highly versatile engineering material, even for complex components.

| Polymer | Advantages | Disadvantages |
|---------|-----------|---------------|
| PTFE | Outstanding chemical resistance, Low friction , High operational Tmax | Low stiffness , strength and hardness |
| ETFE | Good creep . tensile and wear properties. | Expensive , Attacked by esters , aromatics |
| PCTFE | Stiffer than PTFE | Very expensive , Attacked by – Esters , ethers and halogenated hydrocarbons. |
| PFA | Highest Tmax of fluoroplastics | Very expensive , Low stiffness, strength and hardness |
| POM | Tough and stiff . Good abrasion , creep and chemical resistance . | Attacked by acid and alkalis |
| UHMWPE | Good abrasion and chemical resistance | Low Tmax |
|  |  |  |

*Table 8 Thermoplastic comparison*

Distinction is made between acetal homopolymers (POM-H) & acetal copolymers (POM-C) in regard to their properties. Due to it's higher crystallinity, properties of POM H include slightly higher density, hardness & strength. POM C material, however has the higher chemical resistance & lower melting point than POM H. As we require low density and high chemical resistance , POM-C was selected as our material for cell holders .

Density of POM-C plastic – 1.41 g/cm3

Below is the properties of POM-C Plastic.

| | Test method | Unit | Guideline Value |
|---|---|---|---|
| **General properties** | | | |
| Density | DIN EN ISO 1183-1 | g / cm$^3$ | 1,41 |
| Water absorption | DIN EN ISO 62 | % | 0,2 |
| Flammability (Thickness 3 mm / 6 mm) | UL 94 | | HB / HB |
| **Mechanical properties** | | | |
| Yield stress | DIN EN ISO 527 | MPa | 67 |
| Elongation at break | DIN EN ISO 527 | % | 30 |
| Tensile modulus of elasticity | DIN EN ISO 527 | MPa | 2800 |
| Notched impact strength | DIN EN ISO 179 | kJ / m$^2$ | 6 |
| Shore hardness | DIN EN ISO 868 | scale D | 81 |
| **Thermal properties** | | | |
| Melting temperature | ISO 11357-3 | °C | 165 |
| Thermal conductivity | DIN 52612-1 | W / (m * K) | 0,31 |
| Thermal capacity | DIN 52612 | kJ / (kg * K) | 1,50 |
| Coefficient of linear thermal expansion | DIN 53752 | 10$^{-6}$ / K | 110 |
| Service temperature, long term | Average | °C | -50 ... 100 |
| Service temperature, short term (max.) | Average | °C | 140 |
| Heat deflection temperature | DIN EN ISO 75, Verf. A, HDT | °C | 110 |
| **Electrical properties** | | | |
| Dielectric constant | IEC 60250 | | 3,8 |
| Dielectric dissipation factor (50 Hz) | IEC 60250 | | 0,002 |
| Volume resistivity | DIN EN 62631-3-1 | Ω * cm | 10$^{13}$ |
| Surface resistivity | DIN EN 62631-3-2 | Ω | 10$^{13}$ |
| Comparative tracking index | IEC 60112 | | 600 |
| Dielectric strength | IEC 60243 | kV / mm | 40 |

*Figure 26 POM-C plastic Properties*

## 3.5 Thickness of Nickel & Copper Plates

Maximum current that will be drawn from 12V battery is 700 A . Therefore, our nickel and copper busbars must be able to conduct 700A . The nickel sheet is spot welded to the cells that we are going to use , hence the nickel sheet thickness cannot be more than 0.15mm . As Nickel has very high resistance , we will use a copper sheet on top of nickel sheet to conduct the current.

| Metal | Resistance ( μΩ-cm) (ρ) |
|---|---|
| Silver | 1.59 |
| Copper | 1.68 |
| Nickel | 6.84 |
| Aluminium | 2.65 |

*Table 9 Resistance comparison of different metals*

We can calculate voltage drop per cm of copper in the following way -

Copper plate cross sectional area

$$A_{copper} = width * thickness \qquad Equation\ 5$$

Copper resistance per unit cm

$$R_C = \rho_c * A_c \qquad Equation\ 6$$

$$R_{total,copper} = R_C * L_{total,copper} \qquad Equation\ 7$$

$$V_{drop,copper} = I * R_{total,copper} \qquad Equation\ 8$$

We can also calculate heat dissipation due to resistance :-

$$Q_{resistance} = I^2 * R_{Total} \qquad Equation\ 9$$

| $A_{copper}$ | 0.85 Cm$^2$ |
|---|---|
| $R_C$ | 7.9*10$^{-5}$ $\Omega$/cm |
| $R_{Total,copper}$ | 55.34 $\mu\Omega$ |
| $V_{drop,copper}$ | 0.0387 V |
| $Q_{resistance}$ | 27W |

*Table 10 Copper plate dimension & heat generated values*

According to data given in,

0.254 mm thick and 50.8mm nickel can handle 700 Amps of current , Here we are using 285.25 mm wide and 0.15mm thick Nickel as our current direction is as shown below .
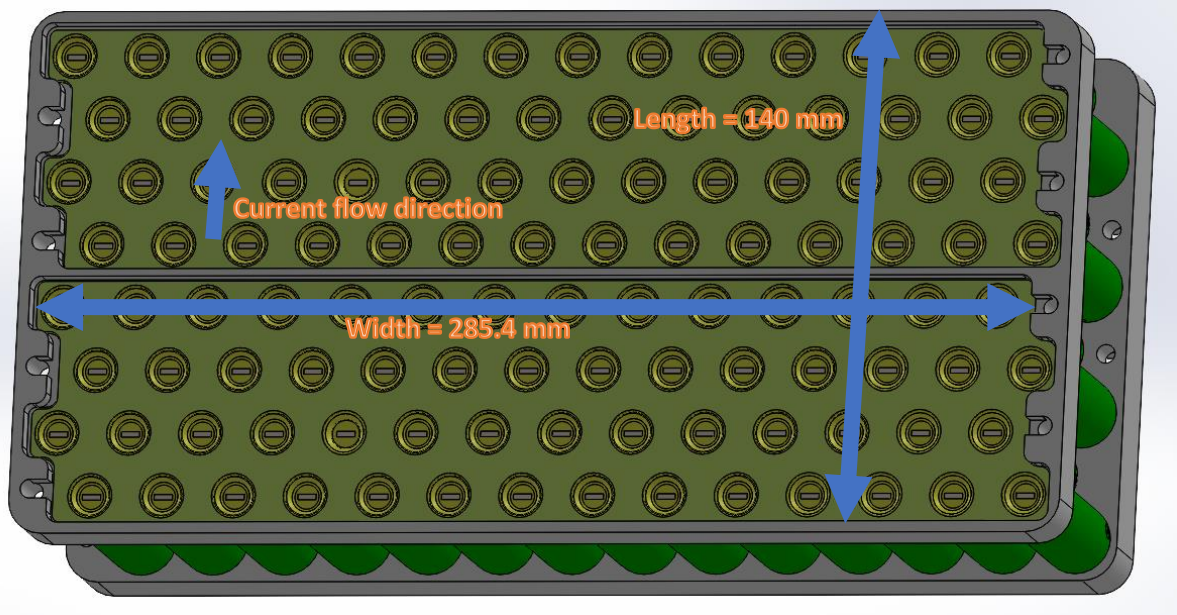
*Figure 27  Model of 12V battery cell pack*

As we are using nickel-plate instead of small nickel strips , we have a high cross sectional area for conducting .

| $L_{Nickel}$ | 285.25 mm |
|---|---|
| **Thickness** | 0.15 |
| $R_{total,nickel}$ | $456*10^{-6} \ \Omega$ |
| $A_{nickel}$ | 42.48 mm$^2$ |

*Table 11 Nickel plate resistance and dimensions*

Now Copper and Nickel plates are in series , therefore total resistance of copper and nickel combined can be calculated as –

$$R_{total} = R_{total,nickel} + R_{total,copper} \qquad \textit{Equation 10}$$

and Heat generated can be calculated as –

$$Q_{nickel,copper} = I^2 * R_{total} \qquad \textit{Equation 11}$$

| $R_{total}$ | 511 $\mu\Omega$ |
|---|---|
| $Q_{nickel,copper}$ | 250 W |

As the end collectors we will use copper end collectors. Copper bus bar must be able to handle 700 Amps . According to data by Austral wrights [6], 10mm2 copper can conduct 66 Amps. We need to conduct 700 Amps, hence required cross-section area is 106mm$^2$.

| Copper busbar Thickness | 4 mm |
|---|---|
| Width of copper busbar | 26.5 mm |
| Length of Copper busbar | 300 mm |

*Table 12 Copper busbar dimensions*

We can again calculate voltage drop and heat generated due to resistance in copper bus bar .

$$R_{busbar} = \frac{\rho_{copper} * L_{busbar}}{A_{busbar}} \qquad \text{Equation 12}$$

Hence Total resistance = 1.68*10^(-6) * 30 / 1.06 = 47.54*10^(-6) ohm

$$Q_{busbar} = 2 * I^2 * R_{busbar} \qquad \text{Equation 13}$$

Heat Generated = 700^2 * 47.54*10^(-6) = 23 W

We have 2 copper end collectors . hence

Heat generation = 23*2 = 46 W

Our Sony Murata 18650 cells have a internal resistance = $R_{internal}$ = 12.8 * 10$^{-3}$ $\Omega$

Therefore total resistance of cells for a 4s28p configuration is = 4*12.8*10^(-3) / 28 = 1.82 mili ohm

$$R_{internal,total} = \frac{4 * R_{internal}}{28} \qquad \text{Equation 14}$$

Therefore total heat generation = 1.82*10^(-3) * 700^2 = 891 W

$$Q_{cells} = I^2 * R_{internal,total} \qquad \text{Equation 15}$$

Hence total heat generation will be = 891 + 293 = 1184 W

$$Q_{battery} = Q_{cells} + Q_{busbar} + Q_{nickel,copper} \qquad \text{Equation 16}$$

| | |
|---|---|
| $R_{interna,cells}$ | $1.82*10^{-3}\ \Omega$ |
| $Q_{busbar}$ | 46 W |
| $Q_{cells}$ | 891W |
| $Q_{battery}$ | 1184 W |

## 3.6 Immersive Cooling Fluid

Out of all the types of insulating fluid stated in 2.8.2.1, hydrocarbon-based fluid suits best for our application as it is cost-effective and has low viscosity and high dielectric strength. Moreover they are highly biodegradable.

3M is one of largest manufacturers of dielectric fluids , which has a whole range of fluid for specific application . Some of the fluids specifications are listed below.

# 3M™ Thermal Management Fluids Properties

## 3M™ Novec™ Engineered Fluids

| | Unit | Novec 7000 | Novec 7100 | Novec 7200 | Novec 7300 | Novec 7500 | Novec 7600 |
|---|---|---|---|---|---|---|---|
| Boiling Point | °C | 34 | 61 | 76 | 98 | 128 | 131 |
| Pour Point | °C | -122 | -135 | -138 | -38 | -100 | -98 |
| Molecular Weight | g/mol | 200 | 250 | 264 | 350 | 414 | 346 |
| Critical Temperature | °C | 165 | 195 | 210 | 243 | 261 | 260 |
| Critical Pressure | MPa | 2.48 | 2.23 | 2.01 | 1.88 | 1.55 | 1.67 |
| Vapor Pressure | kPa | 65 | 27 | 16 | 5.9 | 2.1 | 0.96 |
| Heat of Vaporization | kJ/kg | 142 | 112 | 119 | 102 | 89 | 116 |
| Liquid Density | kg/m³ | 1400 | 1510 | 1420 | 1660 | 1614 | 1540 |
| Coefficient of Expansion | K⁻¹ | 0.0022 | 0.0018 | 0.0016 | 0.0013 | 0.0013 | 0.0011 |
| Kinematic Viscosity | cSt | 0.32 | 0.38 | 0.41 | 0.71 | 0.77 | 1.1 |
| Absolute Viscosity | cP | 0.45 | 0.58 | 0.58 | 1.18 | 1.24 | 1.65 |
| Specific Heat | J/kg-K | 1300 | 1183 | 1220 | 1140 | 1128 | 1319 |
| Thermal Conductivity | W/m-K | 0.075 | 0.069 | 0.068 | 0.063 | 0.065 | 0.071 |
| Surface Tension | mN/m | 12.4 | 13.6 | 13.6 | 15.0 | 16.2 | 17.7 |
| Solubility of Water in Fluid | ppm by weight | ~60 | 95 | 92 | 67 | 45 | 410 |
| Solubility of Fluid in Water | ppm by weight | <50 | 12 | <20 | <1 | <3 | <10 |
| Dielectric Strength, 0.1" gap | kV | ~40 | ~40 | ~40 | ~40 | ~40 | ~40 |
| Dielectric Constant @ 1kHz | – | 7.4 | 7.4 | 7.3 | 6.1 | 5.8 | 6.4 |
| Volume Resistivity | Ohm-cm | $10^8$ | $10^8$ | $10^8$ | $10^{11}$ | $10^8$ | $10^{10}$ |
| Global Warming Potential | GWP | 420 | 297 | 59 | 210 | 100 | 700 |

*Figure 28 3M Novec 7200 fluid*

As we can see above from the table , the vapour pressure and boiling point of Novec fluids is fairly low .

As we are using single-phase  immersive cooling , the fluid needs to have the following properties :-

- High Dielectric Strength
- High heat capacity
- Low density
- Low viscosity
- High boiling point
- Easily available
- Low price
- low vapour pressure

After analysing the properties of novec fluids , Novec 7200 suits best to our application as its boiling point is reasonably high along with relatively high vapour pressure and low density and high heat capacity.

Fluid Chosen – 3M Novec 7200

Density = 1420 Kg/m^3

## 3.7  Battery Case Material Battery

Out of all the options proposed in 2.5.3 Aluminium machined block is the best option for our design as it is cost-effective and at the same time provides high strength and surface finish, and it also fulfils the need for having a non flammable battery enclosure.

**Selecting Aluminium Grade**

Aluminium Alloys are assigned a four-digit number, in which first digit identifies general class, or series, characterized by its main alloying elements.

| Series Number | Alloying Element | Alloy Category | Typical Applications |
|---|---|---|---|
| 1XXX | Aluminum | Commercially Pure | Electrical, Power Grid & Transmission |
| 2XXX | Copper | Heat-Treatable | Aircraft, Cylinders and Pistons |
| 3XXX | Manganese | Non Heat-Treatable | Cooking Utensils, Beverage cans |
| 4XXX | Silicon | Non Heat-Treatable | Structural and Automotive |
| 5XXX | Magnesium | Non Heat-Treatable | Storage Tanks, Marine, Pressure Vessels |
| 6XXX | Magnesium and Silicon | Heat-Treatable | Structural and Automotive |
| 7XXX | Zinc | Heat-Treatable | Aircraft |

*Table 13 Table comparing all the aluminium series*

Aluminium 6000 series is best suitable for our application .

Al-6061 and Al-6082 are the most common aluminium alloys used in automotive . A brief comparison chart is shown below.

| Alloy | Specimens | $\sigma_{yield}$ [MPa] | $\sigma_{rupt}$ [MPa] | E [GPa] | Elongation [%] |
|---|---|---|---|---|---|
| 6082-T6 | 1 | 276.0 | 322.6 | 65.9 | 18.9 |
| | 2 | 276.0 | 323.4 | 64.7 | 16.4 |
| | 3 | 276.5 | 322.7 | 70.7 | 17.2 |
| | **Average** | **276.2** | **322.9** | **67.1** | **17.5** |
| 6061-T6 | 1 | 307.0 | 343.5 | 67.2 | 17.7 |
| | 2 | 301.0 | 337.3 | 73.7 | 16.9 |
| | 3 | 311.0 | 345.2 | 64.4 | 16.9 |
| | **Average** | **306.3** | **342.0** | **68.5** | **17.1** |

*Figure 29 Comparison of AL 6082-T6 and AL 6061-T6*

Aluminium 6061 provides greater yield strength which is paramount to our design . A detailed specification for 6061 is given below .

| Property | Al 6061-T6 |
|---|---|
| Young's modulus | 68.9 GPa |
| Poisson's ratio | 0.33 |
| Tensile yield stress | 276 MPa |
| Ultimate tensile strength | 310 MPa |
| Elongation at break for 12.7mm (1/2 in.) diameter | 17% |
| Brinell hardness | 95 |
| Fracture toughness $K_{Ic}$ (T-L orientation) | 29 MPa√m |

*Figure 30 Properties of Aluminium 6061-T6*

### 3.7.1 Type of Coating

It's critical to determine whether or not coatings are required. One of the most important reasons for coatings is to protect electronics and battery cells from grounding and shorting. Furthermore, the coating acts as an isolator for the battery system. This can be accomplished with a variety of materials and types. One frequent application is to use an isolating film with an adhesive on one side that may be applied directly to the metal surface and provides the necessary isolation.

Powder coating or liquid coating are two more types of coatings that can be used. This sort of coating provides additional environmental protection in addition to isolation. As we are using Aluminium as our battery enclosure, it is essential to have anodization for isolation and corrosion-resistant. Some of the advantages of anodization are listed below.

- Corrosion resistance.
- Natural metallic anodised finish.
- No risk of adhesion failure of the anodic film.
- No risk of surface finish fading.
- Anodised aluminium is non conductive

Anodization has a huge advantage over other forms of coating. A layer of 60 microns can resist up to 800V DC. [6] As we are manufacturing a 12V battery, a 50 microns thickness provides the necessary electrical system isolation and corrosion resistance. The variation of breakdown voltage and anodization coating thickness is given below.
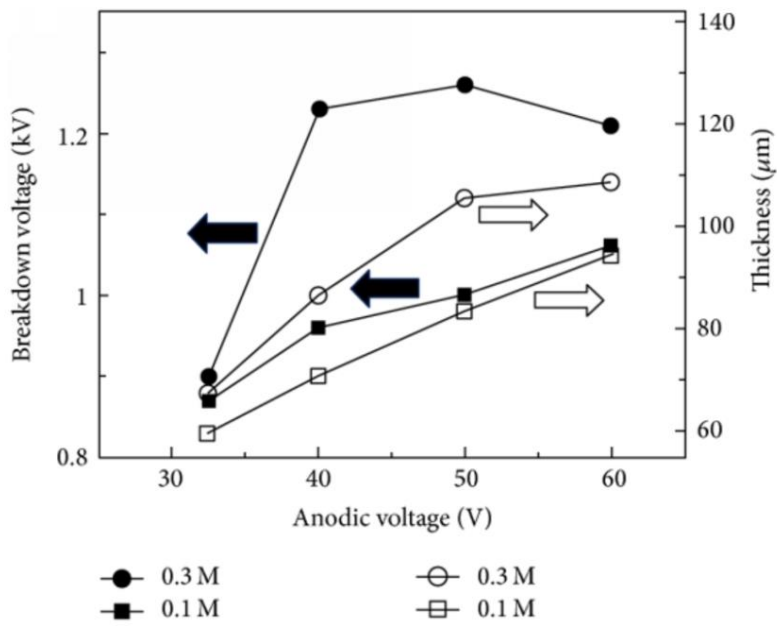
*Figure 31 Graph of Breakdown voltage vs Anodisation coating thickness*

## 3.8  12 V Battery weight Estimation

For battery weight estimation first, we require the dimensions and weight of the cells that we are using.

### 3.8.1 Cell



| SIZE | Weight | 45.50 g |
|---|---|---|
| | Diameter, max. | 18.50 mm |
| | Height, max. | 65.20 mm |
| VOLTAGE | Voltage, charge max. | 4.20 V |
| | Voltage, nominal | 3.60 V |
| | Voltage, discharge end | 2.00 V |
| CAPACITY | Capacity, max. | 3000.00 mAh |
| CURRENT | Charge constant standard | 3 A |
| | Max. continuous discharge current | 20.00 A |
| | Peak discharge theoretic, 4 sec | 35 A |
| | C-rate (discharge, max.) | 6.67 C |
| POWER | Watts (discharge, max.) | 72 W |
| ENERGY | Energy, max. | 10.80 Wh |
| | Density volumetric theoretic | 617 Wh/L |
| | Density gravimetric theoretic | 237.00 Wh/kg |
| | E-rate (discharge, max.) | 6.67 E |
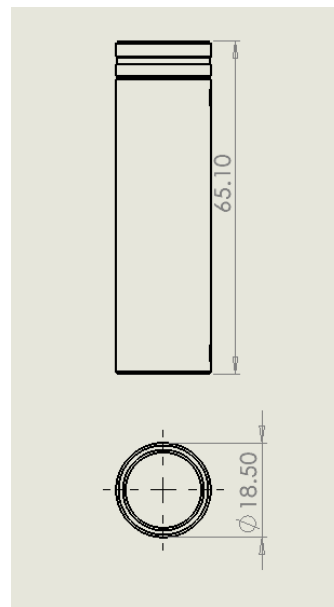
*Figure 32 SONY VTC618650 Specifications*

As our configuration is 4s28p total no. of cells is  112.

| Number of cells | 112 |
|---|---|
| Weight of the cells ( $W_{cells}$) | 5152 g |

## 3.9 Cell holder

Material used = POM-C Delrin

| Density | 1.41 g/cm$^3$ |
|---|---|
| Rectangle sheet size | 285 x 140 x 15 mm |
| Cell hole radius | 9.25 mm |
| Number of cells | 112 |
| Volume of Cell holder | 146.91 cm$^3$ |
| Weight of cell holder ($W_{cell\ holder}$ ) | 415 g |

## 3.10 Immersive Cooling fluid weight

Novec 7200 Immersive cooling weight can be calculated by subtracting the volume of cells and cell holder from the cell pack volume

| Cell Pack Size | 285 x 140 x 75 mm |
|---|---|
| Cell height | 65.10 |
| 3M Novec 7200 volume | $5.71*10^{-4}$ m$^3$ |
| 3M Novec 7200 Density | 1400 Kg/m$^3$ |
| Weight of the fluid ( $W_{fluid}$) | 800 g |

## 3.11 Battery case weight

| Battery Case dimensions | 295 x 150 x 5 mm |
|---|---|
| Aluminium Density | 2400 Kg/m$^3$ |
| Weight of Aluminim case ( $W_{Al}$) | 1960 g |
| | |
| | |

## 3.12 Total weight of the battery

$$W_{battery} = W_{cells} + W_{cellholder} + W_{fluid} + W_{al} + W_{miscellaneous}$$ 

*Equation 17*

| $W_{miscellaneous}$ | 4500 |
|---|---|
| $W_{battery}$ | 12847 |

The miscellaneous weight consists of weight of BMS and copper as well as nickel plates and busbars.

## 3.13 Thermal analysis of Battery

Now that we have estimated the weight of the battery and also the amount of cooling fluid which will be used , we can perform a thermal analysis of our battery .

At 700 amperes we already calculated before how much of the heat will be generated i.e $Q_{battery}$, which means that if maximum current was drawn for 5 seconds total energy generated will be ,

$$E_{gen} = Q_{battery} * 5 \qquad \textit{Equation 18}$$

$$\Delta T = E_{gen}/(W_{fluid} * C_{p,novec}) \qquad \textit{Equation 19}$$

| $Q_{battery}$ | 1184 |
|---|---|
| $E_{gen}$ in a 5 second pulse | 5920 J |
| $C_{p,novec}$ | 1214 J/Kg-K |
| $W_{fluid}$ | 0.8 Kg |
| $\Delta T$ novec | 6 Cº |

Therefore we can say that the heat generated during a 5 second pulse of 700 A current will be dissipated through Novec 7200 with an increase 6 deg Celsius in the temperature.

This heat will be further dissipated into the atmosphere via aluminium case .

## 3.14 Assembly

### 3.14.1    Nickel Plate

The nickel sheet was made by sheet forming . Dies were manufactured with aluminium 7075 which are shown below, and pure nickel sheet was pressed with 10 ton of force. Operation sheet of the dies are attached in Appendix
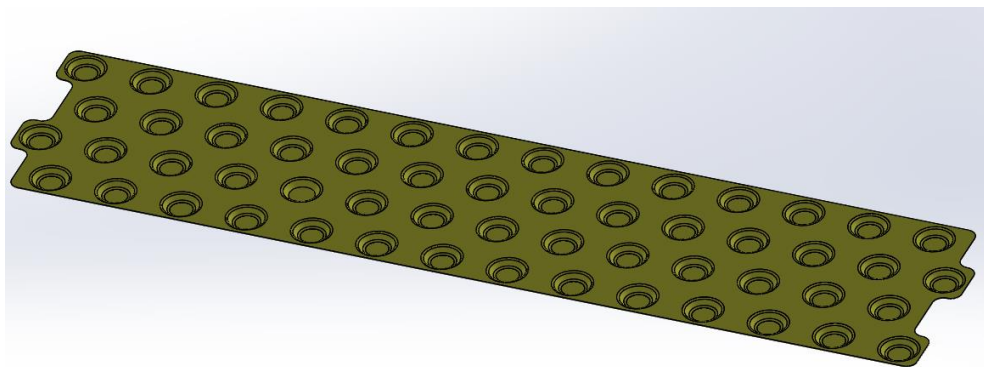


*Figure 33 Nickel plate*

*Figure 34 Bottom die*



*Figure 35 Top Die*



*Figure 36 Nickel sheet*

# 3.15 Assembly
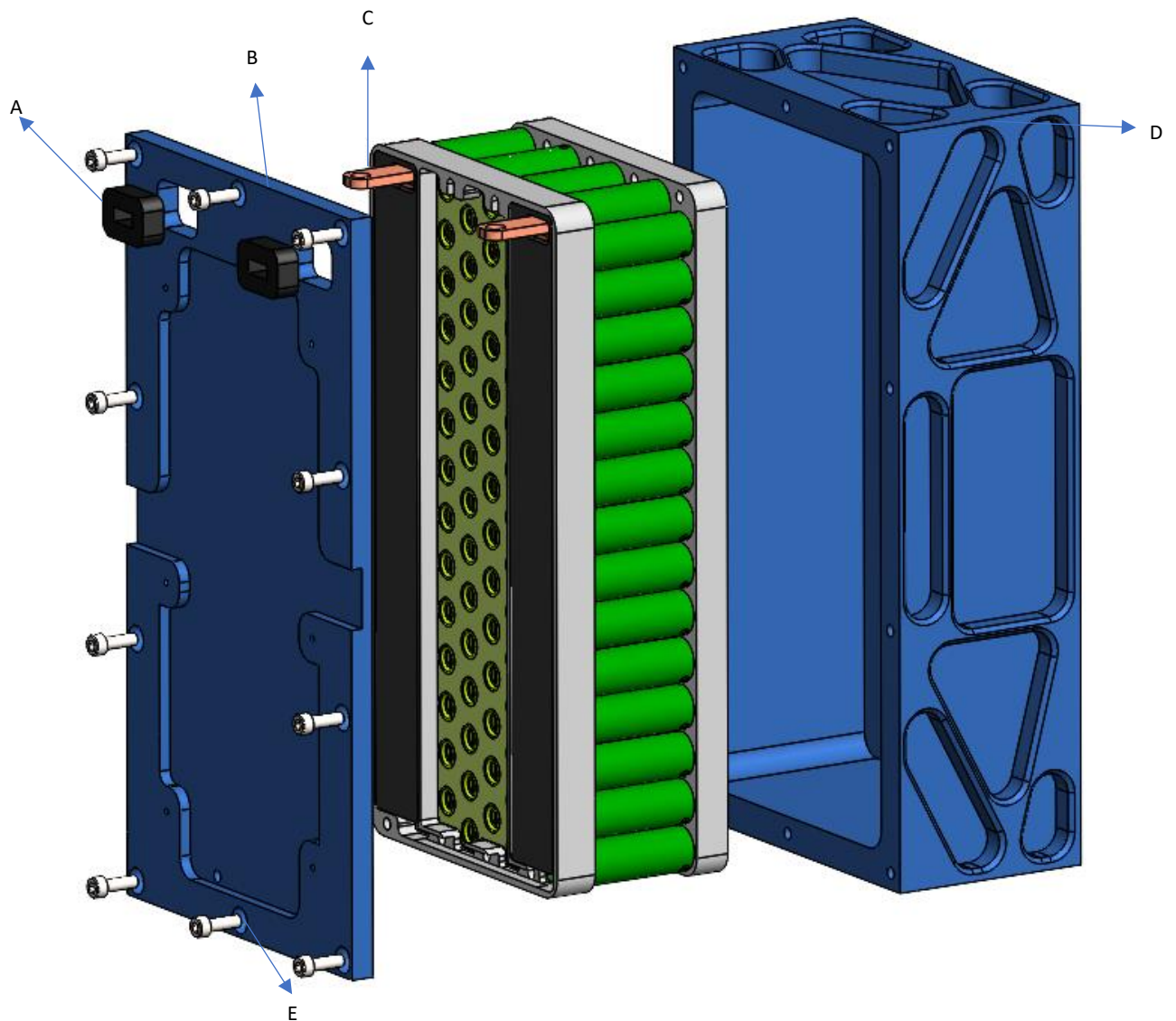


*Figure 37 Exploded view of 12V battery with battery case and cover*

| Label | Component Name |
|-------|----------------|
| A | Busbar bushings |
| B | Battery cover |
| C | Busbar |
| D | Battery Case |
| E | Battery bolts |
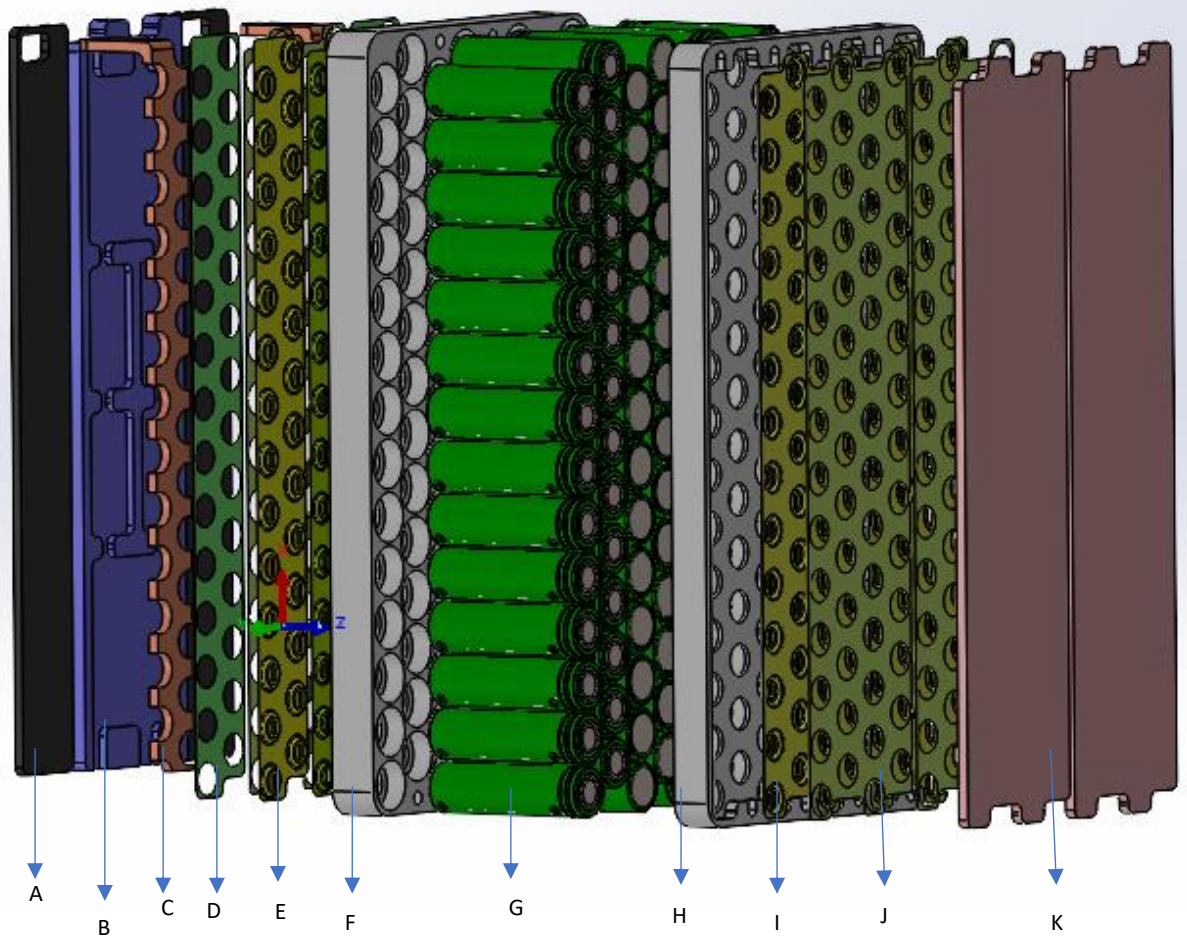
*Figure 38 Exploded view of 12V with all the components*

| Label | Component Name |
|-------|----------------|
| A | Busbar cover |
| B | Top cell cover |
| C | Busbar |
| D | Copper plate |
| E | Nickel plate |
| F | Top Cell holder |
| G | Cells |
| H | Bottom Cell holder |
| I | Bottom nickel plate |
| J | Copper plate |
| K | Bottom cell cover |

*Table 14  12V battery component list*

Drawings and Operation sheet  of all the components are attached in appendix A & Appendix
B respectively.

## 3.16 Manufacturing

For manufacturing our parts we will use HAAS VF-7 CNC machine which is present in the Corbellati production hall.



*Figure 39 HAAS VF7*

## 3.17 Breakdown Voltage of Battery Case

### 3.17.1 Test Equipment

Applying an increasing reverse voltage to the device until a specific test current is reached indicates that the device is in breakdown is how breakdown voltage is measured. This test is generally called HiPot test or High Potential Test. The equipment shown in Figure 22 is Breakdown voltage tester present in the lab of Czech technical University. The Gmbh equipment can provide upto 6000V at 50 Hz.

*Figure 40 Gmbh Breakdown Voltage tester*

## 3.17.2 Test Setup
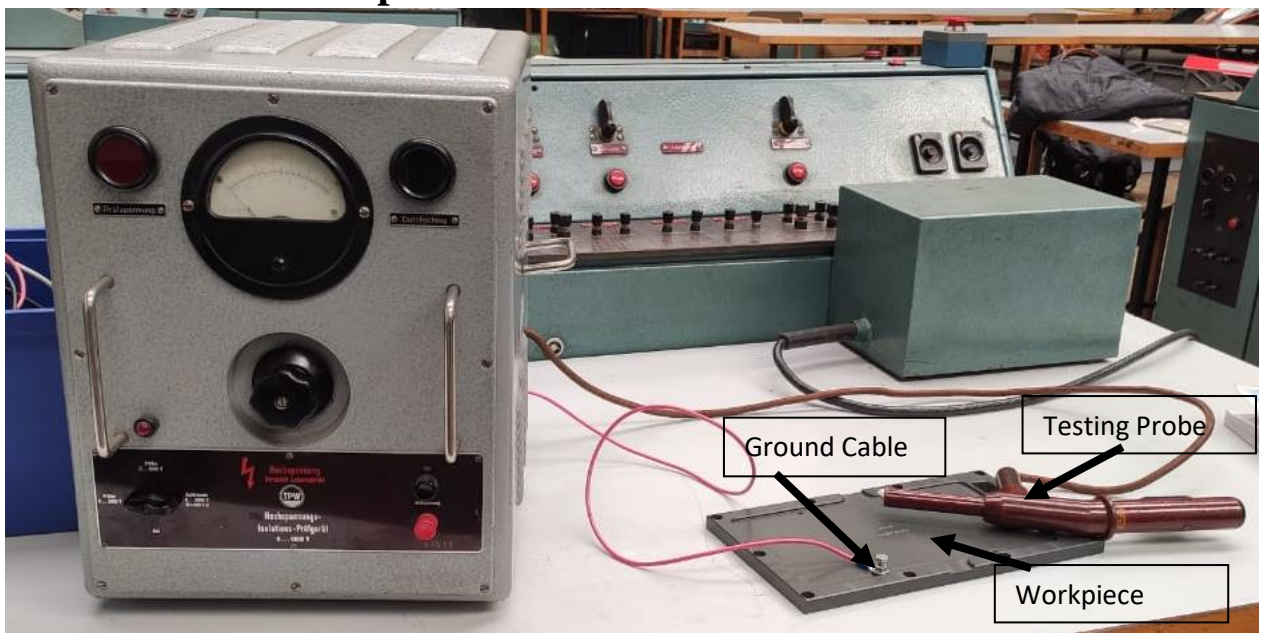


*Figure 41 Breakdown Voltage Test Setup*

## 3.17.3 Test Procedure

The ground cable is attached to the workpiece through a bolt to maintain a permanent contact between ground cable and workpiece. The person performing the experiment must wear high voltage protection gloves for safety and take the probe in hand that is shown in the above picture. The person must touch the probe to workpiece firmly and then turn on the Gmbh breakdown voltage tester. The Gmbh BVT will start applying high voltage across the probe

and will start increasing the voltage gradually . The voltage increase can be seen on the voltmeter on the Gmbh BVT. The BVt trips when it detects current across the workpiece at the breakdown voltage .

### 3.17.4     Results

- **Battery Cover**
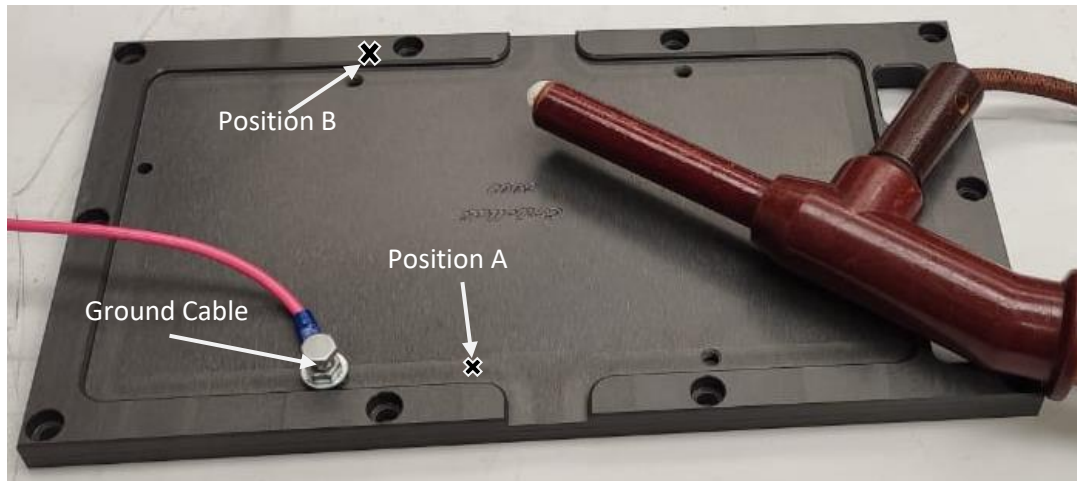


*Figure 42 Battery cover*

The Battery case and cover are shown in the picture have an anodization thickness of 50 microns, and breakdown voltage values are given below in the table.

| Position | Breadown Voltage |
|----------|------------------|
| A | 350 V AC 50 Hz |
| B | 700 V AC 50 Hz |

- **Battery Case**
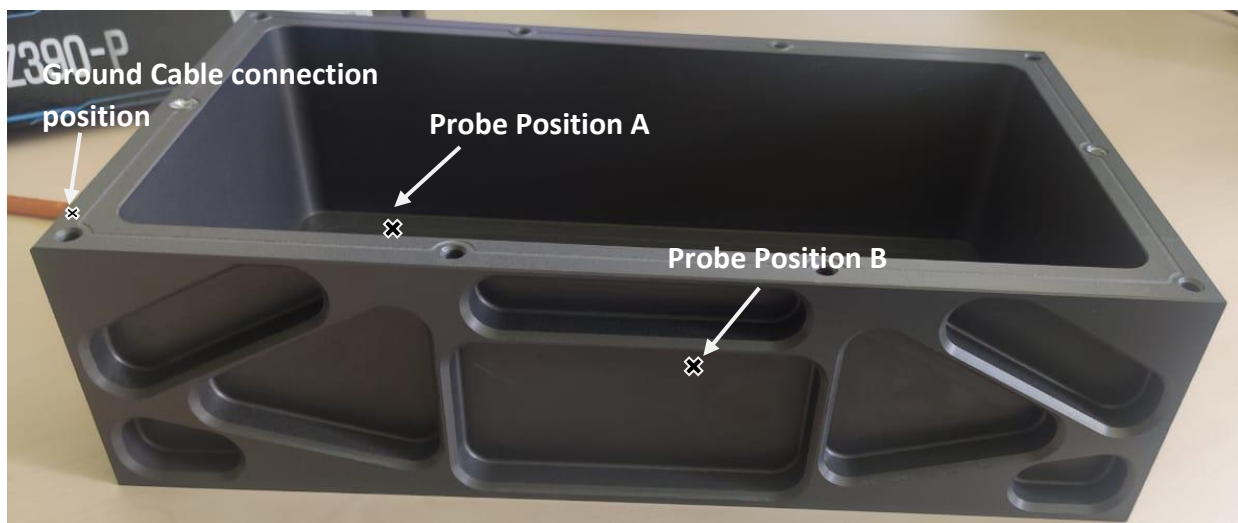


*Figure 43 battery case*

| Position | Breakdown Voltage |
|---|---|
| A | 400 V |
| B | 500 V |
| | |

### 3.17.5  Conclusion

By observing the results of our experiment we can conclude that our battery case and cover have enough insulation for for a 12V battery . But for a 400V battery the insulation is not enough. Therefore we have to increase the anodization thickness in order to have sufficient insulation.

## 3.18 BMS Wiring
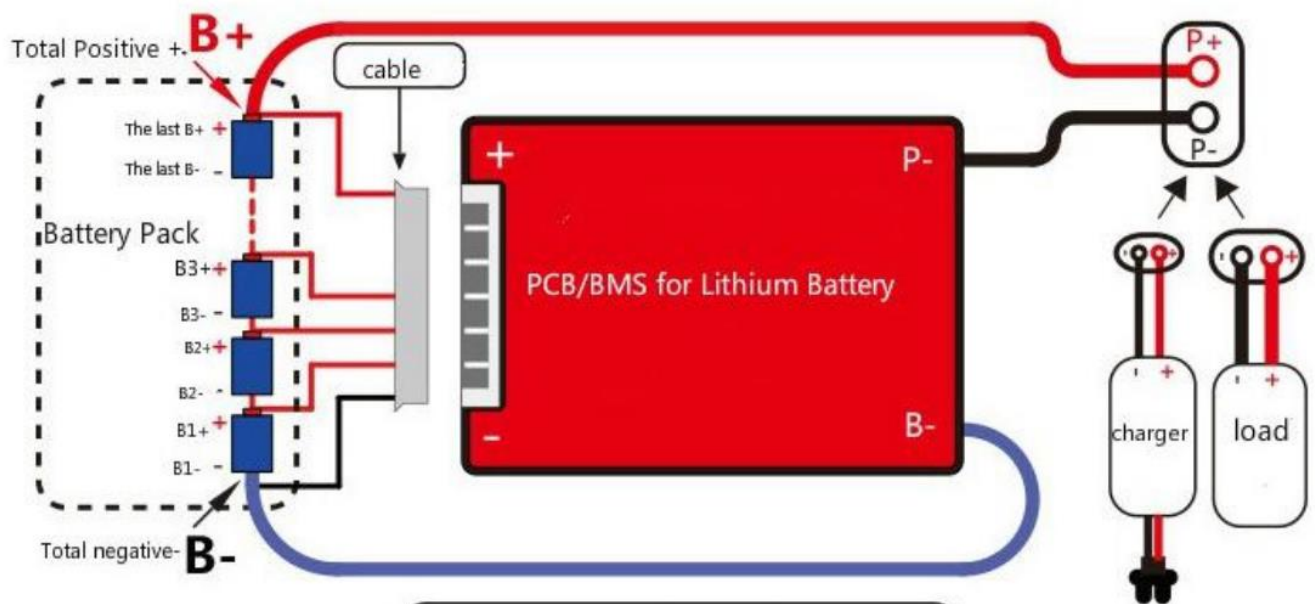


*Figure 44 BMS Wiring Diagram*

The BMS have one B- connection and P- connection . The B- has to be connected to total negative of the battery . The balance wires needs to be connected in the right order as shown above. So P- will be the final negative terminal of the battery and total positive of the battery will be the main positive . Load and charger both can be connected as shown above.

## 3.19 12V Battery
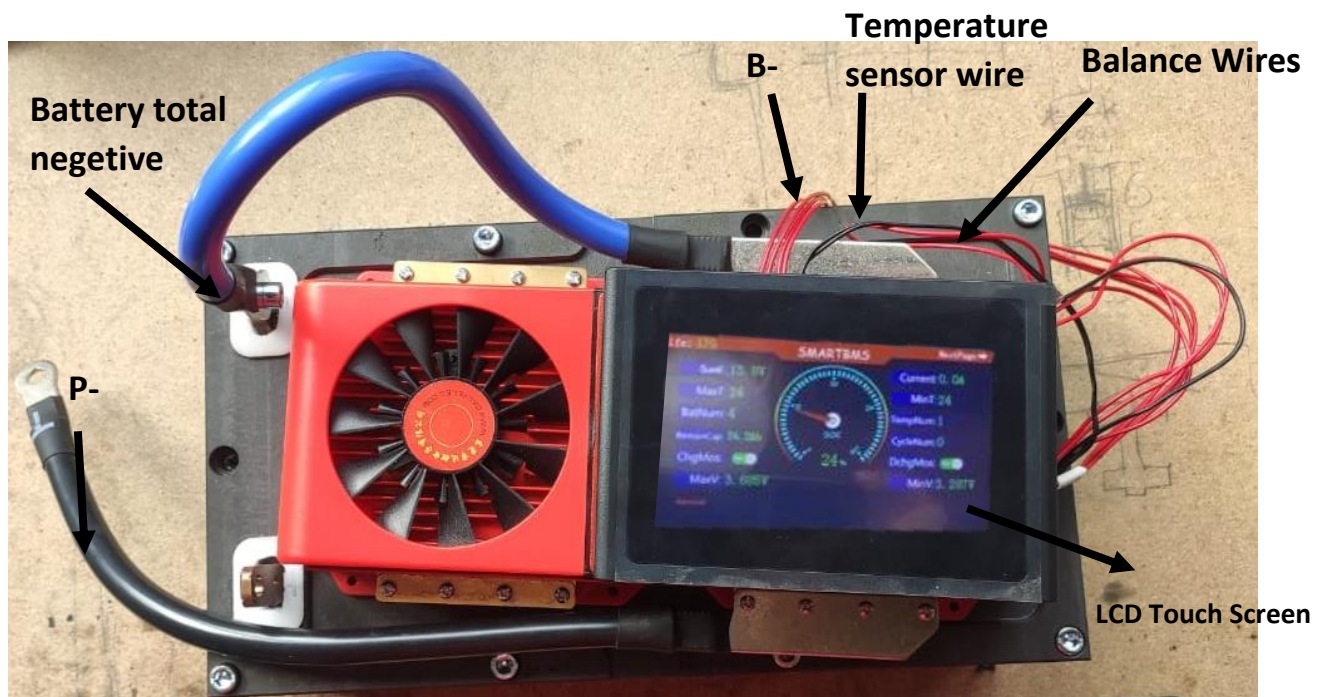


*Figure 45 12V lithium ion Battery Assembly*

In the above figure we can see the assembly of the 12V Lithium-ion immersive cooled battery with a smart BMS. The smart BMS enables us to see and monitor the SOC , temperature and individual voltage of the cells via the LCD touch screen.

# 4 Design Of 400V Battery

## 4.1 Design Constraints
### 4.1.1 Position & Mounting

In the present automotive market, various hybrid and electric car manufacturers have used different approaches for positioning and mounting the batteries. Relatively small battery of micro-hybrid cars are placed in the engine compartment only. The larger batteries of mild and full hybrids like Toyota Prius are placed under trunk in place of the spare wheel.Cars like Volvo XC 90 Hybrid have batteries in the central tunnel.
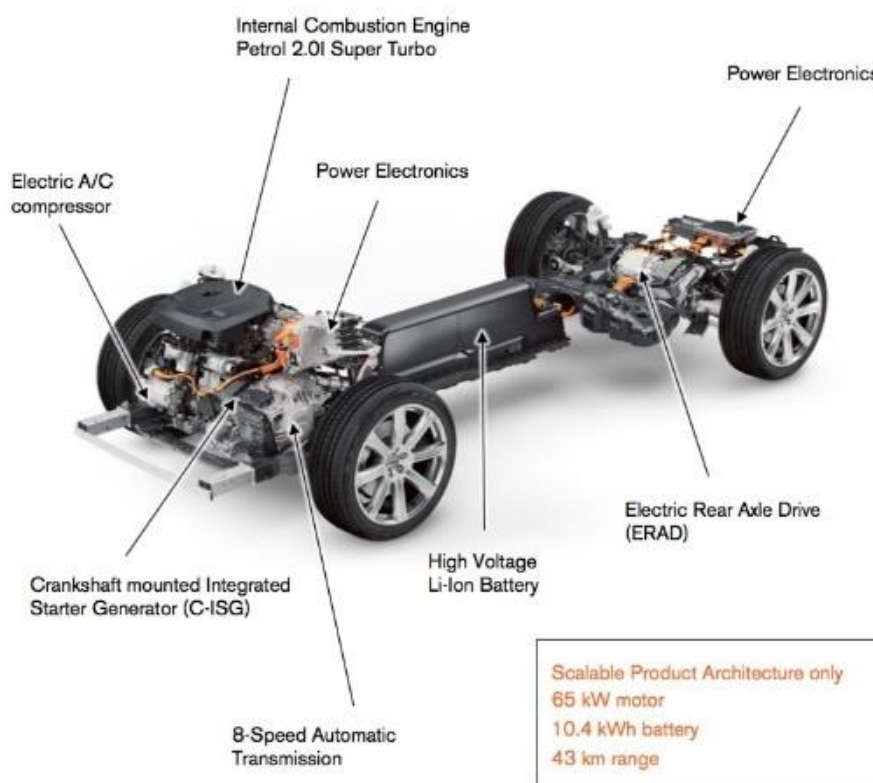
*Figure 46 Volvo XC90 Battery*

Cars like Audi e-Tron , Volkswagen ID , Tesla model 3 all have the battery in the double floor.
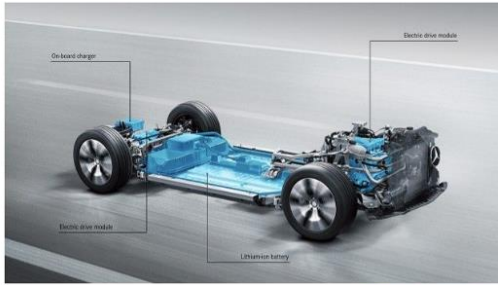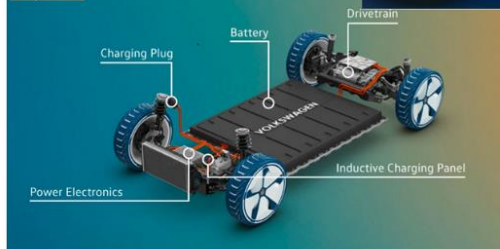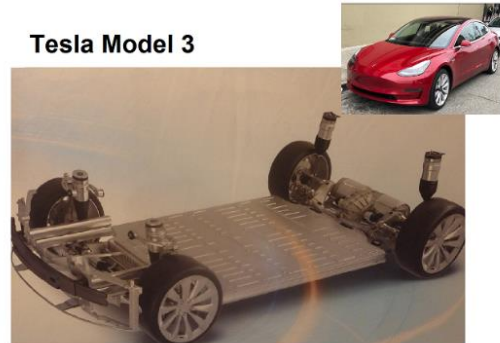
*Figure 47 Mercedes benz EQ series , Audi e-Tron , VW ID , Tesla model 3 battery positions*

In our car, mounting at the rear subframe is the best suitable position for our battery as it does'nt take space in boot.

## 4.1.2 Dimension and Size

Dimension and size is the main design constraint in our battery design as our battery is mounted on the rear subframe of our vehicle, and the space for the battery is limited . Therefore space available at the rear subframe must be taken into account while doing calculations and designing.

## 4.1.2.1     Rear Subframe

Our vehicle is  Classic Minicooper . To get the dimensions of the rear subframe, we used a 3d scanner to scan the rear part of the car and reverse-engineered it. We used Shining HX laser 3D scanner to scan the subframe, datasheet of which is mentioned in Appendix 3

*Figure 48 SHINING 3d Einscan HX 3d Scanner*

The Shining HX laser scanner has an accuracy of 0.04mm. Therefore our scan results will be of high detail and accuracy. Below are the scan results of the rear subframe of the Minicooper.

## 4.1.2.2    Scan Result
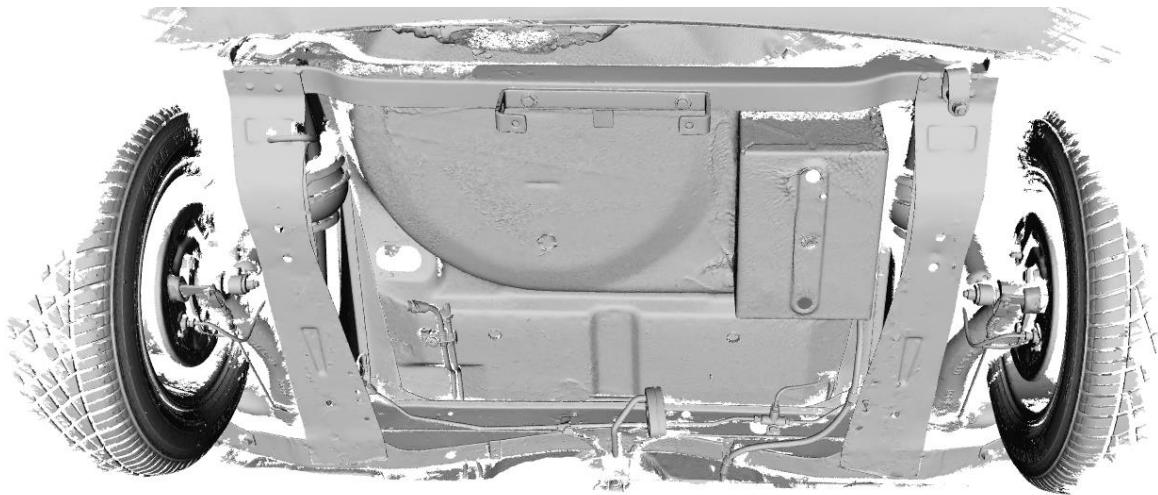


*Figure 49 Minicooper rear subframe scan*

In Figure 49, we have the result of the scan. We get the scan as a mesh file that we import in the Autodesk Recap Photo software to measure our dimensions accurately. According to our measurements , maximum dimension of our battery can be 760mm x 530mm x 150mm .

The height of our battery is also limited to have enough ground clearance for our vehicle.

## 4.1.3 Module Design

Each high voltage battery is made of a number of modules which are connected together in series or parallel connection to get the desired voltage level or capacity .

For example the Tesla model S has a battery of nominal Voltage 350.4 V and capacity of 102.4 Kwh, and is made of 16 modules connected in series.
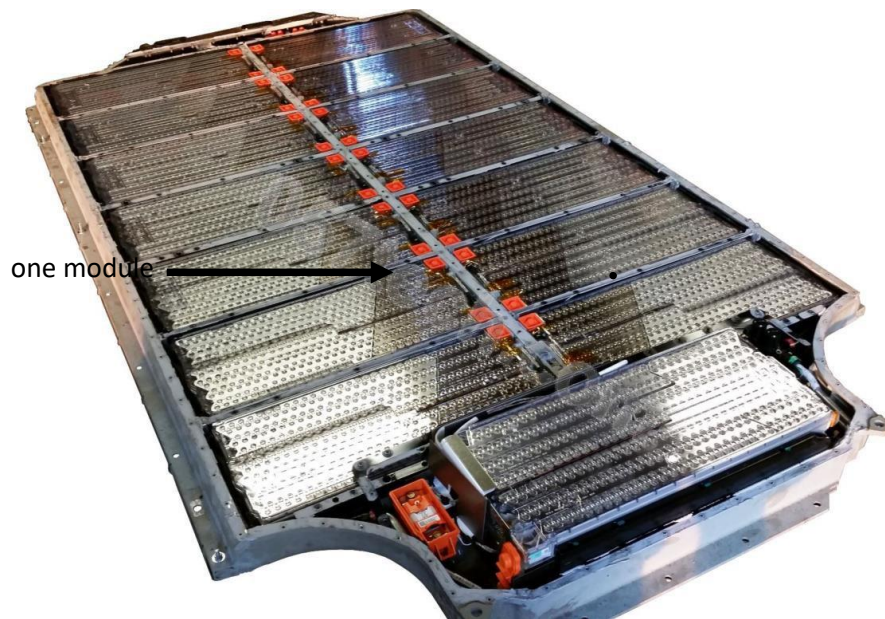
one module

*Figure 50 Tesla model S battery*
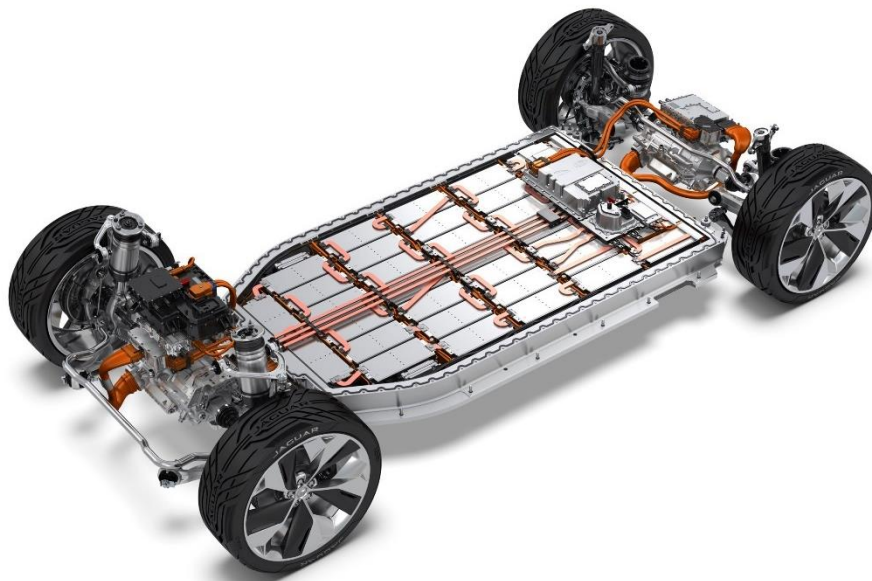
*Figure 51 Jaguar I Pace Battery*

This type of construction give us many benefits;

- We can arrange the modules in various ways according to our design
- While doing the assembly we do not handle hundreds of volts at once which is a crucial design aspect of the battery.

The cell pack that we have designed for the 12V battery will be suitable for our design for our battery.

## 4.1.4 Single module
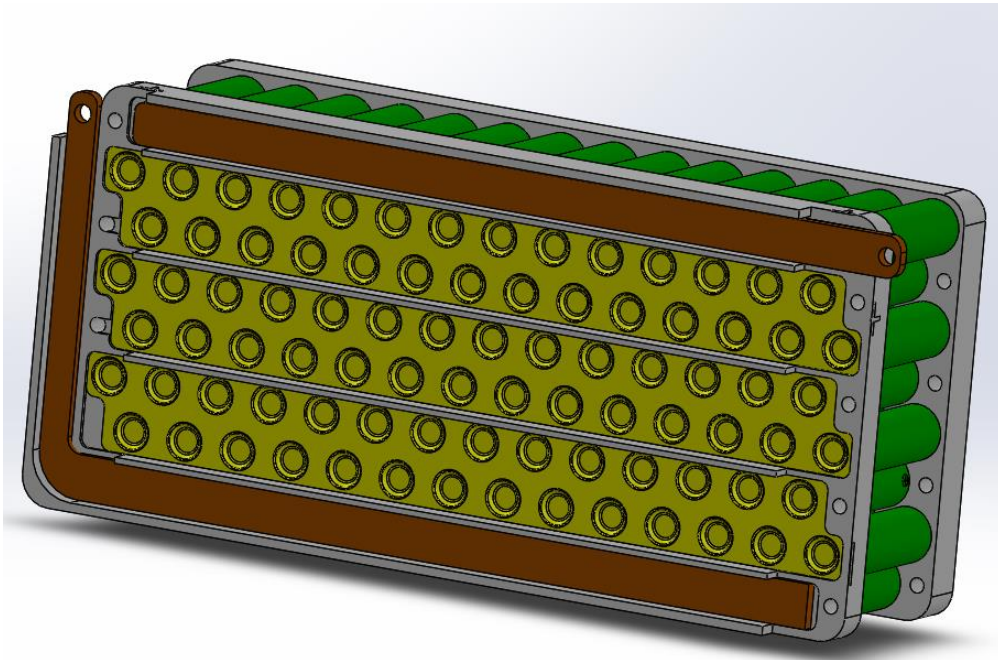


*Figure 52 400V battery single module*

The configuration of the single module shown above is 8s14p . That means a single module is of maximum 33.6 V and capacity of 42 Ah. To get the desired voltage of 400 V we need to connect 12 of these modules in series . The assembly of the modules is shown below.
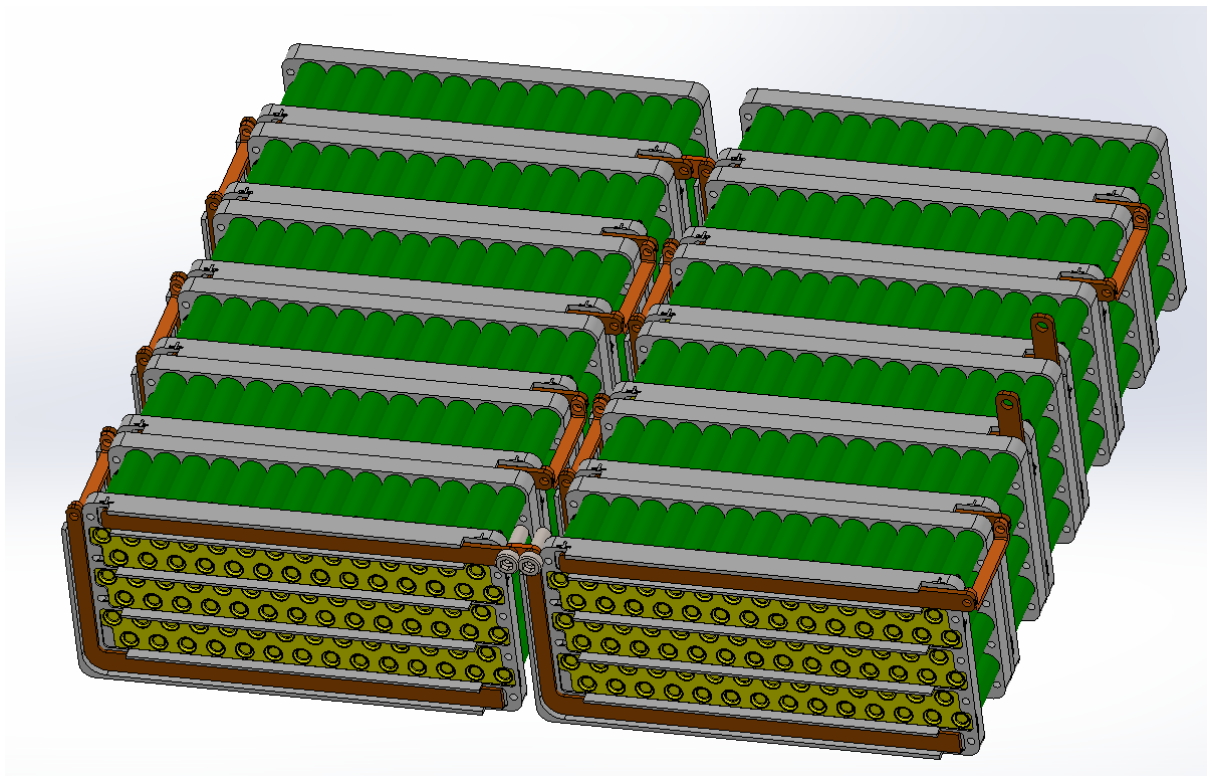


*Figure 53 400V Battery module assembly*

## 4.1.5 Battery Specification

| | |
|---|---|
| Total number of cells | 1344 |
| Peak Voltage | 403.2 V |
| Capacity | 42 Ah |
| Peak Discharge Current | 490 A |
| Maximum Continuous Current | 280 A |
| Peak Battery power | 169.344 KW |
| Peak Battery Energy | 16.9344 Kwhr |

*Table 15 400V battery specification*

## 4.2 Battery Assembly
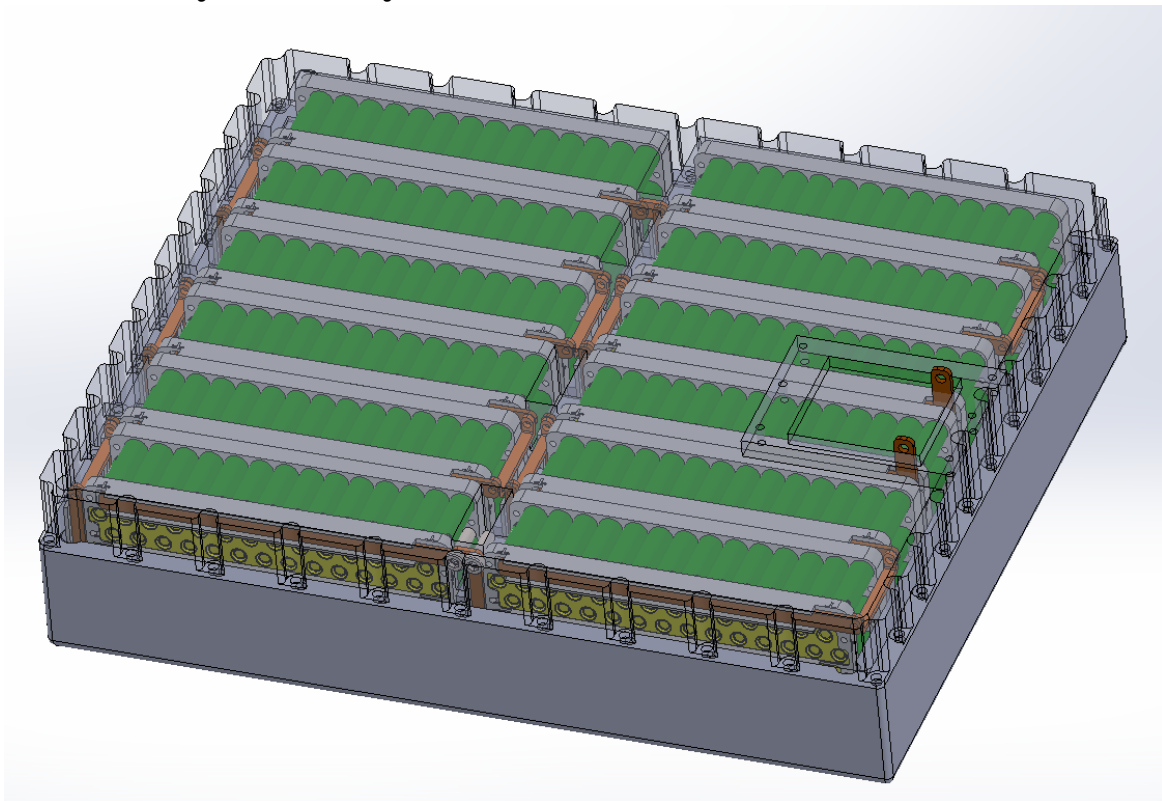


*Figure 54 400V battery assembly with case*

## 4.2.1 FEA Analysis of Battery Case

The battery case material is Aluminium 6061-T6. Dynamic analysis of the cover was performed.

Weight of the battery was calculated for the analysis in the same way we calculated for 12V battery.

| Number of cells | 1344 |
|---|---|
| $W_{cells,400}$ | 64.824 Kg |
| $W_{cellholder,400V}$ | 3 Kg |
| $W_{battery\ case,400V}$ | 20 Kg |
| $W_{fluid,400V}$ | 8 Kg |
| $W_{miscellaneous,400V}$ | 5 Kg |
| $W_{batter,400V}$ | 98 Kg |

We are using the same holder that we used on 12V lithium ion battery . In 400V we are using 12 modules , hence total weight of the cell holder is 3 kg. Weight of the immersive cooling fluid was estimated by subtracting the cell and cell holder volume from the case volume. Miscellaneous Weight comprises all the nickel and copper plates and bus bars, estimated to be 5 kgs.

We require maximum acceleration of the vehicle's Sprung mass during riding on a bump for the dynamic analysis. A Simulink quarter car model was made to calculate the acceleration of the sprung mass of the vehicle. The model and model results are shown below.

The parameters for the Simulink model are given below

| Sprung Mass | 900 Kg |
|---|---|
| Unsprung Mass | 100 Kg |
| Spring Stiffness | 100000 N/m |
| Damping Coefficient | 12000 |
| Tire Stiffness | 225000 N/m |
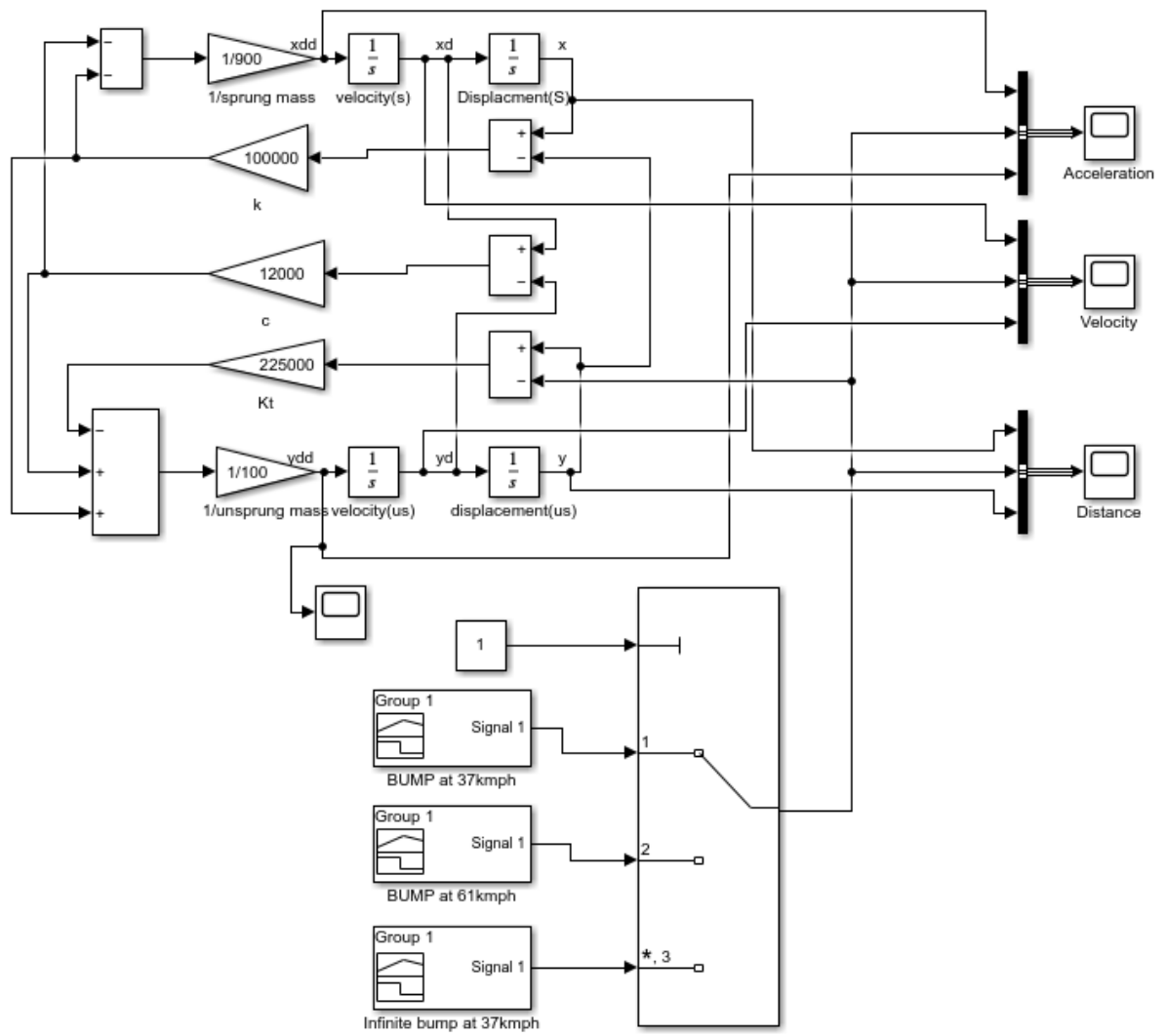
*Figure 55 Quarter Car Model*
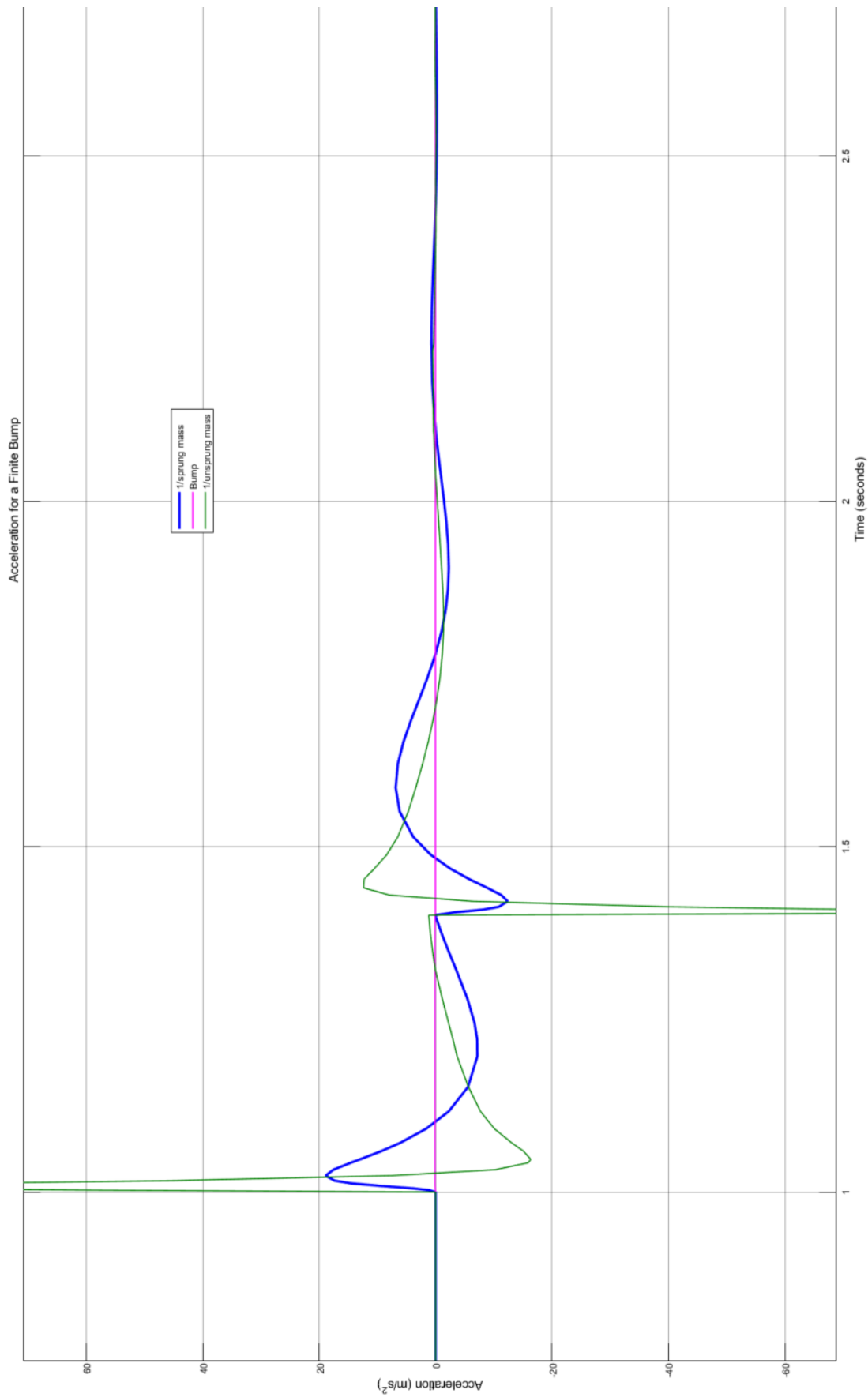
*Figure 56 Acceleration Graph of sprung and unsprung mass on a bump*

The above graph gives us the result for acceleration of sprung and unsprung mass on a bump . The acceleration came out to be 20m/s^2 .

Therefore force on the case = mass* Accelaration = 98 * 20 = 19600 N

Therefore a force of 2000N was applied and FEA analysis was done .
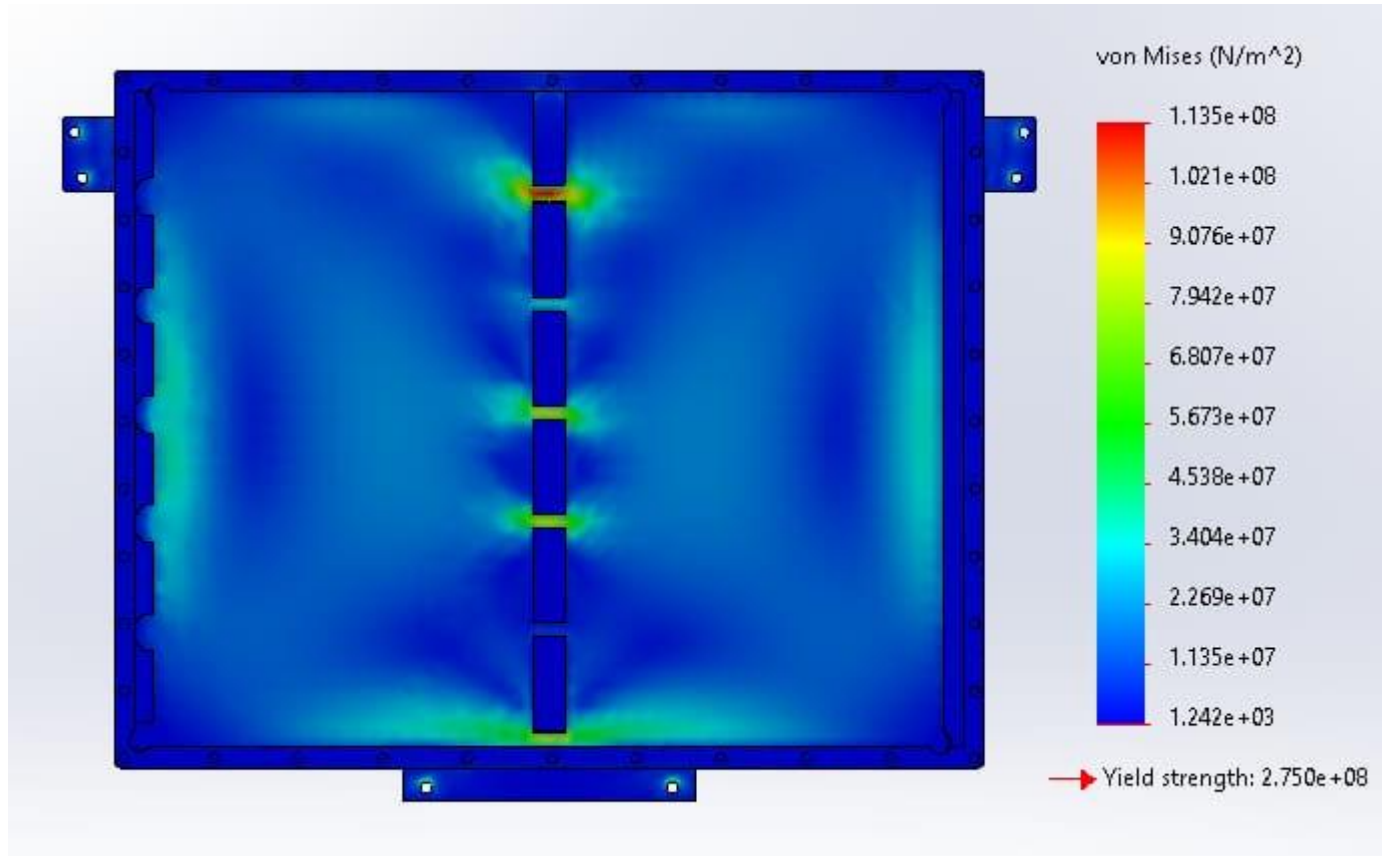


*Figure 57 FEA analysis result of battery case*

| Battery Case Material | Aluminium 6061-T6 |
|---|---|
| Yield Strength | 276 Mpa |
| Maximum Stress | 113.5 Mpa |
| FOS | 2.43 |

### 4.2.2 Battery Case Coating
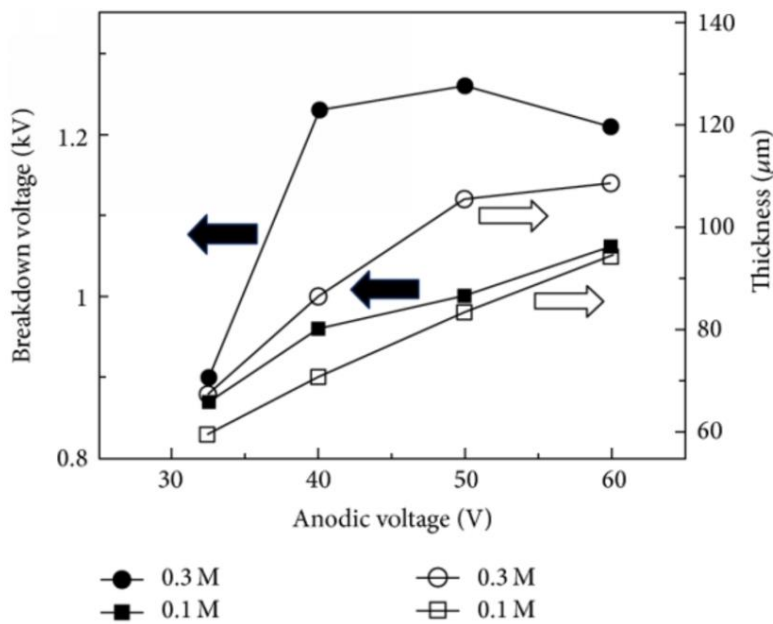


*Figure 58 Graph showing breakdown voltage vs Anodisation thickness*

As we saw earlier in 3.7.1 , 50 microns thick coating of anodized aluminium have a breakdown voltage of 500V. As our battery is 400V , we require a much thicker coating . Therefore, a coating thickness of 120 microns was selected to have a breakdown voltage of at least 1.2 KV, three times the battery voltage .

## 4.3 Components supporting 400 V battery

## 4.3.1 Cooling System

For the design of the cooling system we have to firstly calculate how much heat is generated inside the battery pack during a WLTP cycle. The Worldwide Harmonized Light Vehicles Test Procedure (WLTP) is a chassis dynamometer test cycle for determining light-duty vehicle emissions and fuel consumption. Light-duty vehicle emissions and fuel consumption are measured using a dynamometer test cycle. Characteristics of WLTP cycle are given below.

|  | WLTP Cycle |
|---|---|
| Start Temperature | Cold |
| Cycle Time | 30 min |
| Cycle Length | 23.25 Km |
| Speed | Average : 46.5 Km/h – Maximum: 131 Km/h |
| Stationary Time proportion | 13% |

*Table 16 WLTP Cycle specifications*

The first step in vehicle modelling is to calculate the forces acting on it, in order to determine the total tractive force and power required to drive the vehicle on the WLTP.

rolling resistance force, aerodynamic drag, and inertia force were considered. The other forces like the force required to overcome the angular acceleration of the rotating components because

they were found to be very minimal compared to the other forces. So, the total tractive fore required to overcome the above-mentioned resistive forces is given by equation

$$F_t = F_{aero} + F_{acc}$$      *Equation 20*

Rolling Resistance is given by ,

$$F_{RR} = m * g * f$$      *Equation 21*

Aerodynamic resistance is given by ,

$$F\_aero = 0.5 * \rho * C\_d * A * V^2$$      *Equation 22*

Accelaration Resistance is given by ,

$$F_{acc} = m * g * \delta$$      *Equation 23*

With the above equations we can calculate the the power required at the wheels,

$$P_{wheels} = F_{tractive} * V$$      *Equation 24*

By assuming the transmission efficiencies we can calculate the power required from the motor and battery.

$$P_{motor} = P_{wheels}/(\eta_t)$$

*Equation 25*

*Equation 26*

$$P_{battery} = P_{motor}/(\eta_{motor} * \eta_{converter})$$

## 4.3.2 Battery Modelling

For battery modelling an Internal Resistance model was considered. Following were the formulae used in battery modelling

$$Rint = \frac{Rcell * nseries}{nparallel}$$      Equation 27

$$Idc = \left( \frac{Voc - \left( \sqrt{Vocv - (4 * Rint * Preq)} \right)}{2 * Rint} \right)$$      *Equation 28*

$$Ic = \left( \frac{-Vocv + \sqrt{Vocv + (4 * Rint * Preq)}}{2 * Rint} \right)$$      Equation 29

SOC estimation will be done by current detection method

$$SOC = SOC(t-1) - \left(\frac{1}{C}\right) * \int Itot * dt$$

## 4.3.3 Open circuit voltage

The OCV-SOC modeling is one of the key factors for the OCV-based SOC estimation methods, such as the Shepherd model , Nernst model , Unnewehr universal model , combined model , exponential model , polynomial model , and ECMs model. [7] Fadlaoui Elmahdi performed OCV estimation by fitting the curve using genetic algorithm method .

They used a Samsung 30Q 18650 cell , which have the exact specifications of SONY 18650. They used  a 8th order polynomial equation written below to have the best fitting performance .

$$Vocv = ko + k1 * SOC + k2 * SOC^2 + k3 * SOC^3 + k4 * SOC^4 \quad \textit{Equation 31}$$
$$+ k5 * SOC^5 + k6 * SOC^6 + k7 * SOC^7 + k8$$
$$* SOC^8$$

Where ( k0,k1…k8) are the parameters that were estimated using genetic algorithm method.

Genetic algorithms are heuristic search and optimization techniques inspired by natural evolution that can be used to find the global minimum for highly nonlinear problems. They are based on an evolutionary model .

The (ko , k1 , …k8) parameters are listed below

| ko | k1 | k2 | k3 | k4 | k5 | k6 | k7 | k8 |
|---|---|---|---|---|---|---|---|---|
| 2.85 | 4.80 | -17.80 | 38.59 | 4.91 | -210.52 | 433.98 | -368.45 | 115.81 |

*Table 17 OCV polynomials constants*

The internal resistance of the battery pack will be responsible for heat generation which can be calculated by equation below,

$$Q_{gen} = I^2 * R_{tot} \quad \textit{Equation 32}$$

The total resistance of the battery is the summation of total internal resistance of the cells plus the resistance of the nickel and copper plates used. We calculated in 3.5 the resistance of nickel and copper plates combined . Total resistance of nickel and copper plates was 511 **μΩ.**

**R$_{cell,400V}$ = 0.084 Ω**

**Therefore R$_{internal,400V}$ = 0.090 Ω**

# 4.3.4 SIMULINK MODEL
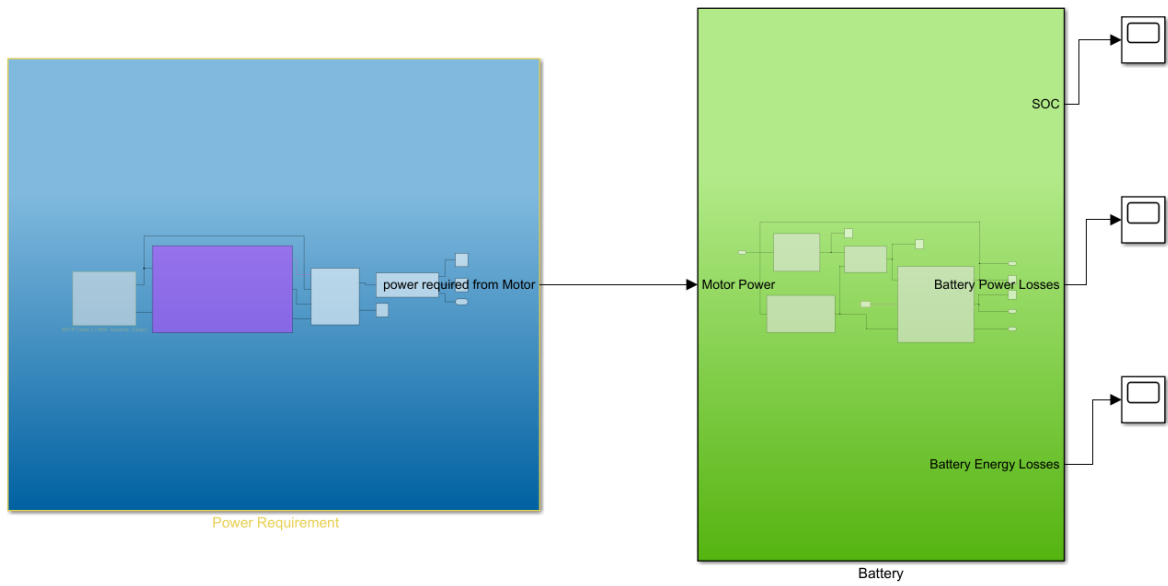


*Figure 59 Lithium ion battery internal resistance model*
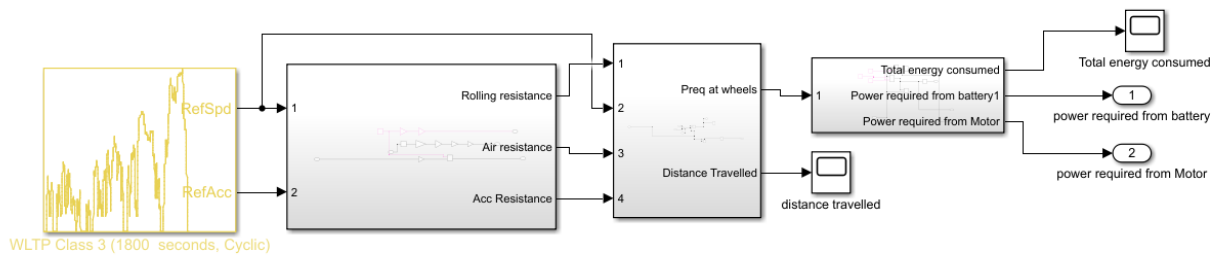


*Figure 60 Power requirement model on a WLTP Cycle*
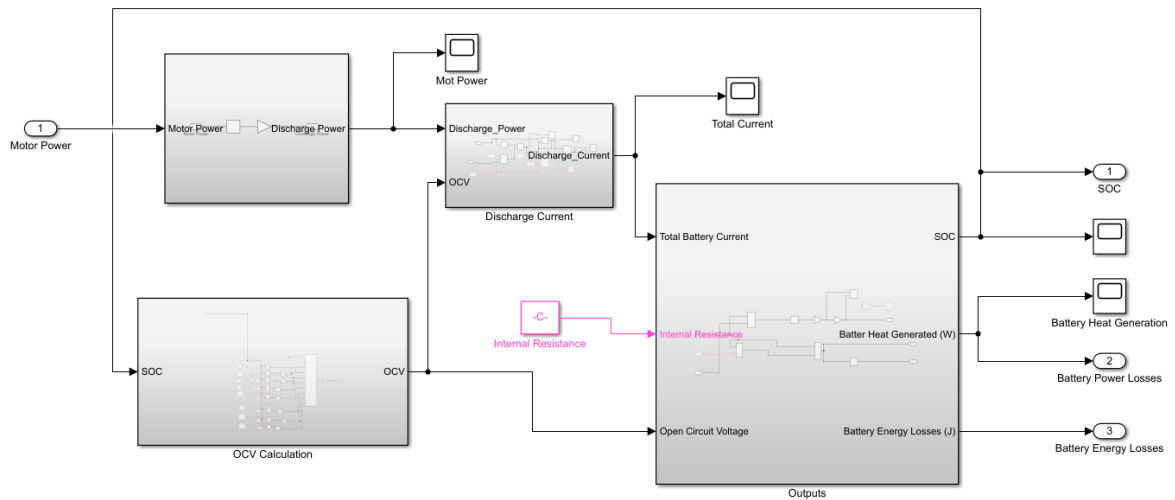


*Figure 61 Lithium Ion Battery Simulink Model*

## 4.3.5 Heat Exchanger Design

An air cooled microchannel type heat exchanger has to be designed . The entire theoritical process begins with Equation given below for the heat transfer rate of the radiator. The subscript 'novec' refers to the immersive fluid 3M Novec 7200.

$$q = m_{air} * Cp_{,air} * (T_{air,in} - T_{air,out,}) = m_{novec} * (T_{(novec,in)} - T_{(novec,out)}) \qquad \text{Equation 33}$$

- **Internal Flow of Water**

The hot Novec fluid travels from the battery , travels through the tubes of the radiator.

$$D_{hydraulic} = \frac{4 * A_{tube}}{P_{tube}} \qquad \text{Equation 34}$$

Because the cross section is not circular, the hydraulic diameter must be used. The Reynolds number can then be calculated using the hydraulic diameter. The wetted perimeter of the tubes is required in the hydraulic diameter equation. The difference in diameter between the outer and inner tubes is so small that the outer perimeter is employed for ease.

- **Mean Temperature of Water**

To determine the fluid's material properties, the average temperature of water must be calculated. At this temperature, the characteristics will be interpolated. Density, thermal conductivity,Prandtl number, and specific heat are required qualities.

- **Velocity**

$$V_{water} = \frac{Q_{water}}{N_{tube} * A_{tube}} \qquad \text{Equation 35}$$

To compute the Reynolds number, the velocity of the Novec fluid through each tube must be determined. The chosen radiator determines the number of tubes

- **Reynolds Number**

$$Re_{novec} = \frac{\rho_{novec} * v_{novec} * D_{hydraulic}}{\mu_{novec}} \qquad \text{Equation 36}$$

- **Nusselt Number**

The air flow can be expected to be similar to parallel flow over a flat plate based on the shape of the tubes. The flow is said to be laminar throughout the operation because it never surpasses the crucial Reynolds number for a flat plate, Re = 5x105.

$$Nu_{air} = 0.664 * Re_{air}^{0.5} \Pr_{air}^{0.5} \qquad \text{Equation 37}$$

- **Convective Heat Transfer Coefficient for Air Flow**

$$h_{air} = \frac{Nu_{air} * K_{air}}{W_{tube}}$$   Equation 38

- **Fin Dimensions and Efficiency**

The radiator's fins have a sinusoidal form. The troughs of the fins are in contact with the lower adjacent tube, while the peaks of the fins are in contact with the upper adjacent tube. The fins disperse the heat from the tubes. The fins and tubes are cooled by the air that is blown over the radiator by the fan.  The fins are considered to be straight rather than sinusoidal to simplify the geometry for ease of calculation. Figure 6 illustrates this. Because the shape and position of the real fins are so near to the straight design, this is a small geometric change. The formulas for calculating fin efficiency are listed below.The fin efficiency equation takes into account the geometry of the fin and its dimensions to find the efficiency the fin will have

$$\eta_{fin} = \frac{\tanh(mL_c)}{mL_c}$$   Equation 39
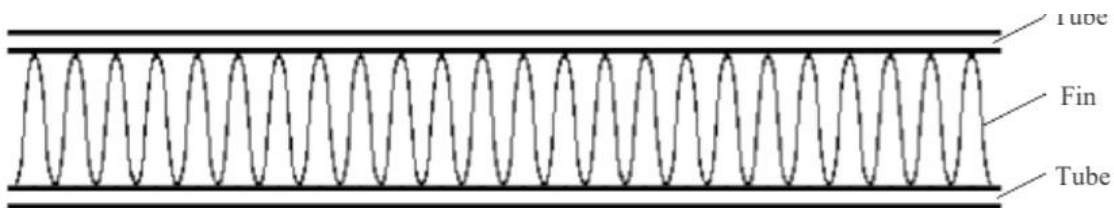


Figure 5: Actual fin geometry
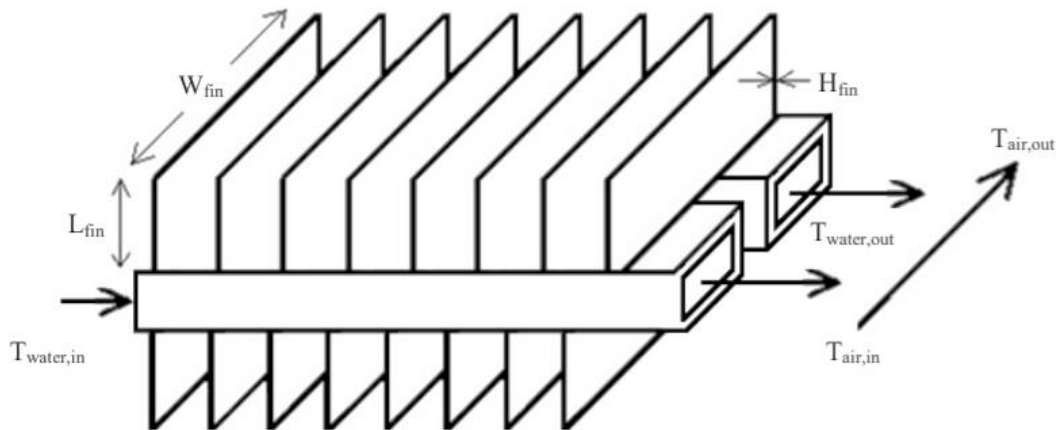


*Figure 62 Fin Geometry*

- **Overall Surface Efficiency**

Because the defects of the flow around the fins must be considered, the overall surface efficiency is required for the external air flow.

$$\eta_o = 1 - \frac{(N_{fin}A_f)}{A_{(fin,base)}}$$   Equation 40

- **Effectiveness-NTU Method**

The effectiveness of the system is determined using the Effectiveness-NTU approach. It is necessary to calculate the entire heat transfer coefficient. Because the defects of the flow surrounding the fins must be considered, the surface efficiency is required for the external flow of air. Using the convective heat transfer coefficients of both the internal and external flows, the UA is calculated. This value is then used to calculate the NTU

- **Overall Heat Transfer Coefficient**

$$UA = 1 / \left( \frac{1}{\eta_o h_{air} A_{external}} + \left( \frac{1}{h_{novec} A_{internal}} \right) \right) \qquad \textit{Equation 41}$$

- **Effectiveness**

Both fluids remain unmixed in the radiator's cross-flow single pass design. This corresponds to a formula for calculating effectiveness. This equation, however, demands that the heat capacity ratio, Cr, be equal to 1. Because the calculated heat capacity ratio is 0.827, the efficiency is merely a near approximation of the genuine number.

$$\varepsilon = 1 - e^{\left[ \left( \frac{1}{C_r} * NTU^{0.22} \right) * \left( e^{\left( -C_r * NTU^{0.78} \right)} - 1 \right) \right]} \qquad \textit{Equation 42}$$

- **Heat Transfer Rate**

To determine the projected heat transfer rate, the maximum heat transfer rate must be determined. Once this is known, a modified version of the initial thermal energy calculation is used to calculate the final output temperature of both the hot and cold fluids. These outlet temperatures must be compared to the originally estimated outlet temperatures until they are equal. The theoretical values for both air and water iterated output temperatures are utilized to compare with the experimental results.

- **Max Heat Transfer Rate**

$$q_{max} = C_{\min(T_{water,in} - T_{air,in})} \qquad \textit{Equation 43}$$

- **Predicted heat transfer**

$$q_{predicted} = \varepsilon * q_{max} \qquad \text{Equation 44}$$

$$T_{air,out} = T_{air,in} - \frac{q_{predicted}}{C_{air}} \qquad \textit{Equation 45}$$

#### 4.3.6 Results
- Heat Generated in Battery
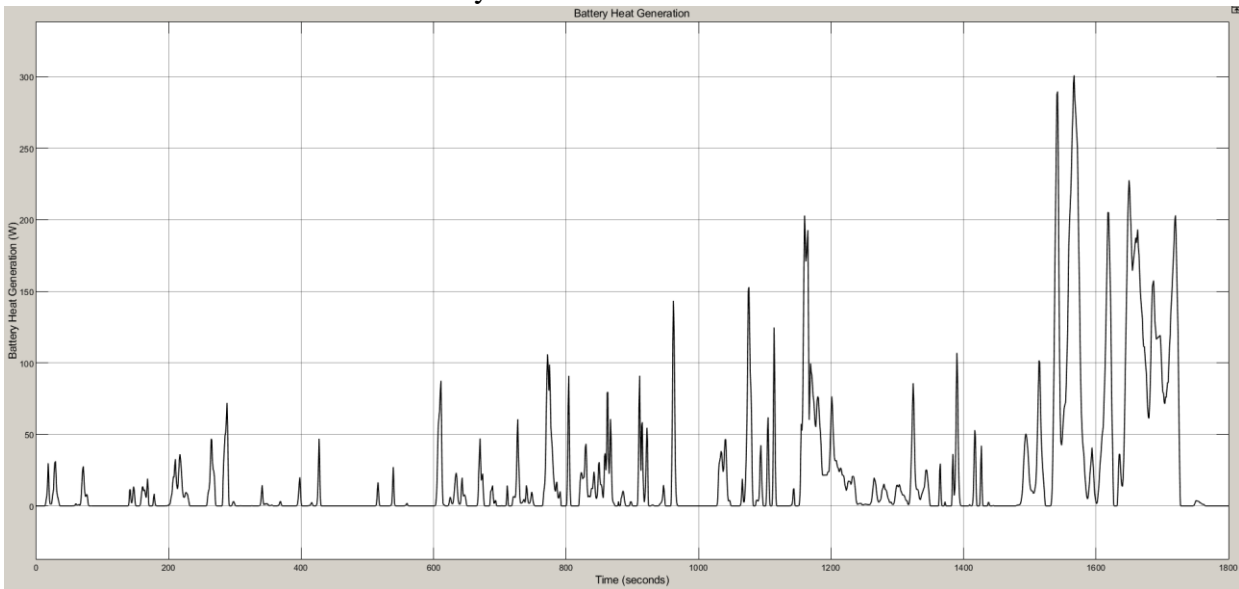


*Figure 63 400V battery heat generated during a WLTP Cycle*

- SOC
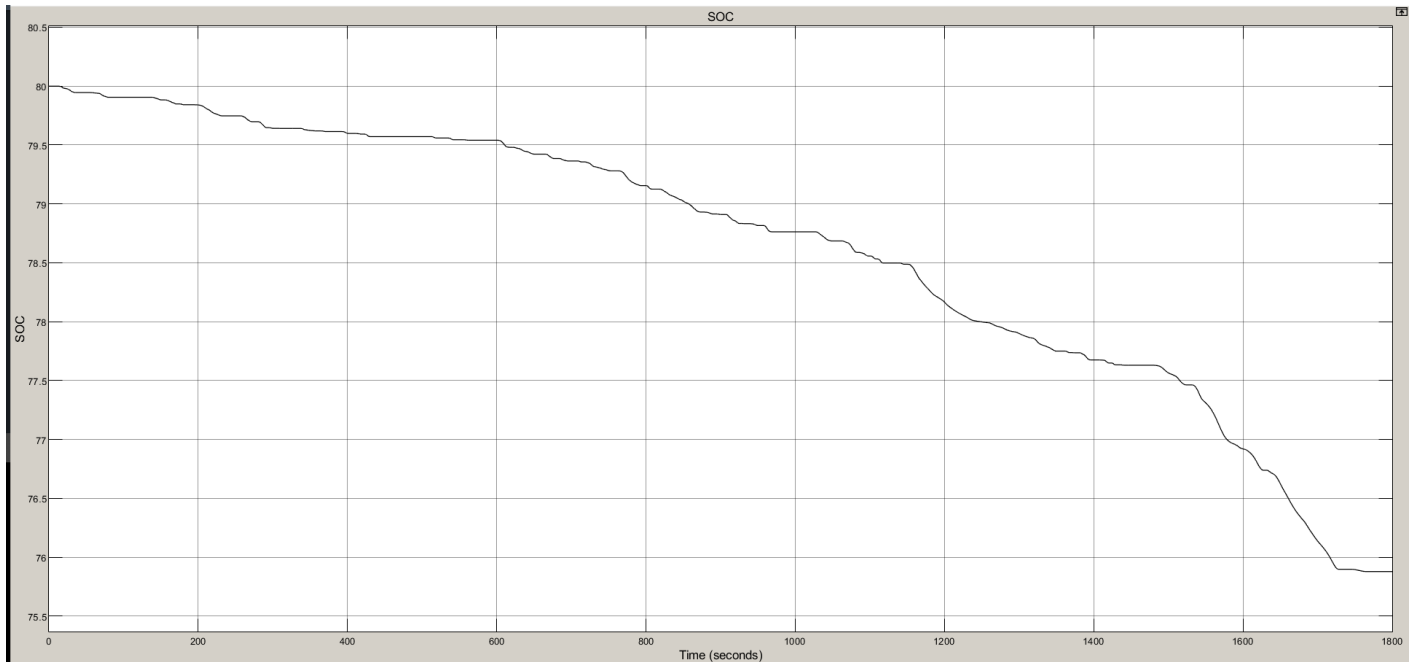


*Figure 64 SOC Curve during a WLTP Cycle*

## 4.3.7 Heat Exchanger Specifications

Many iterations were done with a different flow rate of the Novec fluid to get the desired heat transfer.

We will mount the heat exchanger on the battery pack side , which limits our radiator length and height . As our 400V battery pack height is 150mm , our heat exchanger height can not be more than that. The length of our radiator is kept 500mm.

| $L_{radiator}$ | $H_{Radiator}$ | $W_{Radiator}$ | $W_{tube}$ | $H_{Tube}$ | $L_{fin}$ | $W_{fin}$ | $H_{fin}$ | $N_{tube}$ | $N_{fin}$ |
|---|---|---|---|---|---|---|---|---|---|
| (m) | (m) | (m) | (m) | (m) | (m) | (m) | (m) | | |
| 0.5 | 0.15 | 0.037 | 0.016 | 0.003 | 0.005 | 0.037 | 0.00001 | 37 | 600 |

*Table 18 Heat exchanger dimensions*

| $\rho_{novec}$ | $C_{p,novec}$ | $Pr_{novec}$ | $k_{novec}$ | $\mu_{novec}$ | $LPM_{novec}$ |
|---|---|---|---|---|---|
| (kg/m$^3$) | (J/Kg-K) | | (W/m-k) | Pa.s | (Litres per min) |
| 1463 | 1214.73 | 15.541 | 0.068 | 0.00087 | 6 |

*Table 19 Properties of NOVEC at Average Temperature*

| $\rho_{air}$ | $C_{p,air}$ | $Pr_{air}$ | $k_{air}$ | $V_{air}$ | $Q_{air}$ |
|---|---|---|---|---|---|
| kg/m$^3$ | J/Kg-K | | W/m-k | m/s | m$^3$/s |
| 1.15 | 1004 | 0.74 | 0.027 | 7.17 | 0.14 |

*Table 20 Properties of air at average temperature*

| $h_{novec}$ | $h_{air}$ | UA | NTU | $\varepsilon$ | $q_{predicted}$ |
|---|---|---|---|---|---|
| W/m$^2$K | W/m$^2$K | M$^2$kg/Ks$^3$ | | % | W |
| 160.40 | 58.87 | 86.46 | 0.53 | 0.365 | 1180.84 |

*Table 21 Final Results for radiator*

| $T_{Novec,in}$ | $T_{Novec,out}$ | $T_{air,in}$ | $T_{air,out}$ |
|---|---|---|---|
| deg Celsius | deg Celsius | deg Celsius | deg Celsius |
| 45 | 41 | 25 | 32.3 |

*Table 22  Theoritical Temperature of fluids through radiator*

Apart from the methodology that has been explained so far, another design parameter has an important role in the overall process. That is the pressure drop for both air and Novec sides. To do so, friction factor and the mass flux parameter $G$ which is based on minimum free flow area need to be estimated. For the novec side, it yields

$$G_{a,n} = \rho_{a,n} u_{a,n} \qquad \text{Equation 46}$$

$$f_n = (0.79 \log(Re_w)^{-1.64})^{-2} \qquad \text{Equation 47}$$

And the pressure drop is then calculated with

$$\Delta P_{Novec} = \frac{4000 f_n (L_t G_n^2)}{2 D_h \rho_n} \qquad \text{Equation 48}$$

For the air side, in addition to previous parameters, coefficient of exit and entrance losses and the density at the exit need to be estimated.

This relation is described by the following

$$\sigma = {A_f}\big/{A_r}$$

$$K_e = (1 - \sigma)^2$$

$$K_c = 0.42(1 - \sigma^2)^2$$

The friction factor and the pressure drop are then defined as [8]

$$f_a = {96}\big/{Re_a}$$

$$\Delta P_a = \left(\frac{G_a^2}{2\rho_a}\right)\left((1 - \sigma^2 + K_c) + \left(\frac{4f_a L_c}{D_h}\right)\left(\frac{\rho_a}{\rho_{a_e}}\right) + 2\left(\frac{\rho_a}{\rho_{a_e}}\right) - (1 - \sigma^2 - K_e)\left(\frac{\rho_a}{\rho_{a_e}}\right)\right)$$

| ΔP results | Value | Unit |
|---|---|---|
| $\Delta P_{novec}$ | 15.38 | Kpa |
| $\Delta P_{air}$ | 166 | Pa |

*Table 23 Pressure drop calculation results*

## 4.3.8 Pump Selection

In the above section we calculated pressure drop across the heat exchanger. This information is critical for the selection of the Novec pump. However, we need to know pressure drop across our battery pack too in order to choose the right pump for our cooling system. Prahit Dubey in

his research paper compared immersion cooling and Cold-plate based cooling for automotive Li-ion Battery modules. [9] In his research he did CFD analysis of one module whose dimensions are same as ours. There are 14 cells connected together in the direction of flow which is same as ours . Hence we can use their thesis results to estimate the pressure drop across our battery pack . In the graph below we can comprehense that at 6LPM we a pressure drop of 0.6 psi or 4.13 kpa . We have six of these modules in the direction of flow , so we can assume that a total of 3.6 psi or 24.82 kpa of pressure drop will occur.
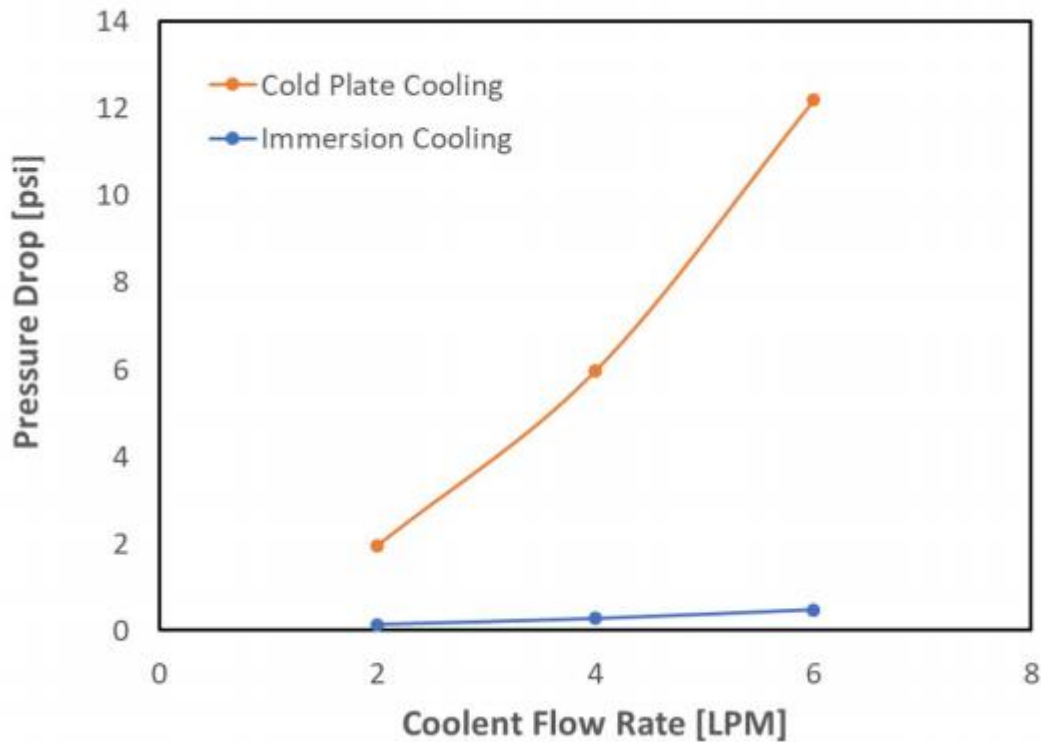


*Figure 65 Pressure drop vs Coolant flow rate for immersive and cold plate cooling*

| LPM | $\Delta P_{battery}$ (kpa) |
|---|---|
| 6 | 24.82 |

From the above calculations, we can determine that we require a pump that can give at least 6 LPM and pressure of 45kpa.

For our purpose AEM high flow rate fuel pump will be suitable. Below is the performance graph of the pump.

There will be other pressure losses as well due to piping connections , hence our pump pressure should be higher that 45Kpa. In the pump's performance curve, we can see that at maximum flow rate of 425 LPH or 7LPM , the pump gives 40 psi or 2.7 bar of pressure , which sufficient for our design
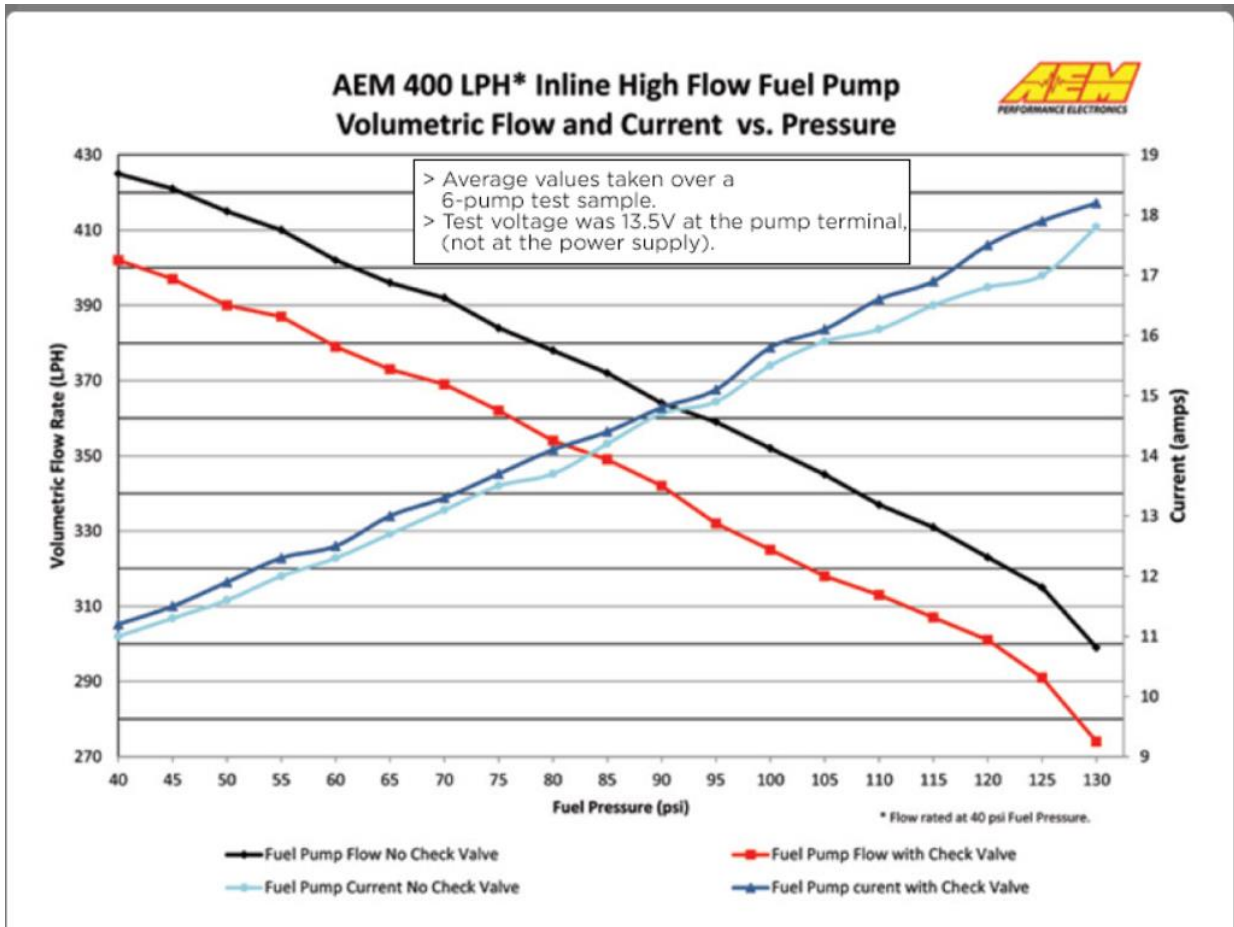
*Figure 66 Novec Pump Performance curve*

## 4.3.9 Fan Selection

AS our heat exchanger is 150 mm in height, the largest possible fan with best performance curve was selected.

SPAL VA39-A101-45S fan was selected. It operates on 12V and can also operate in push or pull configuration and have maximum airflow rate of 520 m$^3$/hr. It has a fan diameter of 140mm and a shroud diameter of 144mm. So this is the biggest fan that can be fitted to a heat exchanger of height 150mm. The fan performance curve is given below.
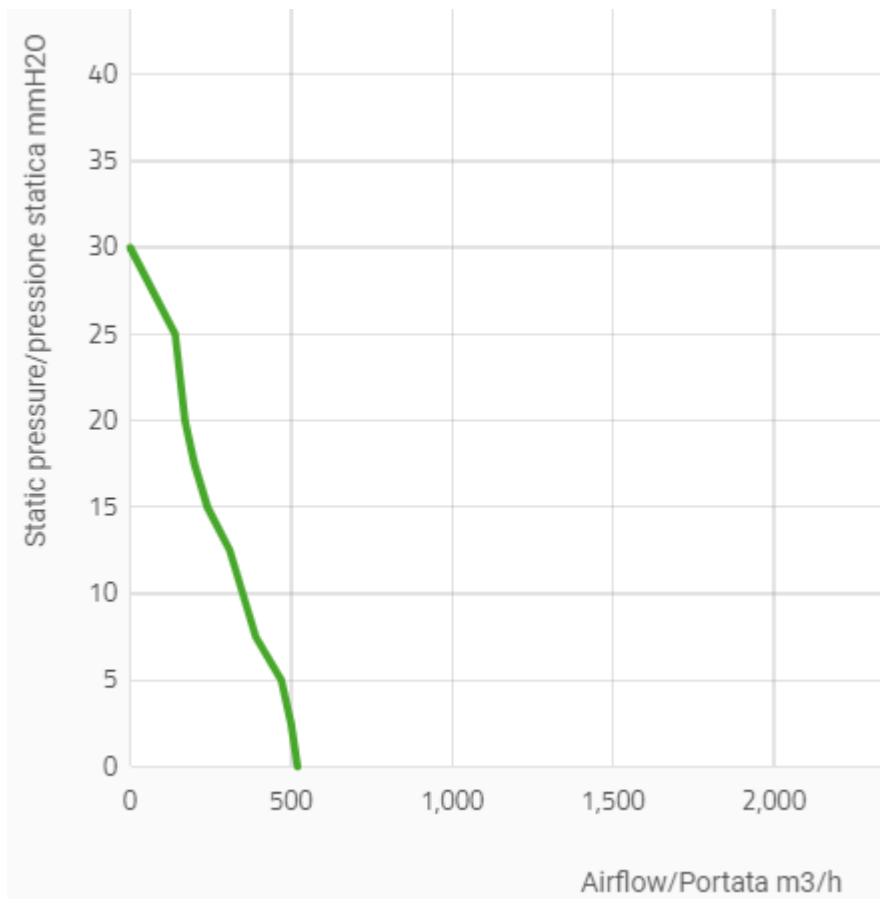
*Figure 67 Fan performance curve*

As the length of our radiator is 500mm, we can use three fans to cover the heat exchanger and have better cooling.



*Figure 68 SPAL VA39-A101-45S*

## 4.4  Cooling Circuit
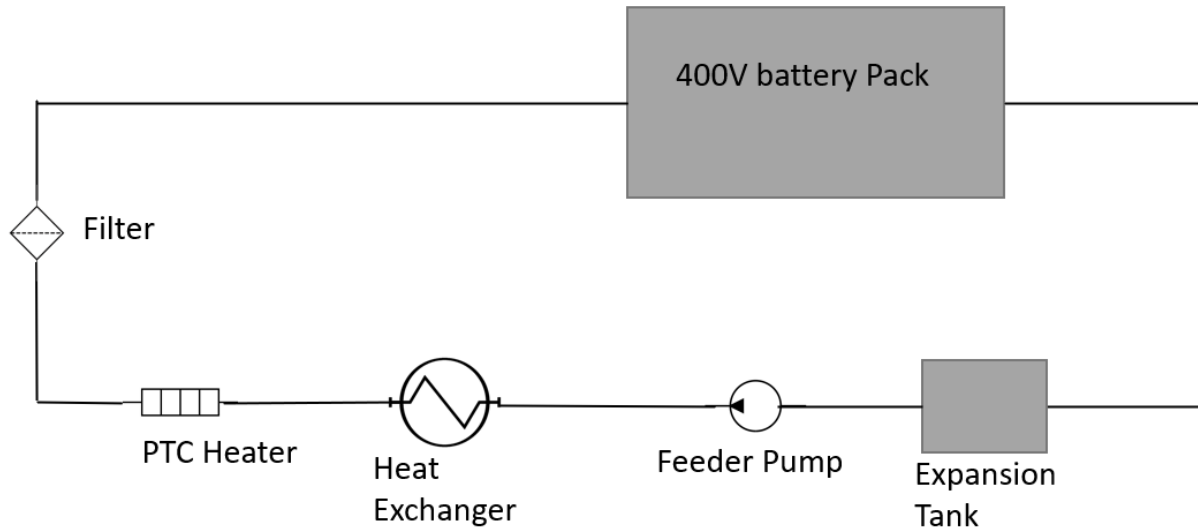


*Figure 69 400V battery Cooling Circuit*

## 4.5  BMS

BMS is the most important component of the battery pack. We are using Orion BMS  by Ewert Energy Systems. It is designed to manage and protect lihium ion battery pack and is suitable for use in electric, plug-in hybrid and hybrid electric vehicles as well as stationary applications. We have 96 cells connected in series, hence we require a BMS which can at least measure 96 cells.  The Orion BMS 2 which we are using can measure upto 180 cells.

## 4.5.1 Discharge Circuit

The discharge circuit consists of an Amphenol PCD 500Amp fuse connected in series with a 500Amp relay which the BMS controls.  The precharge circuit is connected in parallel with the 500 Amp relay.

When a high-voltage system with downstream capacitance is first turned on, it may be subjected to harmful inrush current. This current, if not restrained and controlled, can cause substantial stress or damage to other system components. To slow the charging of the downstream capacitance, a precharge circuit is employed to minimize the inrush currentIt's important for the proper operation and protection of components in high-voltage applications. Precharging extends the life of electric components and improves system reliability. Before the main contactors are allowed to close, a precharge circuit permits the current to flow in a controlled manner until the voltage level rises to very near the source voltage. A separate, more small contactor is frequently linked in series with a resistor in the precharge circuit. The primary contactor is then linked in parallel with these two components. The precharge circuit is often built on the positive terminal, although it might also be installed on the negative

terminal.
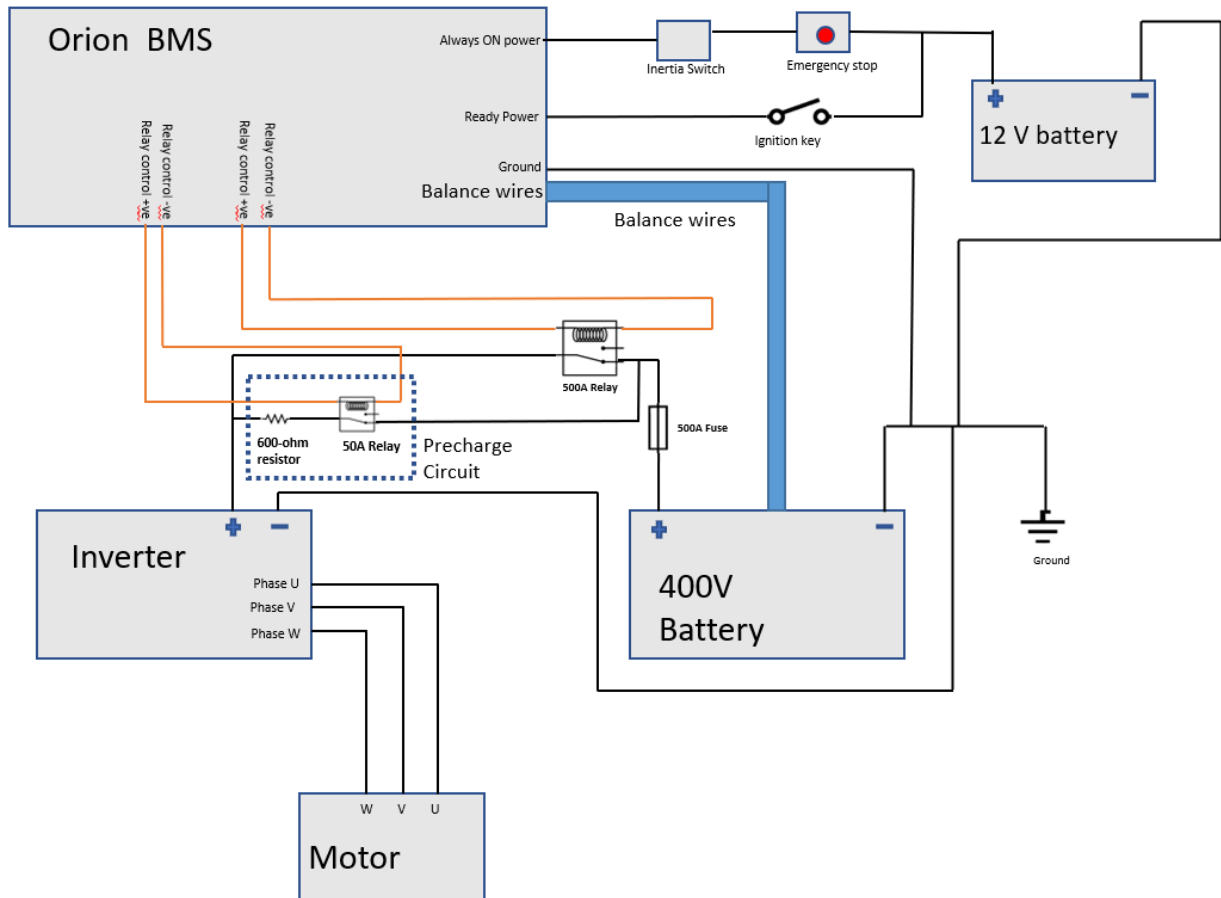


*Figure 70 Discharge Circuit*

## 4.5.2 Charge Circuit

- **Elcon/ TC charger**

    The Elcon charger is deactivated by default in this configuration if the BMS is disconnected or fails (fail safe.) The 12-15V power supply is energized when AC power is present and supplies power to the Orion BMS's CHARGE power supply input. When the BMS senses electricity at the CHARGE power supply input, it performs self-testing and checks to ensure the battery is capable of accepting a charge. When the BMS is ready to take a charge, it pushes the charger safety signal to ground, which activates RELAY2 in the diagram below. When RELAY2 is turned on, the Elcon charger is turned on and the battery pack is charged. When the BMS detects that the battery is full or no longer accepts a charge, it disables the charger safety signal, which floats high and disables RELAY2, thereby turning off the charger.
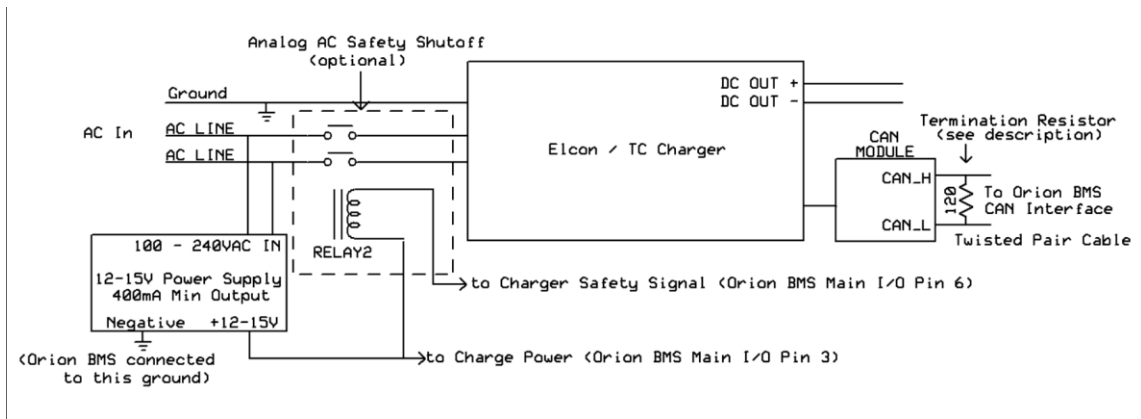
*Figure 71 TC Charger Circuit*

- **Chademo Charger**

CHAdeMO is a common DC fast charging protocol that can provide up to 62.5 kW of DC output power and is widely utilized across the world (500vDC, 125A maximum). Because of the protocol's simple architecture and low integration requirements, it's appropriate for a wide range of automotive and mobile applications. The CHAdeMO protocol communicates with the BMS in two ways: through digital communications (CANBUS) for setting operational parameters and through the Charger Safety relay output for sending the "Charge Enable" signal to the charging station.
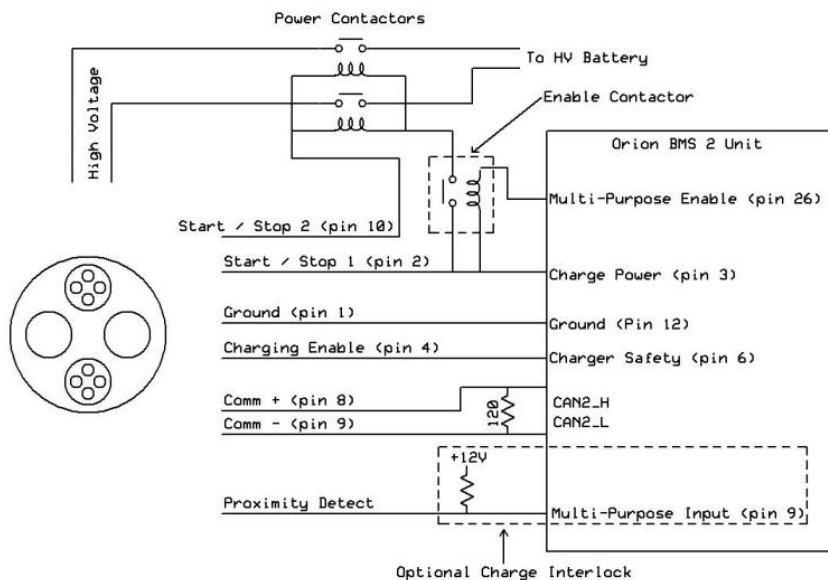


*Figure 72 Chademo Charge Circuit*

## 4.6 Final Assembly
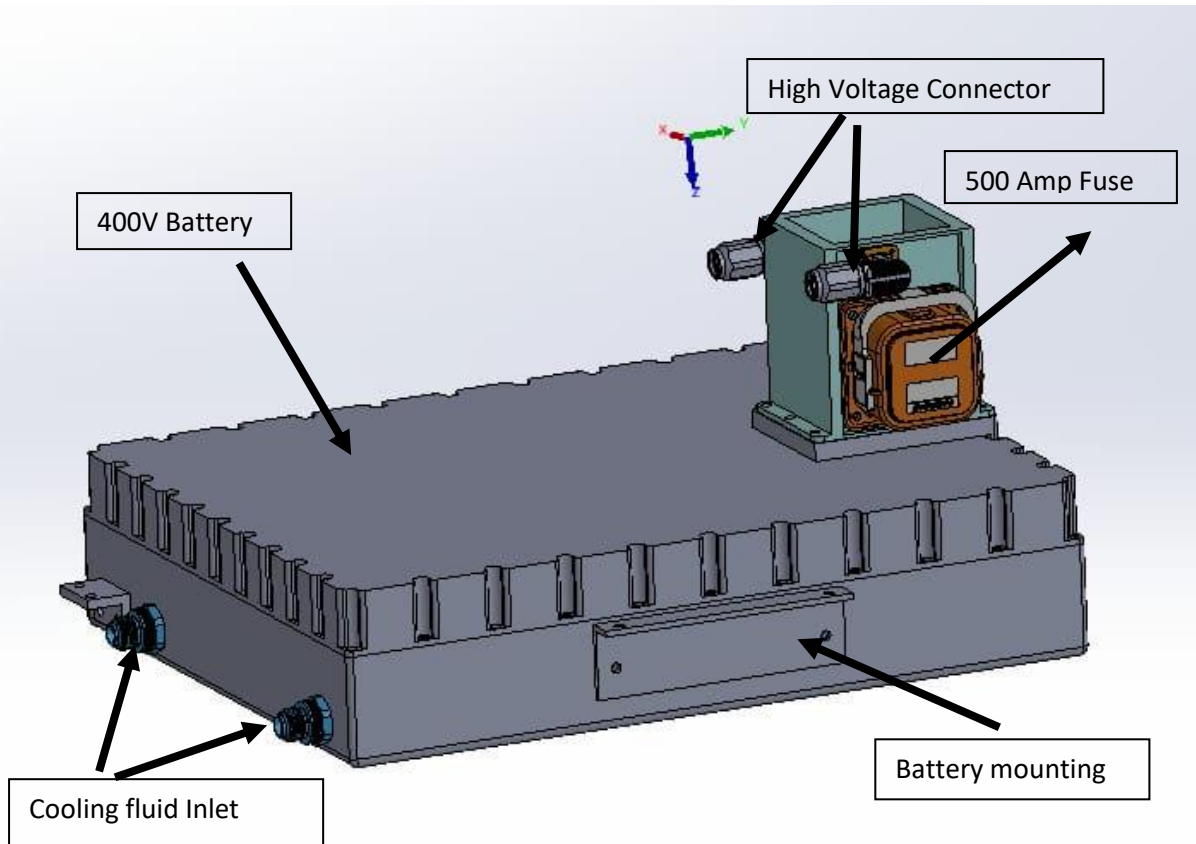


*Figure 73 400V battery final assembly along with high voltage connector*

In the above figure we can see the 400V Battery assembly along with the 500 Amp fuse and high voltage connector. there are two inlet ports on the left side of the battery for a homogenous distribution of the flow.

# 5 Conclusion

This thesis aimed to design and manufacture a 12V immersive cooled lithium-ion battery as well as designing a 400V battery . We have numerous benefits , when compared to a 12V lead acid battery .

Below is a table comparing our 12 Vlithium ion battery to a lead acid battery of same specifications.



*Figure 75 Varta 12V 80 Ah Lead Acid Battery*
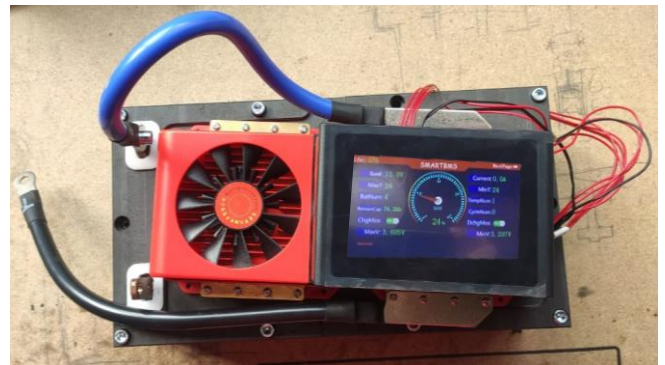


*Figure 74 12V Lithium-ion Immersive Cooled Battery*

| Parameters | 12V Li-Ion Immersive Cooled | Varta AGM 840 |
|---|---|---|
| Battery Capacity ( Ah) | 84 | 80 |
| Peak Current (Amp) | 980 | 800 |
| Battery Weight ( Kg) | 13 | 22.76 |
| Peak Voltage (V) | 16.8 | 13.2 |
| Length (mm) | 295 | 315 |
| Width (mm) | 140 | 175 |
| Height (mm) | 120 | 190 |

*Table 24 Table comparing Varta 12V lead acid and !2V lithium ion battery*

Our lithium-ion battery is 10.3 kg lighter than a standard lead acid battery of the same specification, as shown in the table. Furthermore, because we're utilizing a smart BMS, we can track our battery's state of charge as well as individual cell voltage and temperature. The battery's life cycle can simply be extended by monitoring it. The battery's stiffness and

endurance are ensured by the aluminum battery housing. The battery can even take a massive blow in the event of a vehicle accident, protecting the lithium ion cells. If one of the pack's cells malfunctions and produces a spark, the spark is extinguished instantaneously by the dielectric and nonflammable liquid Novec fluid 3M. It has been found that in the event of an accident, electric automobiles catch fire quite quickly due to battery pack and lithium ion cell penetration. When compared to alternative plastic enclosures, our aluminum case provides the most protection against penetration.

A maximum of 300W of heat is generated during a WLTP cycle, according to the results of the Simulink model for the 400V in 4.3.6, and our cooling system can dissipate 1000W of heat at 6LPM of coolant. Furthermore, we can retain our cell temperature in the ideal range of 30-45 degrees Celsius with the help of the PTC heater.

Furthermore, the cooling system we've included is considerably easier to construct and deploy than alternative liquid cooling systems, such as the one shown in Figure 12 for the Tesla Model 3. Our cooling system has the advantage of being simple to manufacture and assemble. Compared to cold plated cooling system like used in GM Chevrolet Volt again, it is less complex as we don't have to manufacture separately the cold plate with cooling lines that are complex to manufacture.

# 6 References

[1]     P. C. Bhatia, "THERMAL ANALYSIS OF LITHIUM-ION BATTERY PACKS AND THERMAL MANAGEMENT SOLUTIONS," The Ohio State University, 2013.

[2]     S. A. M. F. J. S. Khateeb. S, "Thermal Management of Li-ion Battery with phase change material for electric scooters: Experiment Validation," Journal of Power Sources , 2005.

[3]     C. ,. M. H. G. H. M. a. J. F. Kuper, "Thermal management of Hybrid Vehice Battery Systems," EVS24, Norway.

[4]     Valeo, "Battery Thermal Management for HEV & EV: Technology Overview," 2010.

[5]     P. A. DANIEL CELA, "Study of a 12V Li-ion Battery," Department of Electrical Engineering, CHALMERS UNIVERSITY OF TECHONOLOGY, Gothenburg, SWEDEN, 2018.

[6]     C.-C. C. T.C. Cheng, "The Electrical and Mechanical Properties of Porous Anodic 6061-T6 Aluminum Alloy Oxide Film," *ResearchGate , Journal of Nanomaterials,* 2015.

[7]     L. I. Fadlaoui Elmahdi1, "Fitting the OCV-SOC relationship of a battery lithium-ion using," *ICIES,* 2020.

[8]     O. C. Jones Jr., "An Improvement in the Calculation of Turbulent Friction in Rectangular Ducts," *Journal of Fluid Engineering,* no. ASME, 1976.

[9]     G. P. ,. A. K. S. Prahit Dubey, "Direct Comparison of Immersion and Cold-Plate Based Cooling," *MDPI.*

[10]    "GM cars use plastics in power storage," [Online]. Available: https://www.plasticsnews.com/article/20121119/NEWS/311199979/gm-cars-use-plastics-in-power-storage.

[11]    J. Warner, The handbook of Litium ion Battery pack design.

[12]    "Aluminum Alloys: Do You Know the Difference?," [Online]. Available: http://blog.parker.com/aluminum-alloys-do-you-know-the-difference.

[13]    "The Electrical and Mechanical Properties of Porous Anodic 6061-T6 Aluminum Alloy Oxide Film," [Online]. Available: https://www.researchgate.net/publication/276092462_The_Electrical_and_Mechanical_Properties_of_Porous_Anodic_6061-T6_Aluminum_Alloy_Oxide_Film.

[14]    "Fracture Toughness Measurement for Aluminium 6061-T6 using Notched Round Bars," [Online]. Available:

https://www.researchgate.net/publication/331887724_Fracture_Toughness_Measur
ement_for_Aluminium_6061-T6_using_Notched_Round_Bars.

[15] J. Warner, "The Handbook of Lithium-ion Battery Pack Design , Chemistry ,
Components, Types, & Terminology," ELSEVIER.

[16] A. A. S. B. a. M. K. Pesaran, "An Approach for Designing Thermal," Fourth Vehicle
Thermal Management Systems , 1999.

[17] "Volvo's plug-in hybrid battery system," [Online]. Available:
https://www.drivingthenation.com/volvo-keeps-options-open-for-battery-plans-3-
cyl/.

[18] B. X. ,. B. L. Ruifeng Zhang, "A Study on the Open Circuit Voltage and State of," *MDPI,*
2018.

[19] A. W.M.Kays, Compact Heat Exchangers, McGraw-Hill, 1964.

[20] "COPPER BUSBAR RATING," [Online]. Available:
https://www.australwright.com.au/technical-data/advice/copper-busbar-rating/.

[21] "https://www.australwright.com.au/technical-data/advice/copper-busbar-rating/,"
[Online]. Available: https://multimedia.3m.com/mws/media/569860O/3mtm-
thermal-management-fluids-for-military-aerospace-apps.pdf.

[22] "Insulating Liquids: Basic Properties, Types and Applications Explained," [Online].
Available: https://testguy.net/content/365-Insulating-Liquids-Basic-Properties-Types-
and-Applications-Explained.

[23] Z. Z. JILING LI, "Battery Thermal Management Systems of Electric Vehicles,"
*Department of Applied Mechanics , CHALMERS UNIVERSITY OF TECHNOLOGY.*

[24] "Interfacing with Elcon & TC Chargers," [Online]. Available:
https://www.orionbms.com/charger-integration/interfacing-elcon/.

[25] "CHAdeMO Integration With Orion BMS 2," [Online]. Available:
https://www.orionbms.com/manuals/pdf/chademo_integration.pdf.

[26] J. LaMarre, "FSAE Electric Vehicle Cooling System Design," The University of Akron.

[27] D. G. B. L. A. M. a. X. F. Matthew Carl, "THE THEORETICAL AND EXPERIMENTAL
INVESTIGATION OF THE HEAT TRANSFER PROCESS OF AN AUTOMOBILE RADIATOR,"
Department of Mechanical Engineering, Lamar University.

[28] P. P. C. G. B. P. Alan Keith Hellier, "Fracture Toughness Measurement for Aluminium
6061-T6 using Notched Round Bars," *ResearchGate.*

[29] "Fitting the OCV-SOC relationship of a battery lithium-ion using genetic algorithm method," *ICIES.*

[30] "Lithium-ion battery," Wikipedia, [Online]. Available: https://en.wikipedia.org/wiki/Lithium-ion_battery.

[31] D. Gaur, "Understanding Different Battery Chemistry," *Skill-Lync.*

[32] "A Guide to Understanding Battery Specifications," *MIT .*

[33] X. D. X. ,. ,. C. W.Wang, "Advances in Batteries for Medium and Large-Scale Energy Storage," *ScienceDirect.*

[34] E. Plastics, "POM - Acetal Polyoxymethylene," Ensinger Plastics, [Online]. Available: https://www.ensingerplastics.com/en-us/shapes/engineering-plastics/pom-acetal.

# List Of Figures

# List Of Tables

# 7 APPENDIX A  12V BATTERY COMPONENTS DRAWINGS



*Figure 76 SONY 18650 Cell Drawing*
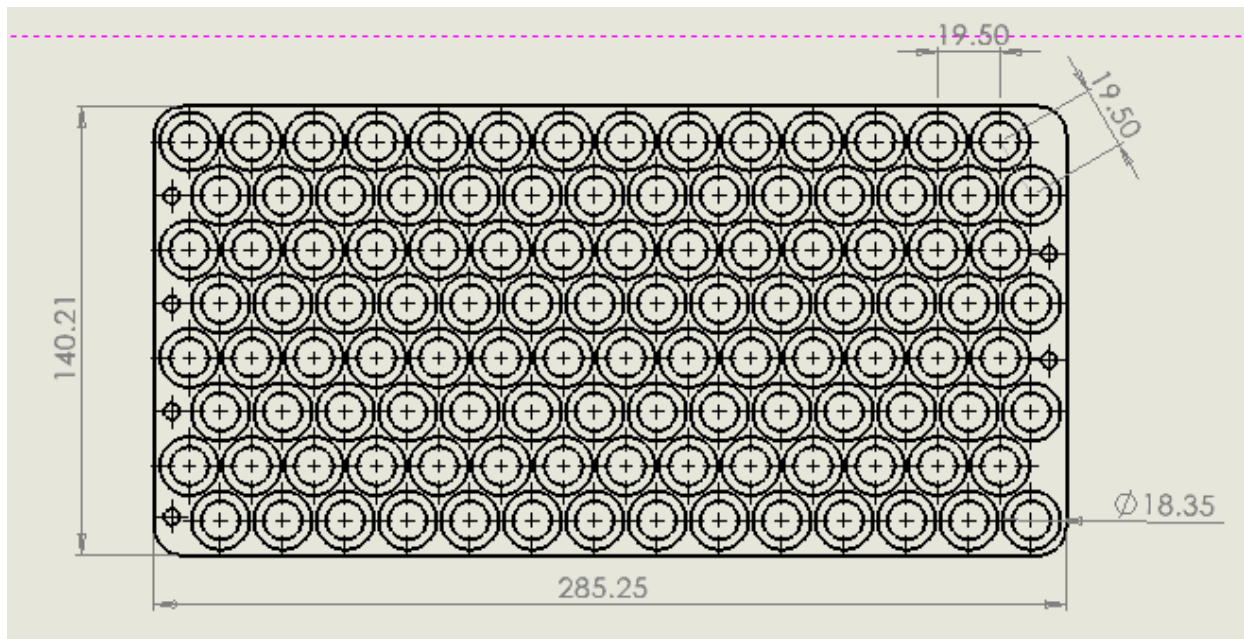


*Figure 77 Top Cell Holder Drawing*
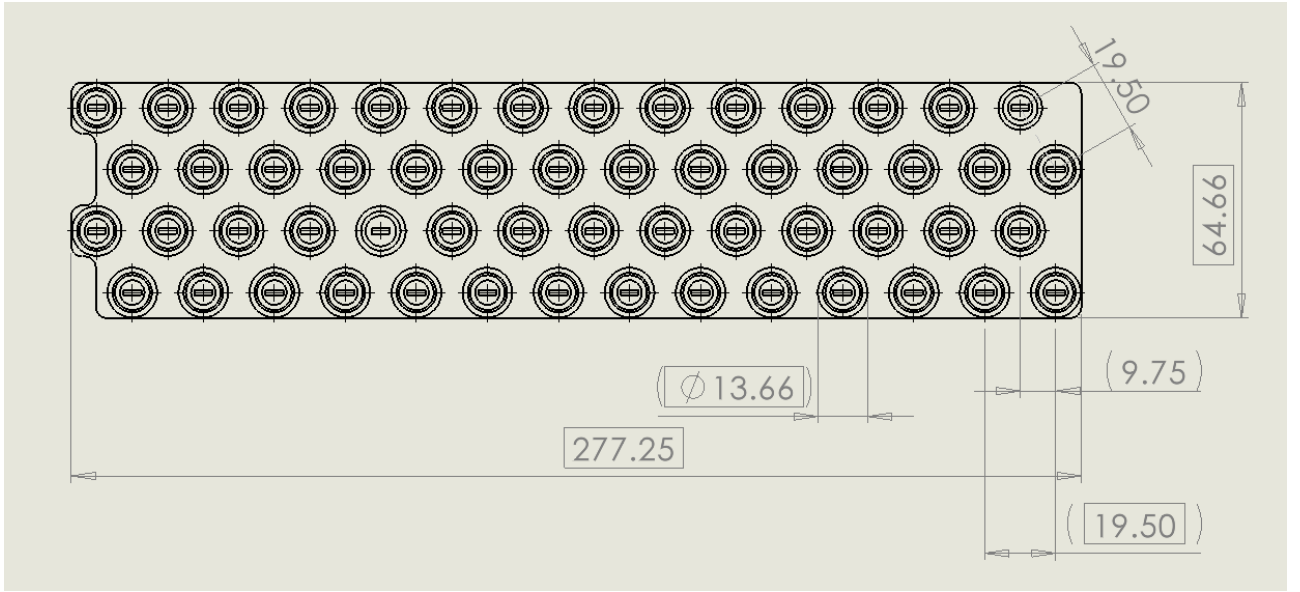
*Figure 78 Nickel plate*
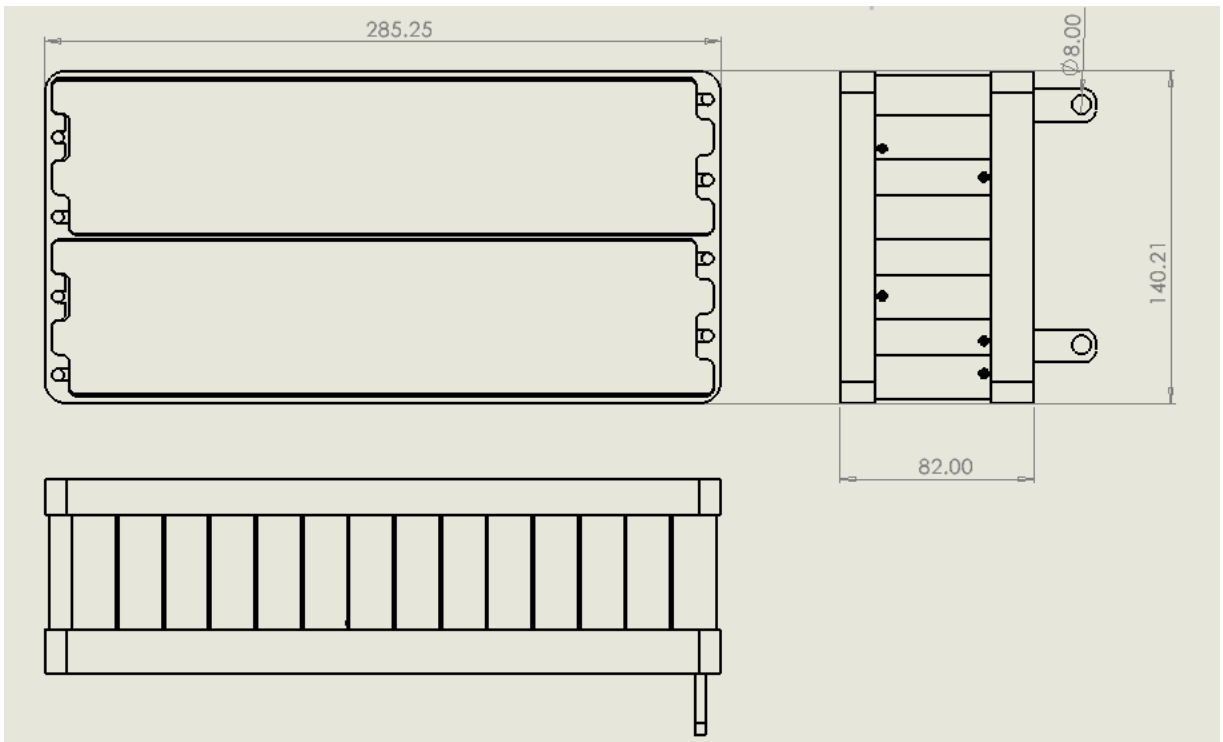


*Figure 79 Cell Pack Drawing*
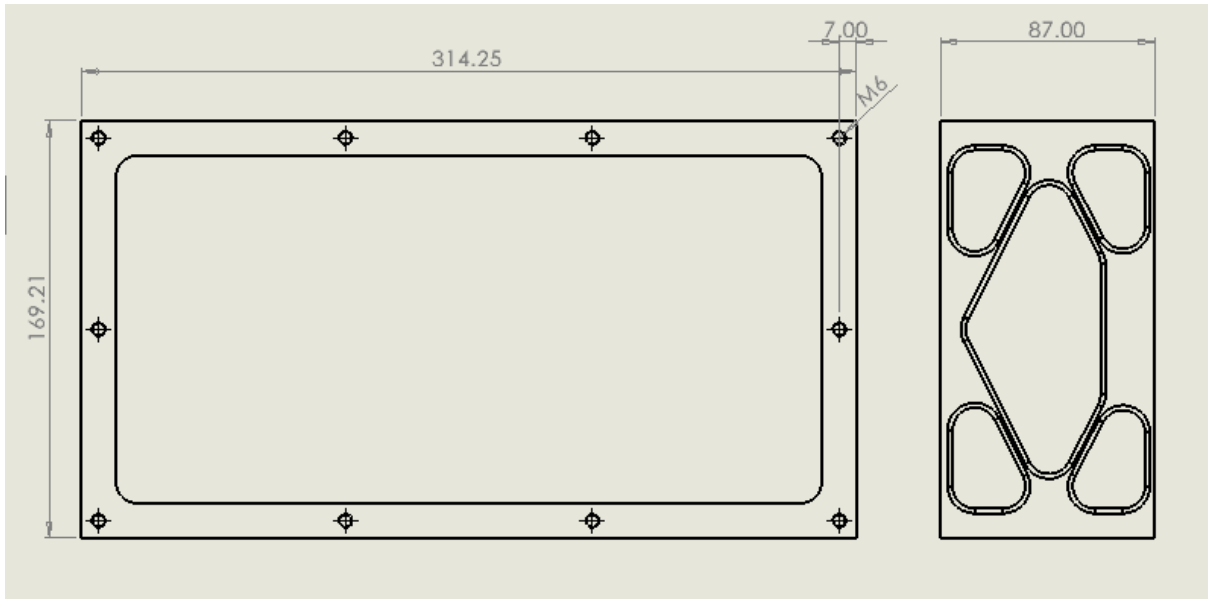
*Figure 80 Battery Case*

# 8 APPENDIX B 12V BATTERY COMPONENTS OPERATION SHEET

| CORBELLATI AUTOMOBILI | **PROCESS ROUTE SHEET** | | Version - 2 |
|---|---|---|---|
| Material: POM-C DELRIN | Part Name: 12V TOP CELL HOLDER<br>Part No: B003<br>Blank: RECTANGLE BLOCK | | |
| Op. | Machine | OPERATION DESCRIPTION | time(min) |
| 10 | HAAS VF-7 | Machining of the middle section of the part | 50 |
| 20 | HAAS VF-7 | Machining of long edge side sections of the part on one side | |
| 30 | HAAS VF-7 | Machining of middle section on the second side of the part | |
| 40 | HAAS VF-7 | Machining of the long edge sides on the second side of the part | |

| CORBELLATI AUTOMOBILI | **PROCESS ROUTE SHEET** | | Version - 2 |
|---|---|---|---|
| Material: POM-C DELRIN | Part Name: 12V BOTTOM CELL HOLDER<br>Part No: B004<br>Blank: RECTANGLE BLOCK | | |
| Op. | Machine | OPERATION DESCRIPTION | time(min) |
| 10 | HAAS VF-7 | Machining of long edge side sections of the part on one side | 50 |
| 20 | HAAS VF-7 | Machining of middle section of the part | |
| 30 | HAAS VF-7 | Machining of the middle section on the second side of the part | |
| 40 | HAAS VF-7 | Machining of the long edge side sections on the second side of the part | |

# OPERATION 10 TOP CELL HOLDER

## Setup

WCS: #5

STOCK:
DX: 285.25mm
DY: 140.21mm
DZ: 15.5mm

PART:
DX: 285.25mm
DY: 140.21mm
DZ: 15mm

STOCK LOWER IN WCS #5:
X: -142.63mm
Y: -70.1mm
Z: -15.5mm

STOCK UPPER IN WCS #5:
X: 142.63mm
Y: 70.1mm
Z: 0mm
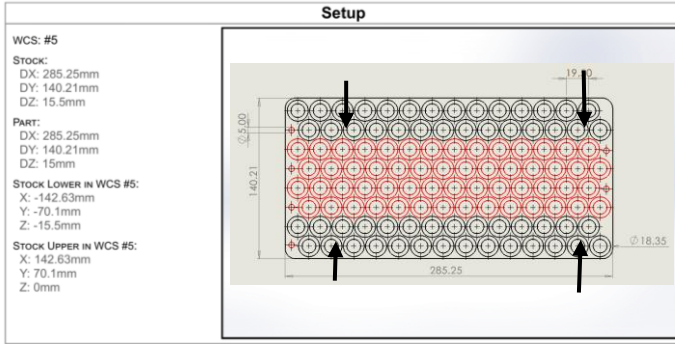
## Total

NUMBER OF OPERATIONS: 6
NUMBER OF TOOLS: 4
TOOLS: T3 T6 T22 T27
MAXIMUM Z: 45mm
MINIMUM Z: -10.5mm
MAXIMUM FEEDRATE: 1782.54mm/min
MAXIMUM SPINDLE SPEED: 12732rpm
CUTTING DISTANCE: 36313.09mm
RAPID DISTANCE: 13512.3mm
ESTIMATED CYCLE TIME: 45m:15s

## Tools

**T3** D3 L3
TYPE: drill
DIAMETER: 5mm
TIP ANGLE: 135°
LENGTH: 55mm
FLUTES: 2
DESCRIPTION: for m6 (5)
MINIMUM Z: -8.47mm
MAXIMUM FEED: 475.089mm/min
MAXIMUM SPINDLE SPEED: 2000rpm
CUTTING DISTANCE: 114.6mm
RAPID DISTANCE: 607.65mm
ESTIMATED CYCLE TIME: 22s (0.8%)

**T6** D6 L6
TYPE: face mill
DIAMETER: 50mm
TAPER ANGLE: 45°
LENGTH: 48mm
FLUTES: 4
DESCRIPTION: facemill
MINIMUM Z: -0.5mm
MAXIMUM FEED: 1193.66mm/min
MAXIMUM SPINDLE SPEED: 4000rpm
CUTTING DISTANCE: 655.67mm
RAPID DISTANCE: 20.5mm
ESTIMATED CYCLE TIME: 48s (1.8%)
HOLDER: 60mm BT40

**T22** D22 L22
TYPE: flat end mill
DIAMETER: 10mm
LENGTH: 45mm
FLUTES: 2
DESCRIPTION: HM9/10 D10
MINIMUM Z: -8.5mm
MAXIMUM FEED: 1782.54mm/min
MAXIMUM SPINDLE SPEED: 11141rpm
CUTTING DISTANCE: 1715.89mm
RAPID DISTANCE: 2442.1mm
ESTIMATED CYCLE TIME: 1m:53s (4.2%)
HOLDER: 60mm BT40

**T27** D27 L27
TYPE: flat end mill
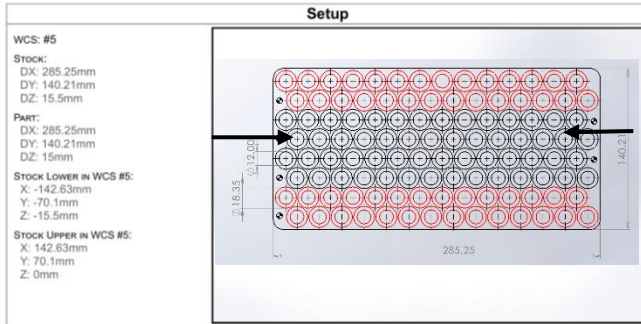DIAMETER: 5mm
LENGTH: 40mm
FLUTES: 2
DESCRIPTION: HM9/04 D5
MINIMUM Z: -10.5mm
MAXIMUM FEED: 1782.54mm/min
MAXIMUM SPINDLE SPEED: 12732rpm
CUTTING DISTANCE: 33826.93mm
RAPID DISTANCE: 10442.04mm
ESTIMATED CYCLE TIME: 41m:12s (91%)
HOLDER: 100mm BT40

## Operations

**Operation 1/6**
DESCRIPTION: Face2
STRATEGY: Facing
WCS: #5
TOLERANCE: 0.01mm
MAXIMUM STEPOVER: 47.5mm
MAXIMUM Z: 15mm
MINIMUM Z: -0.5mm
MAXIMUM SPINDLE SPEED: 4000rpm
MAXIMUM FEEDRATE: 1193.66mm/min
CUTTING DISTANCE: 655.67mm
RAPID DISTANCE: 20.5mm
ESTIMATED CYCLE TIME: 48s (1.8%)
COOLANT: Flood
**T6** D6 L6
TYPE: face mill
DIAMETER: 50mm
TAPER ANGLE: 45°
LENGTH: 48mm
FLUTES: 4
DESCRIPTION: facemill

**Operation 2/6**
DESCRIPTION: 2D Contour7
STRATEGY: Contour 2D
WCS: #5
TOLERANCE: 0.01mm
STOCK TO LEAVE: 0mm
MAXIMUM STEPOVER: 2mm
MAXIMUM Z: 45mm
MINIMUM Z: -8.5mm
MAXIMUM SPINDLE SPEED: 11141rpm
MAXIMUM FEEDRATE: 1782.54mm/min
CUTTING DISTANCE: 1715.89mm
RAPID DISTANCE: 2442.1mm
ESTIMATED CYCLE TIME: 1m:53s (4.2%)
COOLANT: Flood
**T22** D22 L22
TYPE: flat end mill
DIAMETER: 10mm
LENGTH: 45mm
FLUTES: 2
DESCRIPTION: HM9/10 D10

**Operation 3/6**
DESCRIPTION: Drill3
STRATEGY: Drilling
WCS: #5
TOLERANCE: 0.01mm
MAXIMUM Z: 15mm
MINIMUM Z: -8.47mm
MAXIMUM SPINDLE SPEED: 2000rpm
MAXIMUM FEEDRATE: 475.089mm/min
CUTTING DISTANCE: 114.6mm
RAPID DISTANCE: 607.65mm
ESTIMATED CYCLE TIME: 22s (0.8%)
COOLANT: Off
**T3** D3 L3
TYPE: drill
DIAMETER: 5mm
TIP ANGLE: 135°
LENGTH: 55mm
FLUTES: 2
DESCRIPTION: for m6 (5)

**Operation 4/6**
DESCRIPTION: Adaptive5
STRATEGY: Adaptive
WCS: #5
TOLERANCE: 0.1mm
STOCK TO LEAVE: 0.25mm/0mm
MAXIMUM STEPDOWN: 10mm
OPTIMAL LOAD: 2mm
LOAD DEVIATION: 0.2mm
MAXIMUM Z: 15mm
MINIMUM Z: -10.49mm
MAXIMUM SPINDLE SPEED: 12732rpm
MAXIMUM FEEDRATE: 1782.54mm/min
CUTTING DISTANCE: 28177.3mm
RAPID DISTANCE: 6595.75mm
ESTIMATED CYCLE TIME: 32m:47s (72.4%)
COOLANT: Flood
**T27** D27 L27
TYPE: flat end mill
DIAMETER: 5mm
LENGTH: 40mm
FLUTES: 2
DESCRIPTION: HM9/04 D5

**Operation 5/6**
DESCRIPTION: 2D Contour9
STRATEGY: Contour 2D
WCS: #5
TOLERANCE: 0.01mm
STOCK TO LEAVE: 0mm
MAXIMUM STEPOVER: 4.75mm
MAXIMUM Z: 15mm
MINIMUM Z: -8.7mm
MAXIMUM SPINDLE SPEED: 12732rpm
MAXIMUM FEEDRATE: 1782.54mm/min
CUTTING DISTANCE: 3346.19mm
RAPID DISTANCE: 1895.74mm
ESTIMATED CYCLE TIME: 4m:22s (9.6%)
COOLANT: Flood
**T27** D27 L27
TYPE: flat end mill
DIAMETER: 5mm
LENGTH: 40mm
FLUTES: 2
DESCRIPTION: HM9/04 D5

**Operation 6/6**
DESCRIPTION: 2D Contour10
STRATEGY: Contour 2D
WCS: #5
TOLERANCE: 0.01mm
STOCK TO LEAVE: 0mm
MAXIMUM STEPOVER: 4.75mm
MAXIMUM Z: 15mm
MINIMUM Z: -10.5mm
MAXIMUM SPINDLE SPEED: 12732rpm
MAXIMUM FEEDRATE: 1782.54mm/min
CUTTING DISTANCE: 2303.44mm
RAPID DISTANCE: 1950.56mm
ESTIMATED CYCLE TIME: 4m:4s (9%)
COOLANT: Flood
**T27** D27 L27
TYPE: flat end mill
DIAMETER: 5mm
LENGTH: 40mm
FLUTES: 2
DESCRIPTION: HM9/04 D5

# Operation 20 TOP CELL HOLDER

## Setup

WCS: #5

STOCK:
DX: 285.25mm
DY: 140.21mm
DZ: 15.5mm

PART:
DX: 285.25mm
DY: 140.21mm
DZ: 15mm

STOCK LOWER IN WCS #5:
X: -142.63mm
Y: -70.1mm
Z: -15.5mm

STOCK UPPER IN WCS #5:
X: 142.63mm
Y: 70.1mm
Z: 0mm



## Total

NUMBER OF OPERATIONS: 5
NUMBER OF TOOLS: 3
TOOLS: T6 T22 T27
MAXIMUM Z: 50mm
MINIMUM Z: -10.5mm
MAXIMUM FEEDRATE: 1782.54mm/min
MAXIMUM SPINDLE SPEED: 12732rpm
CUTTING DISTANCE: 38031.46mm
RAPID DISTANCE: 34159.35mm
ESTIMATED CYCLE TIME: 49m:53s

## Tools

**T6 D6 L6**
TYPE: face mill
DIAMETER: 50mm
TAPER ANGLE: 45°
LENGTH: 48mm
FLUTES: 4
DESCRIPTION: facemill

MINIMUM Z: -0.5mm
MAXIMUM FEED: 1193.66mm/min
MAXIMUM SPINDLE SPEED: 4000rpm
CUTTING DISTANCE: 2026.26mm
RAPID DISTANCE: 95.89mm
ESTIMATED CYCLE TIME: 2m:30s (5%)

HOLDER: 60mm BT40

**T22 D22 L22**
TYPE: flat end mill
DIAMETER: 10mm
LENGTH: 45mm
FLUTES: 2
DESCRIPTION: HM9/10 D10

MINIMUM Z: -8.5mm
MAXIMUM FEED: 1782.54mm/min
MAXIMUM SPINDLE SPEED: 11141rpm
CUTTING DISTANCE: 3456.4mm
RAPID DISTANCE: 2696.43mm
ESTIMATED CYCLE TIME: 2m:55s (5.8%)

HOLDER: 60mm BT40

**T27 D27 L27**
TYPE: flat end mill
DIAMETER: 5mm
LENGTH: 40mm
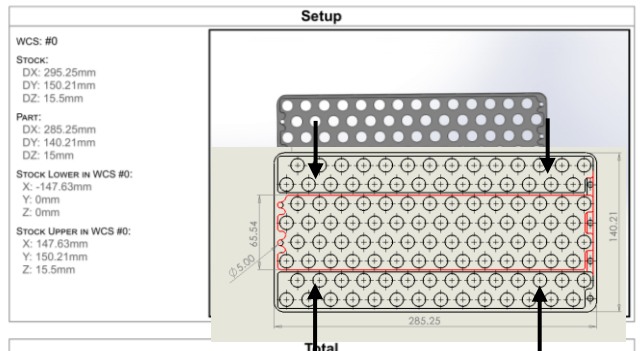FLUTES: 2
DESCRIPTION: HM9/04 D5

MINIMUM Z: -10.5mm
MAXIMUM FEED: 1782.54mm/min
MAXIMUM SPINDLE SPEED: 12732rpm
CUTTING DISTANCE: 32548.8mm
RAPID DISTANCE: 31367.03mm
ESTIMATED CYCLE TIME: 43m:43s (87.6%)

HOLDER: 100mm BT40

## Operations

**Operation 1/5**
DESCRIPTION: Face1
STRATEGY: Facing
WCS: #5
TOLERANCE: 0.01mm
MAXIMUM STEPOVER: 20mm

MAXIMUM Z: 50mm
MINIMUM Z: -0.5mm
MAXIMUM SPINDLE SPEED: 4000rpm
MAXIMUM FEEDRATE: 1193.66mm/min
CUTTING DISTANCE: 2026.26mm
RAPID DISTANCE: 95.89mm
ESTIMATED CYCLE TIME: 2m:30s (5%)
COOLANT: Flood

**T6 D6 L6**
TYPE: face mill
DIAMETER: 50mm
TAPER ANGLE: 45°
LENGTH: 48mm
FLUTES: 4
DESCRIPTION: facemill

**Operation 2/5**
DESCRIPTION: 2D Contour3
STRATEGY: Contour 2D
WCS: #5
TOLERANCE: 0.01mm
STOCK TO LEAVE: 0mm
MAXIMUM STEPOVER: 2mm

MAXIMUM Z: 45mm
MINIMUM Z: -8.5mm
MAXIMUM SPINDLE SPEED: 11141rpm
MAXIMUM FEEDRATE: 1782.54mm/min
CUTTING DISTANCE: 3456.4mm
RAPID DISTANCE: 2696.43mm
ESTIMATED CYCLE TIME: 2m:55s (5.8%)
COOLANT: Flood

**T22 D22 L22**
TYPE: flat end mill
DIAMETER: 10mm
LENGTH: 45mm
FLUTES: 2
DESCRIPTION: HM9/10 D10

**Operation 3/5**
DESCRIPTION: Adaptive2
STRATEGY: Adaptive
WCS: #5
TOLERANCE: 0.1mm
STOCK TO LEAVE: 0.25mm/0mm
MAXIMUM STEPDOWN: 10mm
OPTIMAL LOAD: 2mm
LOAD DEVIATION: 0.2mm

MAXIMUM Z: 45mm
MINIMUM Z: -10.2mm
MAXIMUM SPINDLE SPEED: 12732rpm
MAXIMUM FEEDRATE: 1782.54mm/min
CUTTING DISTANCE: 26899.17mm
RAPID DISTANCE: 20696.32mm
ESTIMATED CYCLE TIME: 33m:55s (68%)
COOLANT: Flood

**T27 D27 L27**
TYPE: flat end mill
DIAMETER: 5mm
LENGTH: 40mm
FLUTES: 2
DESCRIPTION: HM9/04 D5

**Operation 4/5**
DESCRIPTION: 2D Contour1
STRATEGY: Contour 2D
WCS: #5
TOLERANCE: 0.01mm
STOCK TO LEAVE: 0mm
MAXIMUM STEPOVER: 4.75mm

MAXIMUM Z: 45mm
MINIMUM Z: -8.7mm
MAXIMUM SPINDLE SPEED: 12732rpm
MAXIMUM FEEDRATE: 1782.54mm/min
CUTTING DISTANCE: 3346.19mm
RAPID DISTANCE: 5291.21mm
ESTIMATED CYCLE TIME: 5m:3s (10.1%)
COOLANT: Flood

**T27 D27 L27**
TYPE: flat end mill
DIAMETER: 5mm
LENGTH: 40mm
FLUTES: 2
DESCRIPTION: HM9/04 D5

**Operation 5/5**
DESCRIPTION: 2D Contour2
STRATEGY: Contour 2D
WCS: #5
TOLERANCE: 0.01mm
STOCK TO LEAVE: 0mm
MAXIMUM STEPOVER: 4.75mm

MAXIMUM Z: 45mm
MINIMUM Z: -10.5mm
MAXIMUM SPINDLE SPEED: 12732rpm
MAXIMUM FEEDRATE: 1782.54mm/min
CUTTING DISTANCE: 2303.44mm
RAPID DISTANCE: 5379.5mm
ESTIMATED CYCLE TIME: 4m:45s (9.5%)
COOLANT: Flood

**T27 D27 L27**
TYPE: flat end mill
DIAMETER: 5mm
LENGTH: 40mm
FLUTES: 2
DESCRIPTION: HM9/04 D5

# Operation 30 TOP CELL HOLDER

## Setup

WCS: #0

STOCK:
DX: 295.25mm
DY: 150.21mm
DZ: 15.5mm

PART:
DX: 285.25mm
DY: 140.21mm
DZ: 15mm

STOCK LOWER IN WCS #0:
X: -147.63mm
Y: 0mm
Z: 0mm

STOCK UPPER IN WCS #0:
X: 147.63mm
Y: 150.21mm
Z: 15.5mm



## Total

NUMBER OF OPERATIONS: 4
NUMBER OF TOOLS: 4
TOOLS: T3 T22 T27 T99
MAXIMUM Z: 75.5mm
MINIMUM Z: 7mm
MAXIMUM FEEDRATE: 3150mm/min
MAXIMUM SPINDLE SPEED: 12732rpm
CUTTING DISTANCE: 22028.59mm
RAPID DISTANCE: 6930.4mm
ESTIMATED CYCLE TIME: 15m:52s

## Tools

**T3 D3 L3**
TYPE: drill
DIAMETER: 5mm
TIP ANGLE: 135°
LENGTH: 55mm
FLUTES: 2
DESCRIPTION: for m6 (5)

MINIMUM Z: 7mm
MAXIMUM FEED: 475.089mm/min
MAXIMUM SPINDLE SPEED: 2000rpm
CUTTING DISTANCE: 114.6mm
RAPID DISTANCE: 1088.05mm
ESTIMATED CYCLE TIME: 28s (2.9%)

**T22 D22 L22**
TYPE: flat end mill
DIAMETER: 10mm
LENGTH: 45mm
FLUTES: 2
DESCRIPTION: HM9/10 D10

MINIMUM Z: 7mm
MAXIMUM FEED: 1782.54mm/min
MAXIMUM SPINDLE SPEED: 11141rpm
CUTTING DISTANCE: 2395.72mm
RAPID DISTANCE: 3156.96mm
ESTIMATED CYCLE TIME: 2m:24s (15.2%)

HOLDER: 60mm BT40

**T27 D27 L27**
TYPE: flat end mill
DIAMETER: 5mm
LENGTH: 40mm
FLUTES: 2
DESCRIPTION: HM9/04 D5

MINIMUM Z: 10mm
MAXIMUM FEED: 3150mm/min
MAXIMUM SPINDLE SPEED: 12732rpm
CUTTING DISTANCE: 18015.51mm
RAPID DISTANCE: 2661.49mm
ESTIMATED CYCLE TIME: 6m:48s (42.9%)

HOLDER: 100mm BT40

**T99 D99 L99**
TYPE: flat end mill
DIAMETER: 16mm
LENGTH: 120mm
FLUTES: 2
DESCRIPTION: 16mm flat reduced 0001 D16

MINIMUM Z: 15mm
MAXIMUM FEED: 2506.69mm/min
MAXIMUM SPINDLE SPEED: 1592rpm
CUTTING DISTANCE: 1502.75mm
RAPID DISTANCE: 23.9mm
ESTIMATED CYCLE TIME: 5m:12s (32.8%)

HOLDER: 100mm BT40

## Operations

**Operation 1/4**
DESCRIPTION: Face4
STRATEGY: Facing
WCS: #0
TOLERANCE: 0.01mm
MAXIMUM STEPOVER: 15.2mm

MAXIMUM Z: 30.5mm
MINIMUM Z: 15mm
MAXIMUM SPINDLE SPEED: 1592rpm
MAXIMUM FEEDRATE: 2506.69mm/min
CUTTING DISTANCE: 1502.75mm
RAPID DISTANCE: 23.9mm
ESTIMATED CYCLE TIME: 5m:12s (32.8%)
COOLANT: Flood

**T99 D99 L99**
TYPE: flat end mill
DIAMETER: 16mm
LENGTH: 120mm
FLUTES: 2
DESCRIPTION: 16mm flat reduced 0001 D16

**Operation 2/4**
DESCRIPTION: Drill2
STRATEGY: Drilling
WCS: #0
TOLERANCE: 0.01mm

MAXIMUM Z: 60.5mm
MINIMUM Z: 7mm
MAXIMUM SPINDLE SPEED: 2000rpm
MAXIMUM FEEDRATE: 475.089mm/min
CUTTING DISTANCE: 114.6mm
RAPID DISTANCE: 1088.05mm
ESTIMATED CYCLE TIME: 28s (2.9%)
COOLANT: Off

**T3 D3 L3**
TYPE: drill
DIAMETER: 5mm
TIP ANGLE: 135°
LENGTH: 55mm
FLUTES: 2
DESCRIPTION: for m6 (5)

**Operation 3/4**
DESCRIPTION: 2D Contour6
STRATEGY: Contour 2D
WCS: #0
TOLERANCE: 0.01mm
STOCK TO LEAVE: 0mm
MAXIMUM STEPOVER: 2mm

MAXIMUM Z: 75.5mm
MINIMUM Z: 7mm
MAXIMUM SPINDLE SPEED: 11141rpm
MAXIMUM FEEDRATE: 1782.54mm/min
CUTTING DISTANCE: 2395.72mm
RAPID DISTANCE: 3156.96mm
ESTIMATED CYCLE TIME: 2m:24s (15.2%)
COOLANT: Flood

**T22 D22 L22**
TYPE: flat end mill
DIAMETER: 10mm
LENGTH: 45mm
FLUTES: 2
DESCRIPTION: HM9/10 D10

**Operation 4/4**
DESCRIPTION: Adaptive3
STRATEGY: Adaptive
WCS: #0
TOLERANCE: 0.1mm
STOCK TO LEAVE: 0mm
MAXIMUM STEPDOWN: 10mm
OPTIMAL LOAD: 2mm
LOAD DEVIATION: 0.2mm

MAXIMUM Z: 30.5mm
MINIMUM Z: 10mm
MAXIMUM SPINDLE SPEED: 12732rpm
MAXIMUM FEEDRATE: 3150mm/min
CUTTING DISTANCE: 18015.51mm
RAPID DISTANCE: 2661.49mm
ESTIMATED CYCLE TIME: 6m:48s (42.9%)
COOLANT: Flood

**T27 D27 L27**
TYPE: flat end mill
DIAMETER: 5mm
LENGTH: 40mm
FLUTES: 2
DESCRIPTION: HM9/04 D5

# Operation 40 TOP CELL HOLDER

## Setup

WCS: #0

STOCK:
DX: 295.25mm
DY: 150.21mm
DZ: 15.5mm

PART:
DX: 285.25mm
DY: 140.21mm
DZ: 15mm

STOCK LOWER IN WCS #0:
X: -147.63mm
Y: 0mm
Z: 0mm

STOCK UPPER IN WCS #0:
X: 147.63mm
Y: 150.21mm
Z: 15.5mm



32.33
140.21
32.33
285.25

## Total

NUMBER OF OPERATIONS: 3
NUMBER OF TOOLS: 3
TOOLS: T22 T27 T99
MAXIMUM Z: 75.5mm
MINIMUM Z: 7mm
MAXIMUM FEEDRATE: 3150mm/min
MAXIMUM SPINDLE SPEED: 12732rpm
CUTTING DISTANCE: 22723.29mm
RAPID DISTANCE: 7590.16mm
ESTIMATED CYCLE TIME: 17m:25s

## Tools

**T22** D22 L22
TYPE: flat end mill
DIAMETER: 10mm
LENGTH: 45mm
FLUTES: 2
DESCRIPTION: HM9/10 D10
MINIMUM Z: 7mm
MAXIMUM FEED: 1782.54mm/min
MAXIMUM SPINDLE SPEED: 11141rpm
CUTTING DISTANCE: 4136.24mm
RAPID DISTANCE: 2572.34mm
ESTIMATED CYCLE TIME: 3m:16s (18.8%)
HOLDER: 60mm BT40

**T27** D27 L27
TYPE: flat end mill
DIAMETER: 5mm
LENGTH: 40mm
FLUTES: 2
DESCRIPTION: HM9/04 D5
MINIMUM Z: 10mm
MAXIMUM FEED: 3150mm/min
MAXIMUM SPINDLE SPEED: 12732rpm
CUTTING DISTANCE: 16591.2mm
RAPID DISTANCE: 4729.47mm
ESTIMATED CYCLE TIME: 6m:26s (36.9%)
HOLDER: 100mm BT40

**T99** D99 L99
TYPE: flat end mill
DIAMETER: 16mm
LENGTH: 120mm
FLUTES: 2
DESCRIPTION: 16mm flat reduced 0001 D16
MINIMUM Z: 15mm
MAXIMUM FEED: 2506.69mm/min
MAXIMUM SPINDLE SPEED: 1592rpm
CUTTING DISTANCE: 1995.86mm
RAPID DISTANCE: 288.35mm
ESTIMATED CYCLE TIME: 6m:58s (40%)
HOLDER: 100mm BT40

## Operations

**Operation 1/3**
DESCRIPTION: Face3
STRATEGY: Facing
WCS: #0
TOLERANCE: 0.01mm
MAXIMUM STEPOVER: 15.2mm
MAXIMUM Z: 75.5mm
MINIMUM Z: 15mm
MAXIMUM SPINDLE SPEED: 1592rpm
MAXIMUM FEEDRATE: 2506.69mm/min
CUTTING DISTANCE: 1995.86mm
RAPID DISTANCE: 288.35mm
ESTIMATED CYCLE TIME: 6m:58s (40%)
COOLANT: Flood

**T99** D99 L99
TYPE: flat end mill
DIAMETER: 16mm
LENGTH: 120mm
FLUTES: 2
DESCRIPTION: 16mm flat reduced 0001 D16

**Operation 2/3**
DESCRIPTION: 2D Contour5
STRATEGY: Contour 2D
WCS: #0
TOLERANCE: 0.01mm
STOCK TO LEAVE: 0mm
MAXIMUM STEPOVER: 2mm
MAXIMUM Z: 75.5mm
MINIMUM Z: 7mm
MAXIMUM SPINDLE SPEED: 11141rpm
MAXIMUM FEEDRATE: 1782.54mm/min
CUTTING DISTANCE: 4136.24mm
RAPID DISTANCE: 2572.34mm
ESTIMATED CYCLE TIME: 3m:16s (18.8%)
COOLANT: Flood

**T22** D22 L22
TYPE: flat end mill
DIAMETER: 10mm
LENGTH: 45mm
FLUTES: 2
DESCRIPTION: HM9/10 D10

**Operation 3/3**
DESCRIPTION: Adaptive4
STRATEGY: Adaptive
WCS: #0
TOLERANCE: 0.1mm
STOCK TO LEAVE: 0mm
MAXIMUM STEPDOWN: 10mm
OPTIMAL LOAD: 2mm
LOAD DEVIATION: 0.2mm
MAXIMUM Z: 75.5mm
MINIMUM Z: 10mm
MAXIMUM SPINDLE SPEED: 12732rpm
MAXIMUM FEEDRATE: 3150mm/min
CUTTING DISTANCE: 16591.2mm
RAPID DISTANCE: 4729.47mm
ESTIMATED CYCLE TIME: 6m:26s (36.9%)
COOLANT: Flood

**T27** D27 L27
TYPE: flat end mill
DIAMETER: 5mm
LENGTH: 40mm
FLUTES: 2
DESCRIPTION: HM9/04 D5

# APPENDIX B 12V BATTERY CASE OPERATION SHEET

| CORBELLATI AUTOMOBILI | **PROCESS ROUTE SHEET** | Version - 2 |
|---|---|---|
| Material: Aluminium 6061-T6 | Part Name: 12V BATTERY CASE<br>Part No: B001<br>Blank: RECTANGLE BLOCK | |
| Op. | Machine | OPERATION DESCRIPTION | |
| 10 | HAAS VF-7 | Facing and shoulder milling of the block on one side | |
| 20 | HAAS VF-7 | Facing and shoulder milling of the block on second side | |
| 30 | HAAS VF-7 | Pocket milling and drilling of the top surface | |
| 40 | HAAS VF-7 | Pocket milling on the front of the case | |
| 50 | HAAS VF-7 | Pocket milling on the back of the case | |
| 60 | HAAS VF-7 | Pocket milling on the right side of the case | |
| 70 | HAAS VF-7 | Pocket milling on the left side of the case | |

# Operation 10 BATTERY CASE

## Setup

WCS: #5

STOCK:
DX: 319.25mm
DY: 175.96mm
DZ: 100mm

PART:
DX: 314.25mm
DY: 169.21mm
DZ: 87mm

STOCK LOWER IN WCS #5:
X: -159.63mm
Y: -87.98mm
Z: -100mm

STOCK UPPER IN WCS #5:
X: 159.63mm
Y: 87.98mm
Z: 0mm

## Total

NUMBER OF OPERATIONS: 3
NUMBER OF TOOLS: 3
TOOLS: T6 T9 T12
MAXIMUM Z: 15mm
MINIMUM Z: -102mm
MAXIMUM FEEDRATE: 2506.69mm/min
MAXIMUM SPINDLE SPEED: 5600rpm
CUTTING DISTANCE: 62623.32mm
RAPID DISTANCE: 49254.78mm
ESTIMATED CYCLE TIME: 1h:59m:6s

## Tools

**T6 D6 L6**
TYPE: face mill
DIAMETER: 50mm
TAPER ANGLE: 45°
LENGTH: 48mm
FLUTES: 4
DESCRIPTION: facemill
MINIMUM Z: -6.5mm
MAXIMUM FEED: 1193.66mm/min
MAXIMUM SPINDLE SPEED: 4000rpm
CUTTING DISTANCE: 4595.58mm
RAPID DISTANCE: 302.05mm
ESTIMATED CYCLE TIME: 5m:45s (4.8%)
HOLDER: 60mm BT40

**T9 D9 L9**
TYPE: face mill
DIAMETER: 30mm
CORNER RADIUS: 1mm
LENGTH: 185mm
FLUTES: 2
MINIMUM Z: -102mm
MAXIMUM FEED: 1200mm/min
MAXIMUM SPINDLE SPEED: 5000rpm
CUTTING DISTANCE: 42154.01mm
RAPID DISTANCE: 39023.5mm
ESTIMATED CYCLE TIME: 1h:38m:39s (82.8%)

**T12 D12 L12**
TYPE: flat end mill
DIAMETER: 16mm
LENGTH: 88mm
FLUTES: 3
DESCRIPTION: 16mm reduced shank
MINIMUM Z: -53.5mm
MAXIMUM FEED: 2506.69mm/min
MAXIMUM SPINDLE SPEED: 5600rpm
CUTTING DISTANCE: 15873.74mm
RAPID DISTANCE: 9929.23mm
ESTIMATED CYCLE TIME: 13m:57s (11.7%)
HOLDER: 100mm BT40

## Operations

**Operation 1/3**
DESCRIPTION: Face6
STRATEGY: Facing
WCS: #5
TOLERANCE: 0.01mm
MAXIMUM STEPDOWN: 2.5mm
MAXIMUM STEPOVER: 47.5mm
MAXIMUM Z: 15mm
MINIMUM Z: -6.5mm
MAXIMUM SPINDLE SPEED: 4000rpm
MAXIMUM FEEDRATE: 1193.66mm/min
CUTTING DISTANCE: 4595.58mm
RAPID DISTANCE: 302.05mm
ESTIMATED CYCLE TIME: 5m:45s (4.8%)
COOLANT: Flood

**T6 D6 L6**
TYPE: face mill
DIAMETER: 50mm
TAPER ANGLE: 45°
LENGTH: 48mm
FLUTES: 4
DESCRIPTION: facemill

**Operation 2/3**
DESCRIPTION: 2D Contour9
STRATEGY: Contour 2D
WCS: #5
TOLERANCE: 0.01mm
STOCK TO LEAVE: 0mm
MAXIMUM STEPDOWN: 5mm
MAXIMUM STEPOVER: 26.6mm
MAXIMUM Z: 15mm
MINIMUM Z: -102mm
MAXIMUM SPINDLE SPEED: 5000rpm
MAXIMUM FEEDRATE: 1200mm/min
CUTTING DISTANCE: 42154.01mm
RAPID DISTANCE: 39023.5mm
ESTIMATED CYCLE TIME: 1h:38m:39s (82.8%)
COOLANT: Flood

**T9 D9 L9**
TYPE: face mill
DIAMETER: 30mm
CORNER RADIUS: 1mm
LENGTH: 185mm
FLUTES: 2

**Operation 3/3**
DESCRIPTION: 2D Contour10
STRATEGY: Contour 2D
WCS: #5
TOLERANCE: 0.01mm
STOCK TO LEAVE: 0mm
MAXIMUM STEPDOWN: 5mm
MAXIMUM STEPOVER: 4mm
MAXIMUM Z: 15mm
MINIMUM Z: -53.5mm
MAXIMUM SPINDLE SPEED: 5600rpm
MAXIMUM FEEDRATE: 2506.69mm/min
CUTTING DISTANCE: 15873.74mm
RAPID DISTANCE: 9929.23mm
ESTIMATED CYCLE TIME: 13m:57s (11.7%)
COOLANT: Flood

**T12 D12 L12**
TYPE: flat end mill
DIAMETER: 16mm
LENGTH: 88mm
FLUTES: 3
DESCRIPTION: 16mm reduced shank

---

# Operation 20 BATTERY CASE

## Setup

WCS: #0

STOCK:
DX: 314.25mm
DY: 169.21mm
DZ: 93.5mm

PART:
DX: 314.25mm
DY: 169.21mm
DZ: 87mm

STOCK LOWER IN WCS #0:
X: -157.13mm
Y: -169.21mm
Z: 0mm

STOCK UPPER IN WCS #0:
X: 157.13mm
Y: 0mm
Z: 93.5mm

## Total

NUMBER OF OPERATIONS: 3
NUMBER OF TOOLS: 2
TOOLS: T6 T12
MAXIMUM Z: 108.5mm
MINIMUM Z: 37mm
MAXIMUM FEEDRATE: 2506.69mm/min
MAXIMUM SPINDLE SPEED: 5600rpm
CUTTING DISTANCE: 15228.03mm
RAPID DISTANCE: 7563.51mm
ESTIMATED CYCLE TIME: 15m:48s

## Tools

**T6 D6 L6**
TYPE: face mill
DIAMETER: 50mm
TAPER ANGLE: 45°
LENGTH: 48mm
FLUTES: 4
DESCRIPTION: facemill
MINIMUM Z: 87mm
MAXIMUM FEED: 1193.66mm/min
MAXIMUM SPINDLE SPEED: 4000rpm
CUTTING DISTANCE: 4511.72mm
RAPID DISTANCE: 292.15mm
ESTIMATED CYCLE TIME: 5m:38s (35.7%)
HOLDER: 60mm BT40

**T12 D12 L12**
TYPE: flat end mill
DIAMETER: 16mm
LENGTH: 88mm
FLUTES: 3
DESCRIPTION: 16mm reduced shank
MINIMUM Z: 37mm
MAXIMUM FEED: 2506.69mm/min
MAXIMUM SPINDLE SPEED: 5600rpm
CUTTING DISTANCE: 10716.31mm
RAPID DISTANCE: 7271.36mm
ESTIMATED CYCLE TIME: 9m:39s (61.1%)
HOLDER: 100mm BT40

## Operations

**Operation 1/3**
DESCRIPTION: Face8
STRATEGY: Facing
WCS: #0
TOLERANCE: 0.01mm
MAXIMUM STEPDOWN: 2.5mm
MAXIMUM STEPOVER: 47.5mm
MAXIMUM Z: 108.5mm
MINIMUM Z: 87mm
MAXIMUM SPINDLE SPEED: 4000rpm
MAXIMUM FEEDRATE: 1193.66mm/min
CUTTING DISTANCE: 4511.72mm
RAPID DISTANCE: 292.15mm
ESTIMATED CYCLE TIME: 5m:38s (35.7%)
COOLANT: Flood

**T6 D6 L6**
TYPE: face mill
DIAMETER: 50mm
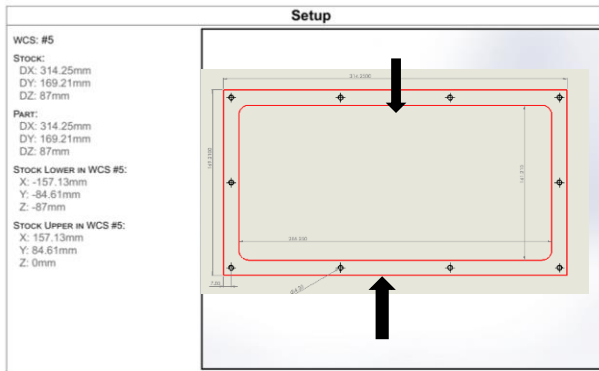TAPER ANGLE: 45°
LENGTH: 48mm
FLUTES: 4
DESCRIPTION: facemill

**Operation 2/3**
DESCRIPTION: 2D Contour11
STRATEGY: Contour 2D
WCS: #0
TOLERANCE: 0.01mm
STOCK TO LEAVE: 0mm
MAXIMUM STEPDOWN: 5mm
MAXIMUM STEPOVER: 15.2mm
MAXIMUM Z: 108.5mm
MINIMUM Z: 72mm
MAXIMUM SPINDLE SPEED: 5600rpm
MAXIMUM FEEDRATE: 2506.69mm/min
CUTTING DISTANCE: 2001.63mm
RAPID DISTANCE: 1916.13mm
ESTIMATED CYCLE TIME: 1m:52s (11.8%)
COOLANT: Flood

**T12 D12 L12**
TYPE: flat end mill
DIAMETER: 16mm
LENGTH: 88mm
FLUTES: 3
DESCRIPTION: 16mm reduced shank

**Operation 3/3**
DESCRIPTION: 2D Contour12
STRATEGY: Contour 2D
WCS: #0
TOLERANCE: 0.01mm
STOCK TO LEAVE: 0mm
MAXIMUM STEPDOWN: 5mm
MAXIMUM STEPOVER: 15.2mm
MAXIMUM Z: 108.5mm
MINIMUM Z: 37mm
MAXIMUM SPINDLE SPEED: 5600rpm
MAXIMUM FEEDRATE: 2506.69mm/min
CUTTING DISTANCE: 8714.67mm
RAPID DISTANCE: 5355.23mm
ESTIMATED CYCLE TIME: 7m:47s (49.3%)
COOLANT: Flood

**T12 D12 L12**
TYPE: flat end mill
DIAMETER: 16mm
LENGTH: 88mm
FLUTES: 3
DESCRIPTION: 16mm reduced shank

# Operation 30 BATTERY CASE

## Setup

WCS: #5

STOCK:
DX: 314.25mm
DY: 169.21mm
DZ: 87mm

PART:
DX: 314.25mm
DY: 169.21mm
DZ: 87mm

STOCK LOWER IN WCS #5:
X: -157.13mm
Y: -84.61mm
Z: -87mm

STOCK UPPER IN WCS #5:
X: 157.13mm
Y: 84.61mm
Z: 0mm

## Total

NUMBER OF OPERATIONS: 4
NUMBER OF TOOLS: 3
TOOLS: T2 T3 T12
MAXIMUM Z: 15mm
MINIMUM Z: -82mm
MAXIMUM FEEDRATE: 2506.69mm/min
MAXIMUM SPINDLE SPEED: 5600rpm
CUTTING DISTANCE: 105972.06mm
RAPID DISTANCE: 71080.72mm
ESTIMATED CYCLE TIME: 1h:8m:22s

## Tools

**T2 D2 L2**
TYPE: bullnose end mill
DIAMETER: 16mm
CORNER RADIUS: 1.5mm
LENGTH: 65mm
FLUTES: 3
DESCRIPTION: 16mm Bullnose Endmill
MINIMUM Z: -81.99mm
MAXIMUM FEED: 2506.69mm/min
MAXIMUM SPINDLE SPEED: 5600rpm
CUTTING DISTANCE: 83882.32mm
RAPID DISTANCE: 56794.34mm
ESTIMATED CYCLE TIME: 53m:11s (77.8%)
HOLDER: 100mm BT40

**T3 D3 L3**
TYPE: drill
DIAMETER: 4.2mm
TIP ANGLE: 135°
LENGTH: 50mm
FLUTES: 2
DESCRIPTION: for m5 (4.2)
MINIMUM Z: -20mm
MAXIMUM FEED: 475.089mm/min
MAXIMUM SPINDLE SPEED: 2375rpm
CUTTING DISTANCE: 291.75mm
RAPID DISTANCE: 1415.09mm
ESTIMATED CYCLE TIME: 54s (1.3%)

### T12 D12 L12

TYPE: flat end mill
DIAMETER: 16mm
LENGTH: 88mm
FLUTES: 3
DESCRIPTION: 16mm reduced shank
MINIMUM Z: -82mm
MAXIMUM FEED: 2506.69mm/min
MAXIMUM SPINDLE SPEED: 5600rpm
CUTTING DISTANCE: 21797.99mm
RAPID DISTANCE: 12871.29mm
ESTIMATED CYCLE TIME: 13m:31s (19.8%)
HOLDER: 100mm BT40

## Operations

**Operation 1/4**
DESCRIPTION: Adaptive4
STRATEGY: Adaptive
WCS: #5
TOLERANCE: 0.1mm
STOCK TO LEAVE: 0.25mm/0mm
MAXIMUM STEPDOWN: 10mm
OPTIMAL LOAD: 6.4mm
LOAD DEVIATION: 0.64mm
MAXIMUM Z: 15mm
MINIMUM Z: -81.99mm
MAXIMUM SPINDLE SPEED: 5600rpm
MAXIMUM FEEDRATE: 2506.69mm/min
CUTTING DISTANCE: 83882.32mm
RAPID DISTANCE: 56794.34mm
ESTIMATED CYCLE TIME: 53m:11s (77.8%)
COOLANT: Flood

**T2 D2 L2**
TYPE: bullnose end mill
DIAMETER: 16mm
CORNER RADIUS: 1.5mm
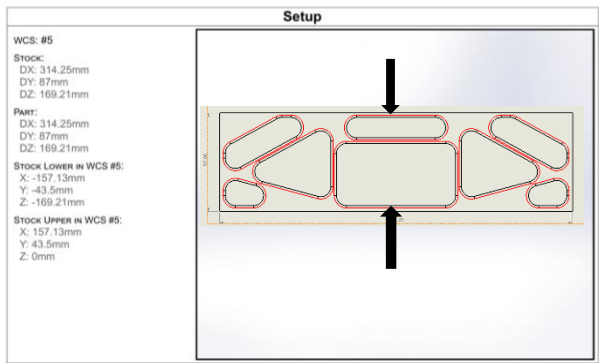LENGTH: 65mm
FLUTES: 3
DESCRIPTION: 16mm Bullnose Endmill

**Operation 2/4**
DESCRIPTION: Adaptive1
STRATEGY: Adaptive
WCS: #5
TOLERANCE: 0.1mm
STOCK TO LEAVE: 0.25mm/0mm
MAXIMUM STEPDOWN: 10mm
OPTIMAL LOAD: 6.4mm
LOAD DEVIATION: 0.64mm
MAXIMUM Z: 15mm
MINIMUM Z: -82mm
MAXIMUM SPINDLE SPEED: 5600rpm
MAXIMUM FEEDRATE: 2506.69mm/min
CUTTING DISTANCE: 16881.86mm
RAPID DISTANCE: 12765.89mm
ESTIMATED CYCLE TIME: 10m:50s (15.8%)
COOLANT: Flood

**T12 D12 L12**
TYPE: flat end mill
DIAMETER: 16mm
LENGTH: 88mm
FLUTES: 3
DESCRIPTION: 16mm reduced shank

**Operation 3/4**
DESCRIPTION: 2D Contour14
STRATEGY: Contour 2D
WCS: #5
TOLERANCE: 0.01mm
STOCK TO LEAVE: 0mm
MAXIMUM STEPDOWN: 15mm
MAXIMUM STEPOVER: 15.2mm
MAXIMUM Z: 15mm
MINIMUM Z: -82mm
MAXIMUM SPINDLE SPEED: 5600rpm
MAXIMUM FEEDRATE: 2506.69mm/min
CUTTING DISTANCE: 4916.14mm
RAPID DISTANCE: 105.4mm
ESTIMATED CYCLE TIME: 2m:42s (3.9%)
COOLANT: Flood

**T12 D12 L12**
TYPE: flat end mill
DIAMETER: 16mm
LENGTH: 88mm
FLUTES: 3
DESCRIPTION: 16mm reduced shank

**Operation 4/4**
DESCRIPTION: Drill3
STRATEGY: Drilling
WCS: #5
TOLERANCE: 0.01mm
MAXIMUM Z: 15mm
MINIMUM Z: -20mm
MAXIMUM SPINDLE SPEED: 2375rpm
MAXIMUM FEEDRATE: 475.089mm/min
CUTTING DISTANCE: 291.75mm
RAPID DISTANCE: 1415.09mm
ESTIMATED CYCLE TIME: 54s (1.3%)
COOLANT: Off

**T3 D3 L3**
TYPE: drill
DIAMETER: 4.2mm
TIP ANGLE: 135°
LENGTH: 50mm
FLUTES: 2
DESCRIPTION: for m5 (4.2)

# Operation 40 BATTERY CASE

## Setup

WCS: #5

STOCK:
DX: 314.25mm
DY: 87mm
DZ: 169.21mm

PART:
DX: 314.25mm
DY: 87mm
DZ: 169.21mm

STOCK LOWER IN WCS #5:
X: -157.13mm
Y: -43.5mm
Z: -169.21mm

STOCK UPPER IN WCS #5:
X: 157.13mm
Y: 43.5mm
Z: 0mm

## Total

NUMBER OF OPERATIONS: 4
NUMBER OF TOOLS: 3
TOOLS: T8 T25 T36
MAXIMUM Z: 15mm
MINIMUM Z: -11.56mm
MAXIMUM FEEDRATE: 2970mm/min
MAXIMUM SPINDLE SPEED: 13500rpm
CUTTING DISTANCE: 94561.73mm
RAPID DISTANCE: 9906.61mm
ESTIMATED CYCLE TIME: 40m:23s

## Tools

**T8 D8 L8**
TYPE: countersink
DIAMETER: 12mm
TIP ANGLE: 90°
LENGTH: 55mm
FLUTES: 3
DESCRIPTION: HM38 D12 90
MINIMUM Z: -2mm
MAXIMUM FEED: 1193.66mm/min
MAXIMUM SPINDLE SPEED: 7958rpm
CUTTING DISTANCE: 1585.71mm
RAPID DISTANCE: 593.23mm
ESTIMATED CYCLE TIME: 1m:47s (4.4%)
HOLDER: 60mm BT40

**T25 D25 L25**
TYPE: chamfer mill
DIAMETER: 10mm
TAPER ANGLE: 45°
LENGTH: 50mm
FLUTES: 2
DESCRIPTION: engrave
MINIMUM Z: -11.56mm
MAXIMUM FEED: 1000mm/min
MAXIMUM SPINDLE SPEED: 9549rpm
CUTTING DISTANCE: 408.6mm
RAPID DISTANCE: 1275.47mm
ESTIMATED CYCLE TIME: 43s (1.8%)

### T36 D36 L36

TYPE: bullnose end mill
DIAMETER: 12mm
CORNER RADIUS: 1.5mm
LENGTH: 88mm
FLUTES: 2
DESCRIPTION: HM92/12.15 DLC
MINIMUM Z: -11mm
MAXIMUM FEED: 2970mm/min
MAXIMUM SPINDLE SPEED: 13500rpm
CUTTING DISTANCE: 92567.43mm
RAPID DISTANCE: 8037.9mm
ESTIMATED CYCLE TIME: 37m:8s (92%)
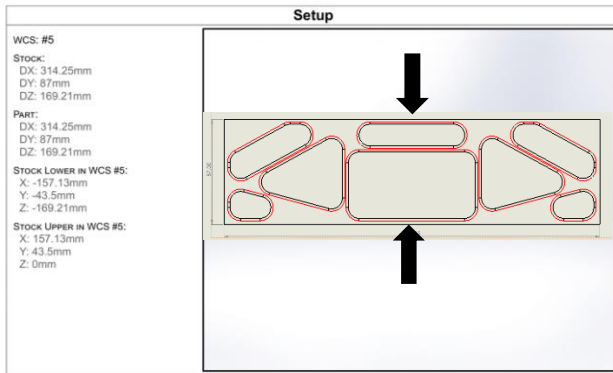HOLDER: 160 shrink

## Operations

**Operation 1/4**
DESCRIPTION: Adaptive2
STRATEGY: Adaptive
WCS: #5
TOLERANCE: 0.1mm
STOCK TO LEAVE: 0.25mm/0mm
MAXIMUM STEPDOWN: 5mm
OPTIMAL LOAD: 1mm
LOAD DEVIATION: 0.1mm
MAXIMUM Z: 15mm
MINIMUM Z: -10.99mm
MAXIMUM SPINDLE SPEED: 13500rpm
MAXIMUM FEEDRATE: 2970mm/min
CUTTING DISTANCE: 88541.35mm
RAPID DISTANCE: 7254.07mm
ESTIMATED CYCLE TIME: 35m:20s (87.5%)
COOLANT: Flood

**T36 D36 L36**
TYPE: bullnose end mill
DIAMETER: 12mm
CORNER RADIUS: 1.5mm
LENGTH: 88mm
FLUTES: 2
DESCRIPTION: HM92/12.15 DLC

**Operation 2/4**
DESCRIPTION: 2D Contour3
STRATEGY: Contour 2D
WCS: #5
TOLERANCE: 0.01mm
STOCK TO LEAVE: 0mm
MAXIMUM STEPDOWN: 5mm
MAXIMUM STEPOVER: 8.55mm
MAXIMUM Z: 15mm
MINIMUM Z: -11mm
MAXIMUM SPINDLE SPEED: 13500rpm
MAXIMUM FEEDRATE: 2970mm/min
CUTTING DISTANCE: 4026.08mm
RAPID DISTANCE: 783.84mm
ESTIMATED CYCLE TIME: 1m:48s (4.4%)
COOLANT: Flood

**T36 D36 L36**
TYPE: bullnose end mill
DIAMETER: 12mm
CORNER RADIUS: 1.5mm
LENGTH: 88mm
FLUTES: 2
DESCRIPTION: HM92/12.15 DLC

**Operation 3/4**
DESCRIPTION: 2D Contour8
STRATEGY: Contour 2D
WCS: #5
TOLERANCE: 0.01mm
STOCK TO LEAVE: 0mm
MAXIMUM STEPOVER: 11.4mm
MAXIMUM Z: 15mm
MINIMUM Z: -2mm
MAXIMUM SPINDLE SPEED: 7958rpm
MAXIMUM FEEDRATE: 1193.66mm/min
CUTTING DISTANCE: 1585.71mm
RAPID DISTANCE: 593.23mm
ESTIMATED CYCLE TIME: 1m:47s (4.4%)
COOLANT: Flood

**T8 D8 L8**
TYPE: countersink
DIAMETER: 12mm
TIP ANGLE: 90°
LENGTH: 55mm
FLUTES: 3
DESCRIPTION: HM38 D12 90

**Operation 4/4**
DESCRIPTION: Engrave2
WCS: #5
TOLERANCE: 0.01mm
MAXIMUM Z: 15mm
MINIMUM Z: -11.56mm
MAXIMUM SPINDLE SPEED: 9549rpm
MAXIMUM FEEDRATE: 1000mm/min
CUTTING DISTANCE: 408.6mm
RAPID DISTANCE: 1275.47mm
ESTIMATED CYCLE TIME: 43s (1.8%)
COOLANT: Flood

**T25 D25 L25**
TYPE: chamfer mill
DIAMETER: 10mm
TAPER ANGLE: 45°
LENGTH: 50mm
FLUTES: 2
DESCRIPTION: engrave

# Operation 50 BATTERY CASE

## Setup

WCS: #5

STOCK:
- DX: 314.25mm
- DY: 87mm
- DZ: 169.21mm

PART:
- DX: 314.25mm
- DY: 87mm
- DZ: 169.21mm

STOCK LOWER IN WCS #5:
- X: -157.13mm
- Y: -43.5mm
- Z: -169.21mm

STOCK UPPER IN WCS #5:
- X: 157.13mm
- Y: 43.5mm
- Z: 0mm

## Operations

### Operation 1/3
- DESCRIPTION: Adaptive3
- STRATEGY: Adaptive
- WCS: #5
- TOLERANCE: 0.1mm
- STOCK TO LEAVE: 0.25mm/0mm
- MAXIMUM STEPDOWN: 5mm
- OPTIMAL LOAD: 1mm
- LOAD DEVIATION: 0.1mm
- MAXIMUM Z: 15mm
- MINIMUM Z: -10.99mm
- MAXIMUM SPINDLE SPEED: 13500rpm
- MAXIMUM FEEDRATE: 2970mm/min
- CUTTING DISTANCE: 88032.12mm
- RAPID DISTANCE: 8063.1mm
- ESTIMATED CYCLE TIME: 35m:19s (89.8%)
- COOLANT: Flood

**T36 D36 L36**
- TYPE: bullnose end mill
- DIAMETER: 12mm
- CORNER RADIUS: 1.5mm
- LENGTH: 88mm
- FLUTES: 2
- DESCRIPTION: HM92/12.15 DLC

### Operation 2/3
- DESCRIPTION: 2D Contour6
- STRATEGY: Contour 2D
- WCS: #5
- TOLERANCE: 0.01mm
- STOCK TO LEAVE: 0mm
- MAXIMUM STEPDOWN: 5mm
- MAXIMUM STEPOVER: 8.55mm
- MAXIMUM Z: 15mm
- MINIMUM Z: -11mm
- MAXIMUM SPINDLE SPEED: 13500rpm
- MAXIMUM FEEDRATE: 2970mm/min
- CUTTING DISTANCE: 4011.15mm
- RAPID DISTANCE: 620.68mm
- ESTIMATED CYCLE TIME: 1m:45s (4.5%)
- COOLANT: Flood

**T36 D36 L36**
- TYPE: bullnose end mill
- DIAMETER: 12mm
- CORNER RADIUS: 1.5mm
- LENGTH: 88mm
- FLUTES: 2
- DESCRIPTION: HM92/12.15 DLC

### Operation 3/3
- DESCRIPTION: 2D Contour1
- STRATEGY: Contour 2D
- WCS: #5
- TOLERANCE: 0.01mm
- STOCK TO LEAVE: 0mm
- MAXIMUM STEPOVER: 11.4mm
- MAXIMUM Z: 15mm
- MINIMUM Z: -2mm
- MAXIMUM SPINDLE SPEED: 7958rpm
- MAXIMUM FEEDRATE: 1193.66mm/min
- CUTTING DISTANCE: 1577.71mm
- RAPID DISTANCE: 540.71mm
- ESTIMATED CYCLE TIME: 1m:46s (4.5%)
- COOLANT: Flood

**T8 D8 L8**
- TYPE: countersink
- DIAMETER: 12mm
- TIP ANGLE: 90°
- LENGTH: 55mm
- FLUTES: 3
- DESCRIPTION: HM38 D12 90

## Total

- NUMBER OF OPERATIONS: 3
- NUMBER OF TOOLS: 2
- TOOLS: T8 T36
- MAXIMUM Z: 15mm
- MINIMUM Z: -11mm
- MAXIMUM FEEDRATE: 2970mm/min
- MAXIMUM SPINDLE SPEED: 13500rpm
- CUTTING DISTANCE: 93620.98mm
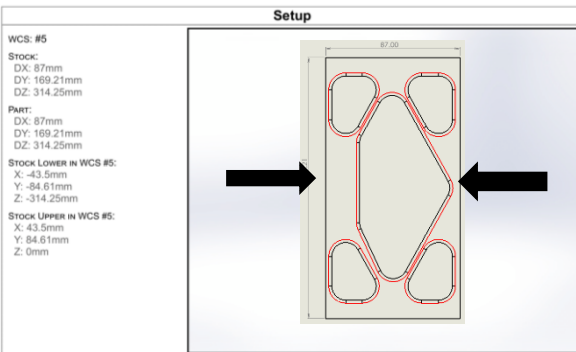- RAPID DISTANCE: 9224.5mm
- ESTIMATED CYCLE TIME: 39m:20s

## Tools

**T8 D8 L8**
- TYPE: countersink
- DIAMETER: 12mm
- TIP ANGLE: 90°
- LENGTH: 55mm
- FLUTES: 3
- DESCRIPTION: HM38 D12 90
- MINIMUM Z: -2mm
- MAXIMUM FEED: 1193.66mm/min
- MAXIMUM SPINDLE SPEED: 7958rpm
- CUTTING DISTANCE: 1577.71mm
- RAPID DISTANCE: 540.71mm
- ESTIMATED CYCLE TIME: 1m:46s (4.5%)
- HOLDER: 60mm BT40

**T36 D36 L36**
- TYPE: bullnose end mill
- DIAMETER: 12mm
- CORNER RADIUS: 1.5mm
- LENGTH: 88mm
- FLUTES: 2
- DESCRIPTION: HM92/12.15 DLC
- MINIMUM Z: -11mm
- MAXIMUM FEED: 2970mm/min
- MAXIMUM SPINDLE SPEED: 13500rpm
- CUTTING DISTANCE: 92043.27mm
- RAPID DISTANCE: 8683.78mm
- ESTIMATED CYCLE TIME: 37m:4s (94.2%)
- HOLDER: 160 shrink

# Operation 60 BATTERY CASE

## Setup

WCS: #5

STOCK:
- DX: 87mm
- DY: 169.21mm
- DZ: 314.25mm

PART:
- DX: 87mm
- DY: 169.21mm
- DZ: 314.25mm

STOCK LOWER IN WCS #5:
- X: -43.5mm
- Y: -84.61mm
- Z: -314.25mm

STOCK UPPER IN WCS #5:
- X: 43.5mm
- Y: 84.61mm
- Z: 0mm

## Operations

### Operation 1/3
- DESCRIPTION: Adaptive5
- STRATEGY: Adaptive
- WCS: #5
- TOLERANCE: 0.1mm
- STOCK TO LEAVE: 0.25mm/0mm
- MAXIMUM STEPDOWN: 5mm
- OPTIMAL LOAD: 1mm
- LOAD DEVIATION: 0.1mm
- MAXIMUM Z: 15mm
- MINIMUM Z: -10.99mm
- MAXIMUM SPINDLE SPEED: 13500rpm
- MAXIMUM FEEDRATE: 2970mm/min
- CUTTING DISTANCE: 38310.26mm
- RAPID DISTANCE: 4976.22mm
- ESTIMATED CYCLE TIME: 16m:20s (87.7%)
- COOLANT: Flood

**T36 D36 L36**
- TYPE: bullnose end mill
- DIAMETER: 12mm
- CORNER RADIUS: 1.5mm
- LENGTH: 88mm
- FLUTES: 2
- DESCRIPTION: HM92/12.15 DLC

### Operation 2/3
- DESCRIPTION: 2D Contour5
- STRATEGY: Contour 2D
- WCS: #5
- TOLERANCE: 0.01mm
- STOCK TO LEAVE: 0mm
- MAXIMUM STEPDOWN: 5mm
- MAXIMUM STEPOVER: 8.55mm
- MAXIMUM Z: 15mm
- MINIMUM Z: -11mm
- MAXIMUM SPINDLE SPEED: 13500rpm
- MAXIMUM FEEDRATE: 2970mm/min
- CUTTING DISTANCE: 2005.24mm
- RAPID DISTANCE: 378.37mm
- ESTIMATED CYCLE TIME: 55s (4.9%)
- COOLANT: Flood

**T36 D36 L36**
- TYPE: bullnose end mill
- DIAMETER: 12mm
- CORNER RADIUS: 1.5mm
- LENGTH: 88mm
- FLUTES: 2
- DESCRIPTION: HM92/12.15 DLC

### Operation 3/3
- DESCRIPTION: 2D Contour4
- STRATEGY: Contour 2D
- WCS: #5
- TOLERANCE: 0.01mm
- STOCK TO LEAVE: 0mm
- MAXIMUM STEPOVER: 11.4mm
- MAXIMUM Z: 15mm
- MINIMUM Z: -2mm
- MAXIMUM SPINDLE SPEED: 7958rpm
- MAXIMUM FEEDRATE: 1193.66mm/min
- CUTTING DISTANCE: 765.06mm
- RAPID DISTANCE: 327.99mm
- ESTIMATED CYCLE TIME: 53s (4.7%)
- COOLANT: Flood

**T8 D8 L8**
- TYPE: countersink
- DIAMETER: 12mm
- TIP ANGLE: 90°
- LENGTH: 55mm
- FLUTES: 3
- DESCRIPTION: HM38 D12 90

## Total

- NUMBER OF OPERATIONS: 3
- NUMBER OF TOOLS: 2
- TOOLS: T8 T36
- MAXIMUM Z: 15mm
- MINIMUM Z: -11mm
- MAXIMUM FEEDRATE: 2970mm/min
- MAXIMUM SPINDLE SPEED: 13500rpm
- CUTTING DISTANCE: 41080.57mm
- RAPID DISTANCE: 5682.57mm
- ESTIMATED CYCLE TIME: 18m:38s
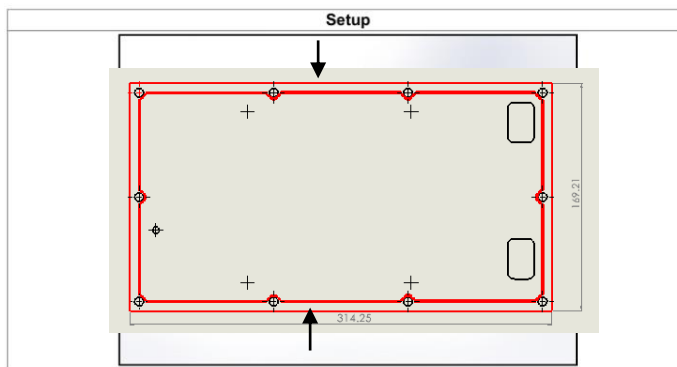
## Tools

**T8 D8 L8**
- TYPE: countersink
- DIAMETER: 12mm
- TIP ANGLE: 90°
- LENGTH: 55mm
- FLUTES: 3
- DESCRIPTION: HM38 D12 90
- MINIMUM Z: -2mm
- MAXIMUM FEED: 1193.66mm/min
- MAXIMUM SPINDLE SPEED: 7958rpm
- CUTTING DISTANCE: 765.06mm
- RAPID DISTANCE: 327.99mm
- ESTIMATED CYCLE TIME: 53s (4.7%)
- HOLDER: 60mm BT40

**T36 D36 L36**
- TYPE: bullnose end mill
- DIAMETER: 12mm
- CORNER RADIUS: 1.5mm
- LENGTH: 88mm
- FLUTES: 2
- DESCRIPTION: HM92/12.15 DLC
- MINIMUM Z: -11mm
- MAXIMUM FEED: 2970mm/min
- MAXIMUM SPINDLE SPEED: 13500rpm
- CUTTING DISTANCE: 40315.5mm
- RAPID DISTANCE: 5354.59mm
- ESTIMATED CYCLE TIME: 17m:15s (92.6%)
- HOLDER: 160 shrink

# Operation 70 BATTERY CASE

## Setup

WCS: #5

STOCK:
 DX: 87mm
 DY: 169.21mm
 DZ: 314.25mm

PART:
 DX: 87mm
 DY: 169.21mm
 DZ: 314.25mm

STOCK LOWER IN WCS #5:
 X: -43.5mm
 Y: -84.61mm
 Z: -314.25mm

STOCK UPPER IN WCS #5:
 X: 43.5mm
 Y: 84.61mm
 Z: 0mm



87.00

## Operations

### Operation 1/3
DESCRIPTION: Adaptive6
STRATEGY: Adaptive
WCS: #5
TOLERANCE: 0.1mm
STOCK TO LEAVE: 0.25mm/0mm
MAXIMUM STEPDOWN: 5mm
OPTIMAL LOAD: 1mm
LOAD DEVIATION: 0.1mm

MAXIMUM Z: 15mm
MINIMUM Z: -10.99mm
MAXIMUM SPINDLE SPEED: 13500rpm
MAXIMUM FEEDRATE: 2970mm/min
CUTTING DISTANCE: 37163.78mm
RAPID DISTANCE: 5289.73mm
ESTIMATED CYCLE TIME: 15m:56s (87.5%)
COOLANT: Flood

**T36** D36 L36
TYPE: bullnose end mill
DIAMETER: 12mm
CORNER RADIUS: 1.5mm
LENGTH: 88mm
FLUTES: 2
DESCRIPTION: HM92/12.15 DLC

### Operation 2/3
DESCRIPTION: 2D Contour7
STRATEGY: Contour 2D
WCS: #5
TOLERANCE: 0.1mm
STOCK TO LEAVE: 0mm
MAXIMUM STEPDOWN: 5mm
MAXIMUM STEPOVER: 8.55mm

MAXIMUM Z: 15mm
MINIMUM Z: -11mm
MAXIMUM SPINDLE SPEED: 13500rpm
MAXIMUM FEEDRATE: 2970mm/min
CUTTING DISTANCE: 1941.88mm
RAPID DISTANCE: 381.12mm
ESTIMATED CYCLE TIME: 54s (5%)
COOLANT: Flood

**T36** D36 L36
TYPE: bullnose end mill
DIAMETER: 12mm
CORNER RADIUS: 1.5mm
LENGTH: 88mm
FLUTES: 2
DESCRIPTION: HM92/12.15 DLC

### Operation 3/3
DESCRIPTION: 2D Contour2
STRATEGY: Contour 2D
WCS: #5
TOLERANCE: 0.01mm
STOCK TO LEAVE: 0mm
MAXIMUM STEPOVER: 11.4mm

MAXIMUM Z: 15mm
MINIMUM Z: -2mm
MAXIMUM SPINDLE SPEED: 7958rpm
MAXIMUM FEEDRATE: 1193.66mm/min
CUTTING DISTANCE: 744.2mm
RAPID DISTANCE: 330.71mm
ESTIMATED CYCLE TIME: 52s (4.7%)
COOLANT: Flood

**T8** D8 L8
TYPE: countersink
DIAMETER: 12mm
TIP ANGLE: 90°
LENGTH: 55mm
FLUTES: 3
DESCRIPTION: HM38 D12 90

## Total

NUMBER OF OPERATIONS: 3
NUMBER OF TOOLS: 2
TOOLS: T8 T36
MAXIMUM Z: 15mm
MINIMUM Z: -11mm
MAXIMUM FEEDRATE: 2970mm/min
MAXIMUM SPINDLE SPEED: 13500rpm
CUTTING DISTANCE: 39849.86mm
RAPID DISTANCE: 6001.56mm
ESTIMATED CYCLE TIME: 18m:12s

## Tools

### T8 D8 L8
TYPE: countersink
DIAMETER: 12mm
TIP ANGLE: 90°
LENGTH: 55mm
FLUTES: 3
DESCRIPTION: HM38 D12 90

MINIMUM Z: -2mm
MAXIMUM FEED: 1193.66mm/min
MAXIMUM SPINDLE SPEED: 7958rpm
CUTTING DISTANCE: 744.2mm
RAPID DISTANCE: 330.71mm
ESTIMATED CYCLE TIME: 52s (4.7%)

HOLDER: 60mm BT40

### T36 D36 L36
TYPE: bullnose end mill
DIAMETER: 12mm
CORNER RADIUS: 1.5mm
LENGTH: 88mm
FLUTES: 2
DESCRIPTION: HM92/12.15 DLC

MINIMUM Z: -11mm
MAXIMUM FEED: 2970mm/min
MAXIMUM SPINDLE SPEED: 13500rpm
CUTTING DISTANCE: 39105.66mm
RAPID DISTANCE: 5670.85mm
ESTIMATED CYCLE TIME: 16m:50s (92.5%)

HOLDER: 160 shrink

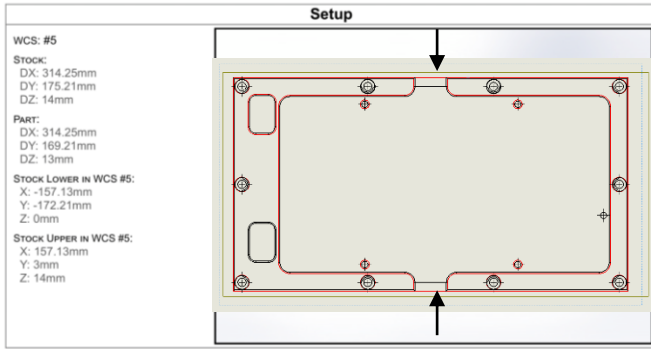| CORBELLATI AUTOMOBILI | **PROCESS ROUTE SHEET** | | Version - 2 |
|---|---|---|---|
| Material: Aluminium 6061-T6 | Part – BATTERY CASE<br>Part Number – B002<br>Blank – Rectangle Block | | |
| Op. | Machine | OPERATION DESCRIPTION | |
| 10 | HAAS VF-7 | Facing , shoulder milling and engraving on one side of the case | |
| 20 | HAAS VF-7 | Facing and shoulder milling and drilling on other side of the case | |

## Operation10 BATTERY COVER



**Setup**

**Total**

Number Of Operations: 4
Number Of Tools: 3
Tools: T6 T25 T42
Maximum Z: 16mm
Minimum Z: -16mm
Maximum Feedrate: 3300mm/min
Maximum Spindle Speed: 15000rpm
Cutting Distance: 33822.71mm
Rapid Distance: 19557.23mm
Estimated Cycle Time: 28m:39s

**Tools**

**T6 D6 L6**
Type: face mill
Diameter: 50mm
Taper Angle: 45°
Length: 48mm
Flutes: 4
Description: facemill
Minimum Z: 0mm
Maximum Feed: 1193.66mm/min
Maximum Spindle Speed: 4000rpm
Cutting Distance: 9405.62mm
Rapid Distance: 377.06mm
Estimated Cycle Time: 11m:49s (41.2%)
Holder: 60mm BT40

**T25 D25 L25**
Type: chamfer mill
Diameter: 10mm
Taper Angle: 45°
Length: 50mm
Flutes: 2
Description: engrave
Minimum Z: -0.5mm
Maximum Feed: 1000mm/min
Maximum Spindle Speed: 9549rpm
Cutting Distance: 924.54mm
Rapid Distance: 27.5mm
Estimated Cycle Time: 1m:10s (4%)

**T42 D42 L42**
Type: bullnose end mill
Diameter: 10mm
Corner Radius: 0.5mm
Length: 50mm
Flutes: 2
Description: HM92/10.05
Minimum Z: -16mm
Maximum Feed: 3300mm/min
Maximum Spindle Speed: 15000rpm
Cutting Distance: 23492.55mm
Rapid Distance: 19152.67mm
Estimated Cycle Time: 14m:55s (52.1%)
Holder: 100mm BT40

**Operations**

Operation 1/4
Description: Face3
Strategy: Facing
WCS: #5
Tolerance: 0.01mm
Maximum Stepdown: 1mm
Maximum Stepover: 27mm
Maximum Z: 16mm
Minimum Z: 0mm
Maximum Spindle Speed: 4000rpm
Maximum Feedrate: 1193.66mm/min
Cutting Distance: 9405.62mm
Rapid Distance: 377.06mm
Estimated Cycle Time: 11m:49s (41.2%)
Coolant: Flood
**T6 D6 L6**
Type: face mill
Diameter: 50mm
Taper Angle: 45°
Length: 48mm
Flutes: 4
Description: facemill

Operation 2/4
Description: 2D Contour2
Strategy: Contour 2D
WCS: #5
Tolerance: 0.01mm
Stock to Leave: 0mm
Maximum Stepdown: 4mm
Maximum Stepover: 1mm
Maximum Z: 16mm
Minimum Z: -7mm
Maximum Spindle Speed: 15000rpm
Maximum Feedrate: 3300mm/min
Cutting Distance: 9310.93mm
Rapid Distance: 5429.62mm
Estimated Cycle Time: 4m:54s (17.1%)
Coolant: Flood
**T42 D42 L42**
Type: bullnose end mill
Diameter: 10mm
Corner Radius: 0.5mm
Length: 50mm
Flutes: 2
Description: HM92/10.05

Operation 3/4
Description: 2D Contour3
Strategy: Contour 2D
WCS: #5
Tolerance: 0.01mm
Stock to Leave: 0mm
Maximum Stepdown: 5mm
Maximum Stepover: 1mm
Maximum Z: 16mm
Minimum Z: -16mm
Maximum Spindle Speed: 15000rpm
Maximum Feedrate: 3300mm/min
Cutting Distance: 14181.62mm
Rapid Distance: 13723.05mm
Estimated Cycle Time: 10m:1s (35%)
Coolant: Flood
**T42 D42 L42**
Type: bullnose end mill
Diameter: 10mm
Corner Radius: 0.5mm
Length: 50mm
Flutes: 2
Description: HM92/10.05

Operation 4/4
Description: Engrave2
WCS: #5
Tolerance: 0.01mm
Maximum Z: 16mm
Minimum Z: -0.5mm
Maximum Spindle Speed: 9549rpm
Maximum Feedrate: 1000mm/min
Cutting Distance: 924.54mm
Rapid Distance: 27.5mm
Estimated Cycle Time: 1m:10s (4%)
Coolant: Flood
**T25 D25 L25**
Type: chamfer mill
Diameter: 10mm
Taper Angle: 45°
Length: 50mm
Flutes: 2
Description: engrave

# Operation 20 BATTERY COVER

## Setup

WCS: #5

STOCK:
DX: 314.25mm
DY: 175.21mm
DZ: 14mm

PART:
DX: 314.25mm
DY: 169.21mm
DZ: 13mm

STOCK LOWER IN WCS #5:
X: -157.13mm
Y: -172.21mm
Z: 0mm

STOCK UPPER IN WCS #5:
X: 157.13mm
Y: 3mm
Z: 14mm

## Total

NUMBER OF OPERATIONS: 15
NUMBER OF TOOLS: 6
TOOLS: T3 T6 T8 T21 T42 T43
MAXIMUM Z: 29mm
MINIMUM Z: -3.24mm
MAXIMUM FEEDRATE: 3300mm/min
MAXIMUM SPINDLE SPEED: 15000rpm
CUTTING DISTANCE: 78066.87mm
RAPID DISTANCE: 38308.16mm
ESTIMATED CYCLE TIME: 48m:21s

## Tools

**T3 D3 L3**
TYPE: drill
DIAMETER: 5mm
TIP ANGLE: 135°
LENGTH: 55mm
FLUTES: 2
DESCRIPTION: for m6 (5)
MINIMUM Z: -2mm
MAXIMUM FEED: 475.089mm/min
MAXIMUM SPINDLE SPEED: 2000rpm
CUTTING DISTANCE: 88.49mm
RAPID DISTANCE: 1483.09mm
ESTIMATED CYCLE TIME: 29s (1%)

**T6 D6 L6**
TYPE: face mill
DIAMETER: 50mm
TAPER ANGLE: 45°
LENGTH: 48mm
FLUTES: 4
DESCRIPTION: facemill
MINIMUM Z: 13mm
MAXIMUM FEED: 1193.66mm/min
MAXIMUM SPINDLE SPEED: 4000rpm
CUTTING DISTANCE: 8833.12mm
RAPID DISTANCE: 369.68mm
ESTIMATED CYCLE TIME: 11m:6s (23%)
HOLDER: 60mm BT40

**T8 D8 L8**
TYPE: countersink
DIAMETER: 12mm
TIP ANGLE: 90°
LENGTH: 55mm
FLUTES: 3
DESCRIPTION: HM38 D12 90
MINIMUM Z: 8mm
MAXIMUM FEED: 2864.79mm/min
MAXIMUM SPINDLE SPEED: 7958rpm
CUTTING DISTANCE: 2090.47mm
RAPID DISTANCE: 1741.27mm
ESTIMATED CYCLE TIME: 1m:28s (3%)
HOLDER: 60mm BT40

**T21 D21 L21**
TYPE: bullnose end mill
DIAMETER: 8mm
CORNER RADIUS: 0.5mm
LENGTH: 55mm
FLUTES: 3
DESCRIPTION: 8mm Bullnose Endmill
MINIMUM Z: -2mm
MAXIMUM FEED: 2506.69mm/min
MAXIMUM SPINDLE SPEED: 13926rpm
CUTTING DISTANCE: 13034.14mm
RAPID DISTANCE: 7282.97mm
ESTIMATED CYCLE TIME: 9m:36s (19.9%)
HOLDER: 100mm BT40

**T42 D42 L42**
TYPE: bullnose end mill
DIAMETER: 10mm
CORNER RADIUS: 0.5mm
LENGTH: 50mm
FLUTES: 2
DESCRIPTION: HM92/10.05
MINIMUM Z: 6mm
MAXIMUM FEED: 3300mm/min
MAXIMUM SPINDLE SPEED: 15000rpm
CUTTING DISTANCE: 53797.03mm
RAPID DISTANCE: 23949.19mm
ESTIMATED CYCLE TIME: 22m:31s (46.6%)
HOLDER: 100mm BT40

**T43 D43 L43**
TYPE: drill
DIAMETER: 6.8mm
TIP ANGLE: 140°
LENGTH: 42mm
FLUTES: 2
DESCRIPTION: 860.1-0680-020A1-GMX1BM
COMMENT: for m8 sandvik
MINIMUM Z: -3.24mm
MAXIMUM FEED: 300mm/min
MAXIMUM SPINDLE SPEED: 5910rpm
CUTTING DISTANCE: 223.62mm
RAPID DISTANCE: 3481.96mm
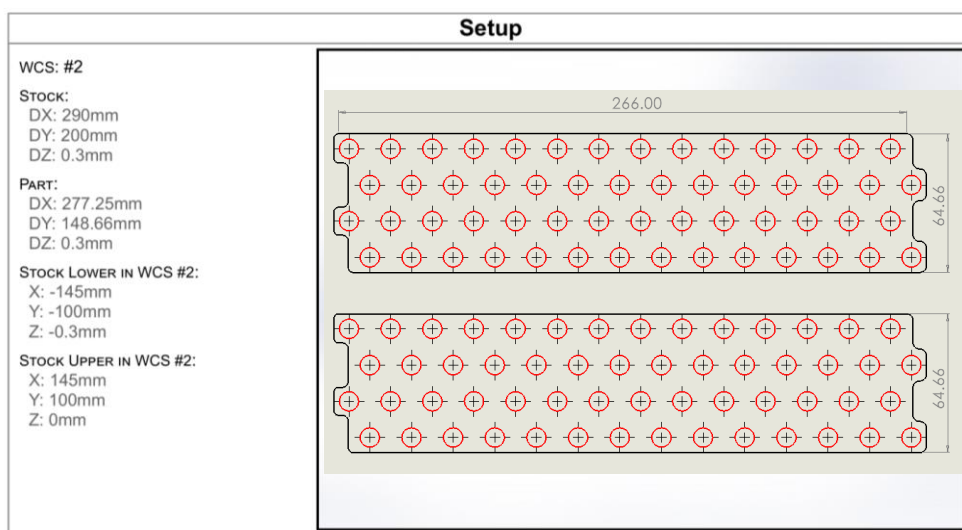ESTIMATED CYCLE TIME: 1m:27s (3%)
HOLDER: 60mm BT40

## Operations

**Operation 1/15**
DESCRIPTION: Face1
STRATEGY: Facing
WCS: #5
TOLERANCE: 0.01mm
MAXIMUM STEPDOWN: 1mm
MAXIMUM STEPOVER: 27mm
MAXIMUM Z: 29mm
MINIMUM Z: 13mm
MAXIMUM SPINDLE SPEED: 4000rpm
MAXIMUM FEEDRATE: 1193.66mm/min
CUTTING DISTANCE: 8833.12mm
RAPID DISTANCE: 369.68mm
ESTIMATED CYCLE TIME: 11m:6s (23%)
COOLANT: Flood
**T6 D6 L6**
TYPE: face mill
DIAMETER: 50mm
TAPER ANGLE: 45°
LENGTH: 48mm
FLUTES: 4
DESCRIPTION: facemill

**Operation 2/15**
DESCRIPTION: 2D Contour1
STRATEGY: Contour 2D
WCS: #5
TOLERANCE: 0.01mm
STOCK TO LEAVE: 0mm
MAXIMUM STEPDOWN: 4mm
MAXIMUM STEPOVER: 1mm
MAXIMUM Z: 29mm
MINIMUM Z: 6mm
MAXIMUM SPINDLE SPEED: 15000rpm
MAXIMUM FEEDRATE: 3300mm/min
CUTTING DISTANCE: 10150.93mm
RAPID DISTANCE: 5453.12mm
ESTIMATED CYCLE TIME: 5m:10s (10.7%)
COOLANT: Flood
**T42 D42 L42**
TYPE: bullnose end mill
DIAMETER: 10mm
CORNER RADIUS: 0.5mm
LENGTH: 50mm
FLUTES: 2
DESCRIPTION: HM92/10.05

**Operation 3/15**
DESCRIPTION: Drill2
STRATEGY: Drilling
WCS: #5
TOLERANCE: 0.01mm
MAXIMUM Z: 29mm
MINIMUM Z: 3.5mm
MAXIMUM SPINDLE SPEED: 2000rpm
MAXIMUM FEEDRATE: 475.089mm/min
CUTTING DISTANCE: 65.99mm
RAPID DISTANCE: 1128.59mm
ESTIMATED CYCLE TIME: 22s (0.8%)
COOLANT: Off
**T3 D3 L3**
TYPE: drill
DIAMETER: 5mm
TIP ANGLE: 135°
LENGTH: 55mm
FLUTES: 2
DESCRIPTION: for m6 (5)

**Operation 4/15**
DESCRIPTION: Drill1
STRATEGY: Drilling
WCS: #5
TOLERANCE: 0.01mm
MAXIMUM Z: 29mm
MINIMUM Z: -2mm
MAXIMUM SPINDLE SPEED: 2000rpm
MAXIMUM FEEDRATE: 475.089mm/min
CUTTING DISTANCE: 22.5mm
RAPID DISTANCE: 354.5mm
ESTIMATED CYCLE TIME: 7s (0.2%)
COOLANT: Off
**T3 D3 L3**
TYPE: drill
DIAMETER: 5mm
TIP ANGLE: 135°
LENGTH: 55mm
FLUTES: 2
DESCRIPTION: for m6 (5)

**Operation 5/15**
DESCRIPTION: Drill3
STRATEGY: Drilling
WCS: #5
TOLERANCE: 0.01mm
MAXIMUM Z: 29mm
MINIMUM Z: -3.24mm
MAXIMUM SPINDLE SPEED: 5910rpm
MAXIMUM FEEDRATE: 300mm/min
CUTTING DISTANCE: 223.62mm
RAPID DISTANCE: 3481.96mm
ESTIMATED CYCLE TIME: 1m:27s (3%)
COOLANT: Flood
**T43 D43 L43**
TYPE: drill
DIAMETER: 6.8mm
TIP ANGLE: 140°
LENGTH: 42mm
FLUTES: 2
DESCRIPTION: 860.1-0680-020A1-GMX1BM
COMMENT: for m8 sandvik

**Operation 6/15**
DESCRIPTION: Adaptive1
STRATEGY: Adaptive
WCS: #5
TOLERANCE: 0.1mm
STOCK TO LEAVE: 0.25mm/0mm
MAXIMUM STEPDOWN: 4mm
OPTIMAL LOAD: 1mm
LOAD DEVIATION: 0.1mm
MAXIMUM Z: 29mm
MINIMUM Z: 10mm
MAXIMUM SPINDLE SPEED: 15000rpm
MAXIMUM FEEDRATE: 3300mm/min
CUTTING DISTANCE: 42768.33mm
RAPID DISTANCE: 18467.07mm
ESTIMATED CYCLE TIME: 17m:3s (35.3%)
COOLANT: Flood
**T42 D42 L42**
TYPE: bullnose end mill
DIAMETER: 10mm
CORNER RADIUS: 0.5mm
LENGTH: 50mm
FLUTES: 2
DESCRIPTION: HM92/10.05

**Operation 7/15**
DESCRIPTION: 2D Contour4
STRATEGY: Contour 2D
WCS: #5
TOLERANCE: 0.01mm
STOCK TO LEAVE: 0mm
MAXIMUM STEPOVER: 8.55mm
MAXIMUM Z: 29mm
MINIMUM Z: 10mm
MAXIMUM SPINDLE SPEED: 15000rpm
MAXIMUM FEEDRATE: 3300mm/min
CUTTING DISTANCE: 877.77mm
RAPID DISTANCE: 29mm
ESTIMATED CYCLE TIME: 18s (0.6%)
COOLANT: Flood
**T42 D42 L42**
TYPE: bullnose end mill
DIAMETER: 10mm
CORNER RADIUS: 0.5mm
LENGTH: 50mm
FLUTES: 2
DESCRIPTION: HM92/10.05

**Operation 8/15**
DESCRIPTION: Adaptive2
STRATEGY: Adaptive
WCS: #5
TOLERANCE: 0.1mm
STOCK TO LEAVE: 0.25mm/0mm
MAXIMUM STEPDOWN: 4mm
OPTIMAL LOAD: 1mm
LOAD DEVIATION: 0.1mm
MAXIMUM Z: 29mm
MINIMUM Z: -1mm
MAXIMUM SPINDLE SPEED: 13926rpm
MAXIMUM FEEDRATE: 2506.69mm/min
CUTTING DISTANCE: 8014.19mm
RAPID DISTANCE: 1442.31mm
ESTIMATED CYCLE TIME: 4m:23s (9.1%)
COOLANT: Flood
**T21 D21 L21**
TYPE: bullnose end mill
DIAMETER: 8mm
CORNER RADIUS: 0.5mm
LENGTH: 55mm
FLUTES: 3
DESCRIPTION: 8mm Bullnose Endmill

**Operation 9/15**
DESCRIPTION: 2D Contour5
STRATEGY: Contour 2D
WCS: #5
TOLERANCE: 0.01mm
STOCK TO LEAVE: 0mm
MAXIMUM STEPDOWN: 4mm
MAXIMUM STEPOVER: 6.65mm
MAXIMUM Z: 29mm
MINIMUM Z: -2mm
MAXIMUM SPINDLE SPEED: 13926rpm
MAXIMUM FEEDRATE: 2506.69mm/min
CUTTING DISTANCE: 633.28mm
RAPID DISTANCE: 170.12mm
ESTIMATED CYCLE TIME: 28s (1%)
COOLANT: Flood
**T21 D21 L21**
TYPE: bullnose end mill
DIAMETER: 8mm
CORNER RADIUS: 0.5mm
LENGTH: 55mm
FLUTES: 3
DESCRIPTION: 8mm Bullnose Endmill

**Operation 10/15**
DESCRIPTION: Adaptive4
STRATEGY: Adaptive
WCS: #5
TOLERANCE: 0.1mm
STOCK TO LEAVE: 0.25mm/0mm
MAXIMUM STEPDOWN: 4mm
OPTIMAL LOAD: 1mm
LOAD DEVIATION: 0.1mm
MAXIMUM Z: 29mm
MINIMUM Z: 6.6mm
MAXIMUM SPINDLE SPEED: 13926rpm
MAXIMUM FEEDRATE: 2506.69mm/min
CUTTING DISTANCE: 3933.64mm
RAPID DISTANCE: 4723.64mm
ESTIMATED CYCLE TIME: 3m:57s (8.2%)
COOLANT: Flood
**T21 D21 L21**
TYPE: bullnose end mill
DIAMETER: 8mm
CORNER RADIUS: 0.5mm
LENGTH: 55mm
FLUTES: 3
DESCRIPTION: 8mm Bullnose Endmill

**Operation 11/15**
DESCRIPTION: 2D Contour6
STRATEGY: Contour 2D
WCS: #5
TOLERANCE: 0.01mm
STOCK TO LEAVE: 0mm
MAXIMUM STEPDOWN: 4mm
MAXIMUM STEPOVER: 6.65mm
MAXIMUM Z: 29mm
MINIMUM Z: 6.6mm
MAXIMUM SPINDLE SPEED: 13926rpm
MAXIMUM FEEDRATE: 2506.69mm/min
CUTTING DISTANCE: 453.03mm
RAPID DISTANCE: 946.9mm
ESTIMATED CYCLE TIME: 48s (1.6%)
COOLANT: Flood
**T21 D21 L21**
TYPE: bullnose end mill
DIAMETER: 8mm
CORNER RADIUS: 0.5mm
LENGTH: 55mm
FLUTES: 3
DESCRIPTION: 8mm Bullnose Endmill

**Operation 12/15**
DESCRIPTION: Drill4
STRATEGY: Drilling
WCS: #5
TOLERANCE: 0.01mm
MAXIMUM Z: 29mm
MINIMUM Z: 8mm
MAXIMUM SPINDLE SPEED: 7958rpm
MAXIMUM FEEDRATE: 397.888mm/min
CUTTING DISTANCE: 28mm
RAPID DISTANCE: 450.6mm
ESTIMATED CYCLE TIME: 10s (0.3%)
COOLANT: Flood
**T8 D8 L8**
TYPE: countersink
DIAMETER: 12mm
TIP ANGLE: 90°
LENGTH: 55mm
FLUTES: 3
DESCRIPTION: HM38 D12 90

**Operation 13/15**
DESCRIPTION: 2D Contour8
STRATEGY: Contour 2D
WCS: #5
TOLERANCE: 0.01mm
STOCK TO LEAVE: 0mm
MAXIMUM STEPOVER: 11.4mm
MAXIMUM Z: 29mm
MINIMUM Z: 12mm
MAXIMUM SPINDLE SPEED: 7958rpm
MAXIMUM FEEDRATE: 2864.79mm/min
CUTTING DISTANCE: 957.82mm
RAPID DISTANCE: 54.2mm
ESTIMATED CYCLE TIME: 23s (0.8%)
COOLANT: Flood
**T8 D8 L8**
TYPE: countersink
DIAMETER: 12mm
TIP ANGLE: 90°
LENGTH: 55mm
FLUTES: 3
DESCRIPTION: HM38 D12 90

**Operation 14/15**
DESCRIPTION: 2D Contour9
STRATEGY: Contour 2D
WCS: #5
TOLERANCE: 0.01mm
STOCK TO LEAVE: 0mm
MAXIMUM STEPOVER: 11.4mm
MAXIMUM Z: 29mm
MINIMUM Z: 12mm
MAXIMUM SPINDLE SPEED: 7958rpm
MAXIMUM FEEDRATE: 2864.79mm/min
CUTTING DISTANCE: 1012.14mm
RAPID DISTANCE: 293.14mm
ESTIMATED CYCLE TIME: 30s (1%)
COOLANT: Flood
**T8 D8 L8**
TYPE: countersink
DIAMETER: 12mm
TIP ANGLE: 90°
LENGTH: 55mm
FLUTES: 3
DESCRIPTION: HM38 D12 90

**Operation 15/15**
DESCRIPTION: Drill5
STRATEGY: Drilling
WCS: #5
TOLERANCE: 0.01mm
MAXIMUM Z: 29mm
MINIMUM Z: 8.75mm
MAXIMUM SPINDLE SPEED: 7958rpm
MAXIMUM FEEDRATE: 397.888mm/min
CUTTING DISTANCE: 92.5mm
RAPID DISTANCE: 943.34mm
ESTIMATED CYCLE TIME: 25s (0.9%)
COOLANT: Flood
**T8 D8 L8**
TYPE: countersink
DIAMETER: 12mm
TIP ANGLE: 90°
LENGTH: 55mm
FLUTES: 3
DESCRIPTION: HM38 D12 90

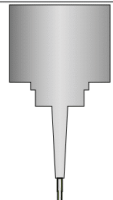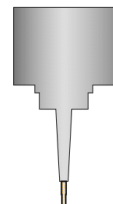| CORBELLATI AUTOMOBILI | **PROCESS ROUTE SHEET** | | Version - 2 |
|---|---|---|---|
| Material:  Copper | Part Name: COPPER PLATES<br>Part No: B004<br>Blank: RECTANGLE SHEET | | |
| Op. | Machine | OPERATION DESCRIPTION | |
| 10 | HAAS VF-7 | Boring of copper plate | |
| 20 | HAAS VF-7 | Shoulder milling to cut the plates | |

## Operation 10 COPPER PLATES
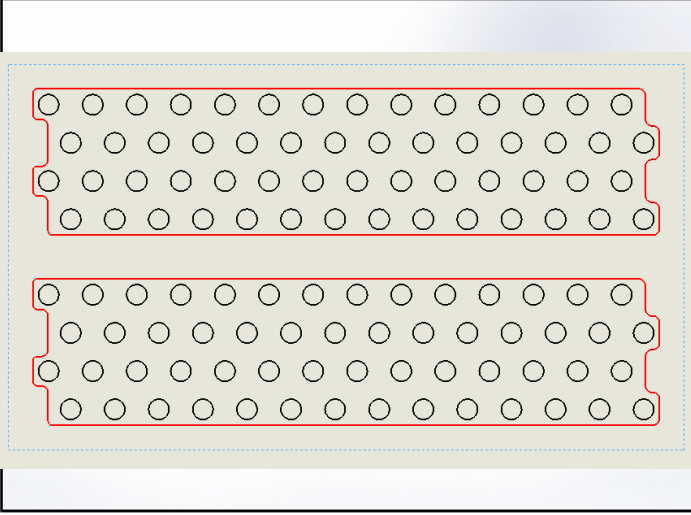


**Setup**

WCS: #2

STOCK:
DX: 290mm
DY: 200mm
DZ: 0.3mm

PART:
DX: 277.25mm
DY: 148.66mm
DZ: 0.3mm

STOCK LOWER IN WCS #2:
X: -145mm
Y: -100mm
Z: -0.3mm

STOCK UPPER IN WCS #2:
X: 145mm
Y: 100mm
Z: 0mm

266.00

64.66

64.66

**Total**

NUMBER OF OPERATIONS: 1
NUMBER OF TOOLS: 1
TOOLS: T27
MAXIMUM Z: 15mm
MINIMUM Z: -2mm
MAXIMUM FEEDRATE: 3150mm/min
MAXIMUM SPINDLE SPEED: 15000rpm
CUTTING DISTANCE: 16464.9mm
RAPID DISTANCE: 3392.27mm
ESTIMATED CYCLE TIME: 21m:17s

**Tools**

**T27** D27 L27
TYPE: flat end mill
DIAMETER: 5mm
LENGTH: 33mm
FLUTES: 3
DESCRIPTION: HM90/05 D5
COMMENT: coated

MINIMUM Z: -2mm
MAXIMUM FEED: 3150mm/min
MAXIMUM SPINDLE SPEED: 15000rpm
CUTTING DISTANCE: 16464.9mm
RAPID DISTANCE: 3392.27mm
ESTIMATED CYCLE TIME: 21m:2s

HOLDER: 100mm BT40

Operation 1/1
DESCRIPTION: 2D Contour2
STRATEGY: Contour 2D
WCS: #2
TOLERANCE: 0.01mm
STOCK TO LEAVE: 0mm
MAXIMUM STEPOVER: 4.75mm

MAXIMUM Z: 15mm
MINIMUM Z: -2mm
MAXIMUM SPINDLE SPEED: 15000rpm
MAXIMUM FEEDRATE: 3150mm/min
CUTTING DISTANCE: 16464.9mm
RAPID DISTANCE: 3392.27mm
ESTIMATED CYCLE TIME: 21m:2s
COOLANT: Flood

**T27** D27 L27
TYPE: flat end mill
DIAMETER: 5mm
LENGTH: 33mm
FLUTES: 3
DESCRIPTION: HM90/05 D5
COMMENT: coated

# Operation 20 COPPER PLATES

## Setup

WCS: #2

STOCK:
  DX: 290mm
  DY: 200mm
  DZ: 0.3mm

PART:
  DX: 277.25mm
  DY: 148.66mm
  DZ: 0.3mm

STOCK LOWER IN WCS #2:
  X: -145mm
  Y: -100mm
  Z: -0.3mm
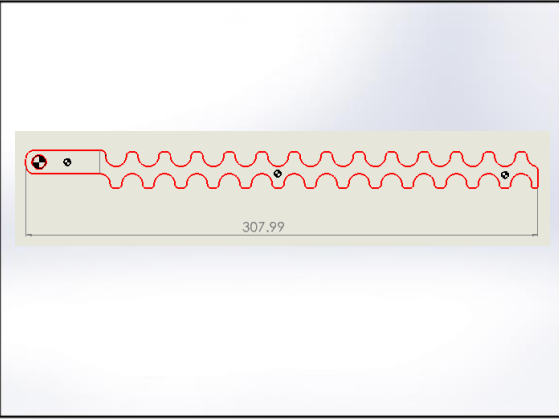
STOCK UPPER IN WCS #2:
  X: 145mm
  Y: 100mm
  Z: 0mm

## Total

NUMBER OF OPERATIONS: 1
NUMBER OF TOOLS: 1
TOOLS: **T27**
MAXIMUM Z: 15mm
MINIMUM Z: -2mm
MAXIMUM FEEDRATE: 500mm/min
MAXIMUM SPINDLE SPEED: 15000rpm
CUTTING DISTANCE: 1704.32mm
RAPID DISTANCE: 229.65mm
ESTIMATED CYCLE TIME: 3m:43s

## Tools

**T27** D27 L27

| | | |
|---|---|---|
| TYPE: flat end mill | MINIMUM Z: -2mm | HOLDER: 100mm BT40 |
| DIAMETER: 5mm | MAXIMUM FEED: 500mm/min | |
| LENGTH: 33mm | MAXIMUM SPINDLE SPEED: 15000rpm | |
| FLUTES: 3 | CUTTING DISTANCE: 1704.32mm | |
| DESCRIPTION: HM90/05 D5 | RAPID DISTANCE: 229.65mm | |
| COMMENT: coated | ESTIMATED CYCLE TIME: 3m:28s | |

| Operation 1/1 | | **T27** D27 L27 |
|---|---|---|
| DESCRIPTION: 2D Contour7 | MAXIMUM Z: 15mm | TYPE: flat end mill |
| STRATEGY: Contour 2D | MINIMUM Z: -2mm | DIAMETER: 5mm |
| WCS: #2 | MAXIMUM SPINDLE SPEED: 15000rpm | LENGTH: 33mm |
| TOLERANCE: 0.01mm | MAXIMUM FEEDRATE: 500mm/min | FLUTES: 3 |
| STOCK TO LEAVE: 0mm | CUTTING DISTANCE: 1704.32mm | DESCRIPTION: HM90/05 D5 |
| MAXIMUM STEPOVER: 4.75mm | RAPID DISTANCE: 229.65mm | COMMENT: coated |
| | ESTIMATED CYCLE TIME: 3m:28s | |
| | COOLANT: Flood | |

| CORBELLATI AUTOMOBILI | **PROCESS ROUTE SHEET** | Version - 2 |
|---|---|---|
| Material:   Copper | Part Name: COPPER PLATES<br>Part No: B004<br>Blank: RECTANGLE SHEET | |

| Op. | Machine | OPERATION DESCRIPTION | |
|---|---|---|---|
| 10 | HAAS VF-7 | Drilling of holes for mounting | |
| 20 | HAAS VF-7 | Shoulder milling of plate into shape | |

## OPERATION 10 BUSBAR

### Setup

WCS: #2

STOCK:
DX: 349.99mm
DY: 40.75mm
DZ: 4mm

PART:
DX: 307.99mm
DY: 22.75mm
DZ: 4mm

STOCK LOWER IN WCS #2:
X: -174.99mm
Y: -20.38mm
Z: -4mm

STOCK UPPER IN WCS #2:
X: 174.99mm
Y: 20.38mm
Z: 0mm

44.49

307.99

### Total

NUMBER OF OPERATIONS: 1
NUMBER OF TOOLS: 1
TOOLS: T3
MAXIMUM Z: 15mm
MINIMUM Z: -5mm
MAXIMUM FEEDRATE: 475.089mm/min
MAXIMUM SPINDLE SPEED: 2375rpm
CUTTING DISTANCE: 18mm
RAPID DISTANCE: 325.46mm
ESTIMATED CYCLE TIME: 21s

### Tools

**T3** D3 L3
TYPE: drill
DIAMETER: 4.2mm
TIP ANGLE: 135°
LENGTH: 50mm
FLUTES: 2
DESCRIPTION: for m5 (4.2)

MINIMUM Z: -5mm
MAXIMUM FEED: 475.089mm/min
MAXIMUM SPINDLE SPEED: 2375rpm
CUTTING DISTANCE: 18mm
RAPID DISTANCE: 325.46mm
ESTIMATED CYCLE TIME: 6s

### Operations

Operation 1/1
DESCRIPTION: Drill2
STRATEGY: Drilling
WCS: #2
TOLERANCE: 0.01mm

MAXIMUM Z: 15mm
MINIMUM Z: -5mm
MAXIMUM SPINDLE SPEED: 2375rpm
MAXIMUM FEEDRATE: 475.089mm/min
CUTTING DISTANCE: 18mm
RAPID DISTANCE: 325.46mm
ESTIMATED CYCLE TIME: 6s
COOLANT: Off

**T3** D3 L3
TYPE: drill
DIAMETER: 4.2mm
TIP ANGLE: 135°
LENGTH: 50mm
FLUTES: 2
DESCRIPTION: for m5 (4.2)

# OPERATION 20 BUSBAR

## Setup

WCS: #2

STOCK:
DX: 349.99mm
DY: 40.75mm
DZ: 4mm

PART:
DX: 307.99mm
DY: 22.75mm
DZ: 4mm

STOCK LOWER IN WCS #2:
X: -174.99mm
Y: -20.38mm
Z: -4mm

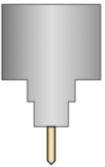STOCK UPPER IN WCS #2:
X: 174.99mm
Y: 20.38mm
Z: 0mm

307.99

## Total

NUMBER OF OPERATIONS: 3
NUMBER OF TOOLS: 2
TOOLS: T25 T27
MAXIMUM Z: 15mm
MINIMUM Z: -5mm
MAXIMUM FEEDRATE: 1400.564mm/min
MAXIMUM SPINDLE SPEED: 12732rpm
CUTTING DISTANCE: 52656.26mm
RAPID DISTANCE: 1034.09mm
ESTIMATED CYCLE TIME: 1h:15m:43s

## Tools

**T25** D25 L25
TYPE: chamfer mill
DIAMETER: 10mm
TAPER ANGLE: 45°
LENGTH: 50mm
FLUTES: 2
DESCRIPTION: engrave
MINIMUM Z: -0.3mm
MAXIMUM FEED: 1000mm/min
MAXIMUM SPINDLE SPEED: 9549rpm
CUTTING DISTANCE: 26.58mm
RAPID DISTANCE: 24.3mm
ESTIMATED CYCLE TIME: 3s (0.1%)

**T27** D27 L27
TYPE: flat end mill
DIAMETER: 5mm
LENGTH: 44mm
FLUTES: 2
DESCRIPTION: HM9/04 D5
MINIMUM Z: -5mm
MAXIMUM FEED: 1400.564mm/min
MAXIMUM SPINDLE SPEED: 12732rpm
CUTTING DISTANCE: 52629.67mm
RAPID DISTANCE: 1009.79mm
ESTIMATED CYCLE TIME: 1h:15m:10s (99.3%)
HOLDER: 100mm BT40

## Operations

### Operation 1/3
DESCRIPTION: Adaptive4
STRATEGY: Adaptive
WCS: #2
TOLERANCE: 0.1mm
STOCK TO LEAVE: 0mm
MAXIMUM STEPDOWN: 1mm
OPTIMAL LOAD: 0.5mm
LOAD DEVIATION: 0.05mm
MAXIMUM Z: 15mm
MINIMUM Z: -5mm
MAXIMUM SPINDLE SPEED: 12732rpm
MAXIMUM FEEDRATE: 1400.564mm/min
CUTTING DISTANCE: 660.23mm
RAPID DISTANCE: 84.15mm
ESTIMATED CYCLE TIME: 48s (1.1%)
COOLANT: Off
**T27** D27 L27
TYPE: flat end mill
DIAMETER: 5mm
LENGTH: 44mm
FLUTES: 2
DESCRIPTION: HM9/04 D5

### Operation 2/3
DESCRIPTION: 2D Contour9
STRATEGY: Contour 2D
WCS: #2
TOLERANCE: 0.01mm
STOCK TO LEAVE: 0mm
MAXIMUM STEPDOWN: 0.5mm
MAXIMUM STEPOVER: 2.5mm
MAXIMUM Z: 15mm
MINIMUM Z: -5mm
MAXIMUM SPINDLE SPEED: 6366rpm
MAXIMUM FEEDRATE: 1300mm/min
CUTTING DISTANCE: 51969.44mm
RAPID DISTANCE: 925.64mm
ESTIMATED CYCLE TIME: 1h:14m:22s (98.2%)
COOLANT: Off
**T27** D27 L27
TYPE: flat end mill
DIAMETER: 5mm
LENGTH: 44mm
FLUTES: 2
DESCRIPTION: HM9/04 D5

### Operation 3/3
DESCRIPTION: 2D Contour11
STRATEGY: Contour 2D
WCS: #2
TOLERANCE: 0.01mm
STOCK TO LEAVE: 0mm
MAXIMUM STEPOVER: 9.5mm
MAXIMUM Z: 15mm
MINIMUM Z: -0.3mm
MAXIMUM SPINDLE SPEED: 9549rpm
MAXIMUM FEEDRATE: 1000mm/min
CUTTING DISTANCE: 26.58mm
RAPID DISTANCE: 24.3mm
ESTIMATED CYCLE TIME: 3s (0.1%)
COOLANT: Off
**T25** D25 L25
TYPE: chamfer mill
DIAMETER: 10mm
TAPER ANGLE: 45°
LENGTH: 50mm
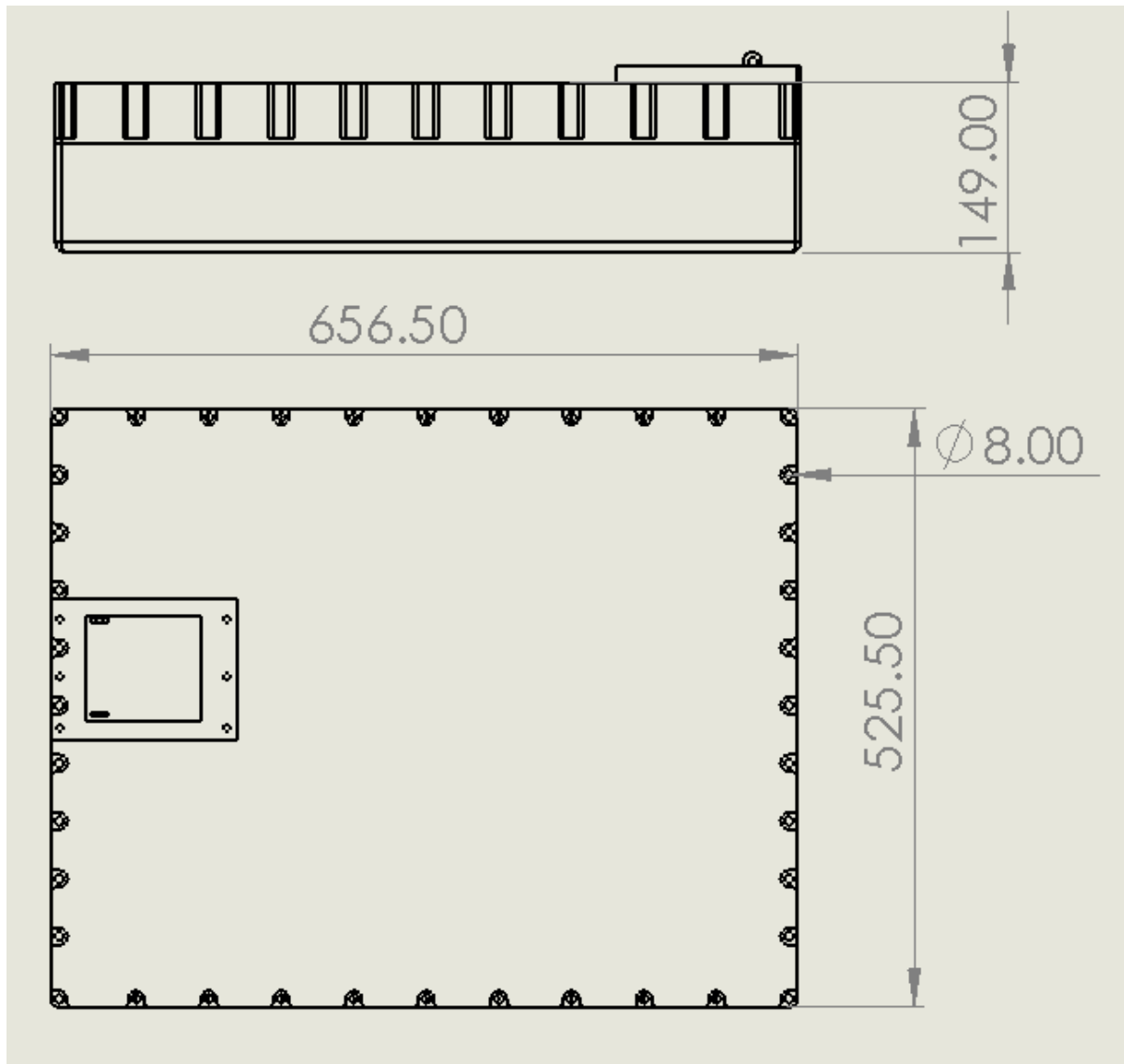FLUTES: 2
DESCRIPTION: engrave

# 9 APPENDIX C 400V BATTERY COMPONENTS DRAWING



*Figure 81 400V battery Drawing*